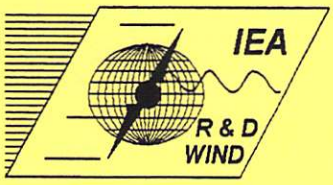

INTERNATIONAL ENERGY AGENCY

Implementing Agreement for Co-operation in the Research and Development of Wind Turbine Systems
ANNEX XI

29th Meeting of Experts

Aero-acoustic Noise of Wind Turbines
Noise Prediction Models

Milano, March 17-18, 1997

Organized by : ENEL, CRE

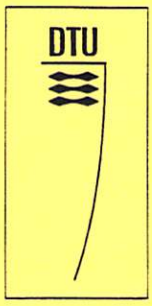

Scientific Coordination :

B. Maribo Pedersen
Dept. of Fluid Mechanics
Technical University of Denmark

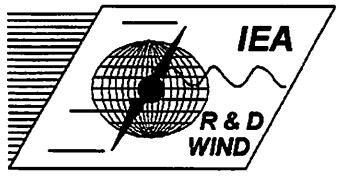

INTERNATIONAL ENERGY AGENCY

Implementing Agreement for Co-operation in the Research and Development of Wind Turbine Systems
ANNEX XI

29th Meeting of Experts

Aero-acoustic Noise of Wind Turbines
Noise Prediction Models

Milano, March 17-18, 1997

Organized by : ENEL, CRE

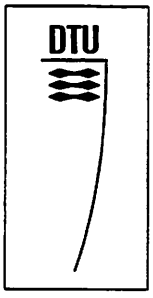

Scientific Coordination :

B. Maribo Pedersen
Dept. of Fluid Mechanics
Technical University of Denmark

ISSN 0590-8809

CONTENTS

NOISE PREDICTION MODELS FOR WIND TURBINES

Introductory Note

To secure the continuing use of wind energy in densely populated areas, it is important that the wind turbines operate silently.

The development of silent wind turbines is dependent upon the understanding of the physics of the noise generating mechanisms and the translation of that understanding into good prediction models. Since knowledge of the aerodynamic noise generating mechanisms is not yet complete, the prediction models still need improvements. Noise prediction models have not reached the maturity of aeroelastic models for wind turbines.

Research projects, past and present ones, funded by the Commission of the European Union, address the problem of wind turbine noise. Some projects have resulted in the development and implementation of semi-empirical prediction models. Semi-empirical models correlate empirically aerodynamic parameters, computed or measured, to the acoustic noise sources. For predictions of the total noise from a wind turbine, semi-empirical models are at present perhaps the most reasonable to use.

However, recently in the late 80s, the discipline computational aeroacoustics (CAA) has emerged. Briefly defined, CAA uses computational fluid dynamics techniques to perform fully numerical computations of sound generated aerodynamically. CAA is, especially in USA, an active area of research, and two recent workshops on benchmark problems have been held. At its present level of maturity, CAA may be a useful tool for prediction of at least some of the different aerodynamic noise contributions from the blades. In the future, CAA is expected to be an important tool for understanding of the noise generating mechanisms and propagation of the noise.

Semi-empirical and CAA noise prediction techniques are the subject of this expert meeting. The meeting offers an opportunity for researchers in the field of noise prediction to present and discuss their models and methods. The meeting may provide answers to the following questions:

What noise sources are the most important?
How are the sources best modeled?
What needs to be done to do better predictions?
Does it boil down to correct prediction of the unsteady aerodynamics around the rotor?
Or is the difficult part to convert the aerodynamics into acoustics?

Improved Prediction of Aerodynamic Noise from Wind Turbines*

G. Guidati, R. Bareiß, S. Wagner

Institute of Aerodynamics and Gasdynamics (IAG), University of Stuttgart
Pfaffenwaldring 21, D-70550 Stuttgart, Germany
Phone: +49 711 695 3421, Fax: +49 711 685 3438, E-mail: guidati@iag.uni-stuttgart.de

CONTENT

1 INTRODUCTION

The dominating aerodynamic noise mechanisms on the blades of large wind turbines (0.5-1.5 MW) are considered to be *trailing-edge noise* and *inflow-turbulence noise*. Trailing-edge noise is caused by the boundary-layer turbulence being convected over the blades trailing edge. DASSEN ET AL. showed that it can be diminished by approx. 6 dB by applying serrations at the trailing edge.[1] Inflow-turbulence noise is caused by the interaction of atmospheric turbulence with the airfoil. Research carried out within the Dutch TWIN project and within the JOULE-III project DRAW (Development of Design Tools for Reduced Aerodynamic Noise Wind Turbines) indicates that the sound radiation is strongly dependent on the exact airfoil shape.[2] This opens the possibility to reduce inflow-turbulence noise by modifying the latter.

Within DRAW, a large number of experiments have been performed in two wind tunnels at the National Aerospace Laboratory NLR (NL). This paper focuses on an improved prediction model for inflow-turbulence noise which takes the true airfoil shape into account. Predictions are compared to the results of acoustic measurements on three 2D-models of 0.25 m chord. Two of the models have NACA–636xx airfoils of 12 % and 18 % relative thickness. The third airfoil was acoustically optimized by using the new prediction model.

In the experiments the turbulence intensity of the flow was strongly increased by mounting a grid with 60 mm wide meshes and 12 mm thick rods onto the tunnel exhaust nozzle. The sound radiated from the airfoil was distinguished by the tunnel background noise by using an acoustic antenna consisting of a cross array of 36 microphones in total. An application of a standard beam-forming algorithm allows to determine how much noise is radiated from different parts of the models. This procedure normally results in a peak at the leading and trailing edge of the airfoil. The strength of the leading-edge peak is taken as the source strength for inflow-turbulence noise.

* Presented at the IEA Meeting on *Aeroacoustic noise of wind turbines, noise prediction models for wind turbines* held in Milano, Italy on 17 March 1997.

2 IMPROVED MODEL FOR INFLOW-TURBULENCE NOISE

The mechanism of noise production by the interaction of a thin airfoil and inflow turbulence was described by AMIET.[3] Although this model is capable of predicting the absolute noise level by relatively thin airfoils (12 %) with a reasonable accuracy it is surely not capable of describing the effect of airfoil shape on noise. A new model is therefore required.

In this section an improved prediction model for inflow turbulence noise is shortly described. For an extensive discussion see GUIDATI ET AL.[4] Starting from the basic equation by HOWE[5] the convected wave equation is reduced to an ordinary wave equation in a fluid at rest (HELMHOLTZ equation). The latter is accomplished by a transform of the acoustic variable. The HELMHOLTZ equation can now be solved by the boundary-element method. The consideration of the mean flow requires the definition of boundary conditions for the acoustic variables at the shear layers which bound the open jet and at the wake.

The main step is however the definition of an appropriate source term for modelling inflow-turbulence noise. The latter is derived by considering the spectral decomposition of a point vortex which is passively convected by the steady base flow around the airfoil. The relation to the well-known convected sinusoidal gusts of thin airfoil theory is indicated and the extension to arbitrary airfoil shapes is introduced.

2.1 Basic acoustic equations

The generation and propagation of aerodynamic sound has been treated by HOWE[5]. He considered the momentum equation and continuity equation and derived an expression for the sound production in a fluid where viscous dissipation and heat conduction can be neglected

$$\left\{\frac{D}{Dt}\left(\frac{1}{c^2}\frac{D}{Dt}\right)+\frac{1}{c^2}\frac{D\mathbf{u}}{Dt}\cdot\nabla-\nabla^2\right\}B=\nabla\cdot(\boldsymbol{\omega}\times\mathbf{u}-T\nabla S)-\frac{1}{c^2}\frac{D\mathbf{u}}{Dt}\cdot(\boldsymbol{\omega}\times\mathbf{u}-T\nabla S). \qquad (1)$$

$\mathbf{u}$ denotes the total fluid velocity, $\boldsymbol{\omega}=\nabla\times\mathbf{u}$ is the vorticity, T the thermodynamic temperature and S the specific entropy. The stagnation enthalpy B assumes the role of the acoustic variable in presence of a mean flow. Eq. (1) shows that the production of sound is always associated with the presence of vorticity or entropy gradients.

Eq. (1) is simplified by linearizing with respect to the acoustic variable B and by assuming a steady, inviscid, irrotational, and isentropic base flow $\mathbf{U}$. The MACH number of the flow shall be small $\left(M_0^2<<1\right)$ so that it can be considered as incompressible with a potential Φ, i.e. $\mathbf{U}=U_0\nabla\Phi$, with U_0 being the free-stream velocity. The acoustic wave speed is taken as constant throughout the field. This yields the convected wave equation

$$\left\{\frac{1}{c_0^2}\left(\frac{\partial}{\partial t}+\mathbf{U}\cdot\nabla\right)^2-\nabla^2\right\}B=\sigma(\mathbf{x},t),\qquad \sigma(\mathbf{x},t)=\nabla\cdot(\boldsymbol{\omega}\times\mathbf{u}). \qquad (2)$$

In the remaining paper B shall denote the *perturbation* stagnation enthalpy. The right hand side $\sigma(\mathbf{x},t)$ acts as a source term and is considered to be an incompressible approximation of the fluctuating (turbulent) flow. The velocity $\mathbf{u}$ is therefore composed of the constant part $\mathbf{U}$ and a fluctuating part which is induced by the vorticity. The latter is assumed to be negligible compared to the base flow. This requires the turbulence to be weak, a condition which is often met in practice. Now a FOURIER transform is performed (indicated by a hat) and the acoustic variable is transformed according to TAYLOR[6]

$$\mathcal{B}=\hat{B}\cdot e^{iM_0k_0\Phi}. \qquad (3)$$

Throughout the text, $\mathcal{B}$ will be referred to as the working variable. If all terms involving M_0^2 are be neglected in a low MACH-number flow, Eq. (2) reduces to the HELMHOLTZ equation for a fluid at rest [7]

$$k_0^2\mathcal{B}+\nabla^2\mathcal{B}=-\hat{\sigma}(\mathbf{x},\omega)e^{iM_0k_0\Phi}. \tag{4}$$

This equation forms the basis for the simulations described in this paper.

Eq. (4) illustrates that the potential Φ of the base flow is required if the influence of the flow onto the propagation of acoustic waves is considered. Now, the determination of the potential for the situation in the experiments is considerably complicated by the fact that the models are placed in an open jet wind tunnel. Depending on the angle of attack the jet is deflected more or less and the airfoil produces less lift than an airfoil in uniform flow.

In order to compute the base flow potential, the following approach is followed: The border of the jet is modeled by two vortex sheets. These sheets are allowed to deform freely until they become a streamline of the flow. The accuracy of this procedure can be seen by comparing the measured and predicted c_l-a curve together with the theoretical curve (see Figure 1). Apparently the reduced slope of the curve is predicted in a satisfactory way. Figure 2 shows an example for the base flow potential. It can be seen that the potential is zero outside the stream, and exhibits a jump through the wake of the airfoil. The discontinuities at the shear layer and at the wake require special attention when dealing with the transform by TAYLOR introduced above.

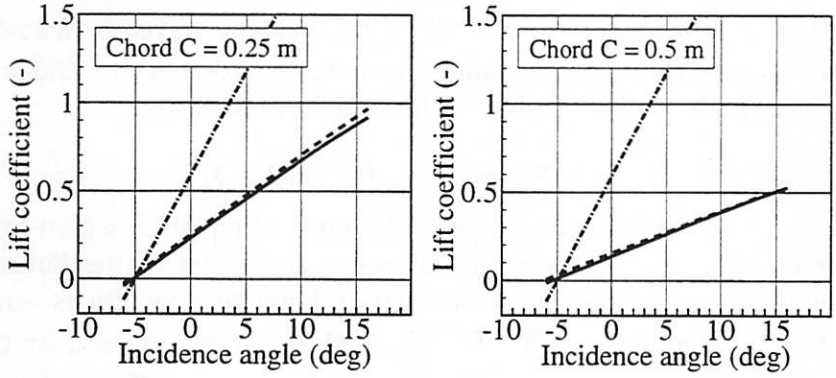

Figure 1: Lift coefficient for two NACA–63612 airfoils of different chord; measurement ——, prediction (open jet) --------, prediction (unbounded flow) -·-·-·-

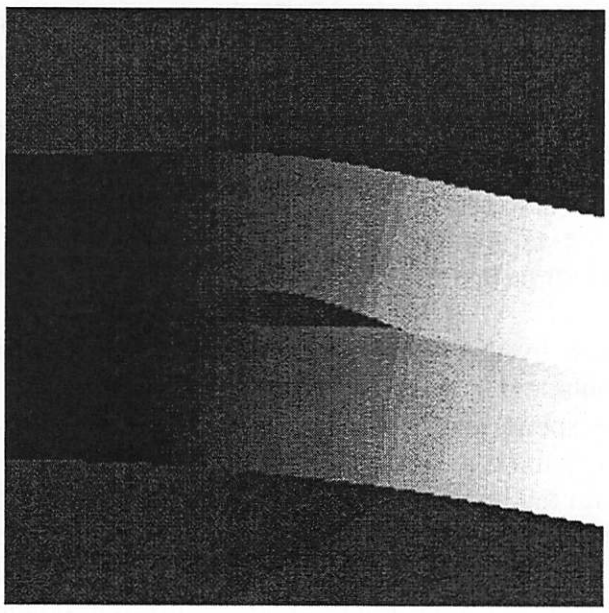

Figure 2: Example for base flow potential.

2.2 Solution of equations

Eq. (4) is well-known in acoustics as it describes the propagation of sound in a fluid which is at rest. If solid surfaces are present, it is most convenient to transform Eq. (4) into a boundary integral equation. This can be accomplished by an application of GREENS third identity. For the general problem of two domains divided by a boundary S, the value of $\mathcal{B}$ at any field point $\mathbf{x}$ is then expressed as a surface integral of a continuous dipole and source (monopole) distribution, the respective strengths being equal to the local boundary value of the working variable $\mathcal{B}$ and its normal derivative $\mathcal{B}^n$

$$\mathcal{B}(\mathbf{x}) = \mathcal{B}^\sigma + \int_S \left(G\left(\mathcal{B}_\mathrm{I}^n - \mathcal{B}_\mathrm{II}^n\right) - G^n\left(\mathcal{B}_\mathrm{I} - \mathcal{B}_\mathrm{II}\right)\right) \mathrm{d}S$$
$$\mathcal{B}^\sigma = \int_V G\hat{\sigma}\, e^{iM_0 k_0 \Phi(\mathbf{y})} \mathrm{d}V \qquad (5)$$

Here use has been made of the following abbreviations

$$\mathcal{B}_\mathrm{I}^n = \left(\nabla \mathcal{B}_\mathrm{I} \cdot \mathbf{n}\right) \quad \mathcal{B}_\mathrm{II}^n = \left(\nabla \mathcal{B}_\mathrm{II} \cdot \mathbf{n}\right) \quad G^n = \left(\nabla G \cdot \mathbf{n}\right). \qquad (6)$$

The subscripts $_\mathrm{I}$ and $_\mathrm{II}$ denote the value on the side of the boundary facing domain Ω_I and Ω_II, respectively (see Figure 3). The volume integral $\mathcal{B}^\sigma$ which is caused by the presence of the acoustic sources $\hat{\sigma}(\mathbf{x}, \omega)$ assumes the role of an incident wave. G denotes the free space Greens function for the Helmholtz equation. It can be regarded as the field which is caused by an acoustic source at the position $\mathbf{y}$. In two dimensions G is given by

$$G(\mathbf{x}, \mathbf{y}, \omega) = -\frac{i}{4} H_0^{(1)}\left(k_0 |\mathbf{x} - \mathbf{y}|\right). \qquad (7)$$

Evaluating Eq. (5) on the boundary S yields the integral equation which forms the basis for the boundary element method. Now the question arises where the boundaries should be located. Generally those surfaces on which certain boundary conditions – i.e. constraints on the initially free distributions of $\mathcal{B}_\mathrm{I}$, $\mathcal{B}_\mathrm{I}^n$, $\mathcal{B}_\mathrm{II}$, and $\mathcal{B}_\mathrm{II}^n$ – are imposed by the physical laws behind the problem, are declared as boundaries which separate different domains.

The obvious choice is the airfoil surface. Here the physics demands that the normal velocity on a rigid surface must vanish. As shown in Figure 2, the base flow potential Φ has a jump through the wake of the airfoil and at the shear layers that bound the open jet. This discontinuity leads in connection with TAYLORS transform to an unphysical jump in pressure and in velocity. Therefore also these surfaces are declared as boundaries, i.e. covered with monopoles and dipoles.

The boundary conditions for the problem of sound refraction at shear layers have been formulated by RIBNER[8] and MILES.[9] They state that the pressure must be continuous through the shear layer and that the shear layer itself must be a stream surface for the flow on both sides. The latter leads to a non-linearity in the boundary conditions and is therefore simplified to the condition that the normal velocity must be continuous through the shear layer.

The error introduced by this simplification is negligible for two reasons: (i) the Mach number is in the simulations is rather low (M_0 = 0.1–0.18) and (ii) that part of the sound which dominates the sound level measured by the microphones crosses the shear layer perpendicular to it and is therefore affected only minimally.

Eq. (5) together with the boundary conditions constitutes a well-posed problem which can be solved by the boundary-element method. The numerical implementation of the method is not a major topic of this paper and is only briefly sketched in Section 3. Figure 4 gives an overview of the boundary conditions imposed on the different boundaries.

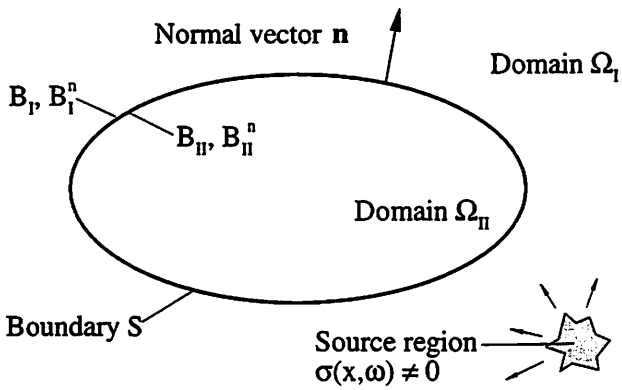

Figure 3: General two-domain problem.

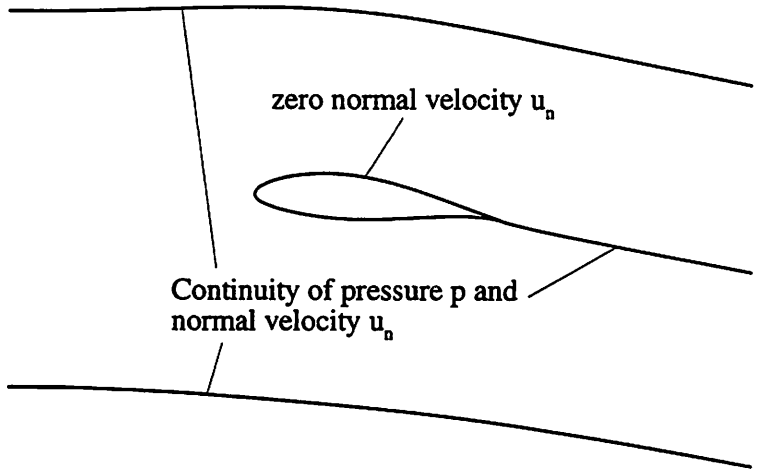

Figure 4: Boundary conditions.

2.3 Introduction of source term

In order to derive an appropriate source term for the problem of turbulence which is convected along an airfoil, the most simple case is considered, i.e. a point vortex which is passively convected along a streamline of the base flow **U**. Thus, the location of the vortex can be described by the path $\mathbf{y}(t)$. The vorticity field is then given by

$$\omega_3 = \Gamma_0 \, \delta(\mathbf{x} - \mathbf{y}(t)) \tag{8}$$

where Γ_0 is the circulation of the vortex. The source term of the convected wave equation is

$$\sigma(\mathbf{x},t) = \nabla \cdot (\boldsymbol{\omega} \times \mathbf{U}) = -U_2 \frac{\partial \omega_3}{\partial x_1} + U_1 \frac{\partial \omega_3}{\partial x_2}. \tag{9}$$

Introducing Eq. (8) gives

$$\sigma(\mathbf{x},t) = U\Gamma_0 \left[n_1 \frac{\partial}{\partial x_1} \delta(x_1 - y_1(t)) \delta(x_2 - y_2(t)) + n_2 \frac{\partial}{\partial x_2} \delta(x_2 - y_2(t)) \delta(x_1 - y_1(t)) \right]. \tag{10}$$

where the normal vector $(n_1 \; n_2)$ is perpendicular to the flow vector **U**. Now consider that all simulation based on the HELMHOLTZ equation are done in the frequency domain. Therefore the FOURIER transform of Eq. (10) has to be performed. The incident wave $\mathcal{B}^\sigma$ is then found by evaluating the volume integral in Eq. (5). This finally reduces to

$$\mathcal{B}^{\sigma}(\mathbf{x},\omega)=\int_{-\infty}^{+\infty}\left[\Gamma_0 U e^{iM_0 k_0 \Phi(y)} e^{i\omega t}(\nabla G\cdot\mathbf{n})\right]\mathrm{d}t. \tag{11}$$

Eq. (11) describes a field of acoustic dipoles which are continuously distributed on the path of the vortex. The dipole axis is perpendicular to the path. The strength varies harmonically with the coordinate t and is furthermore modulated by the local velocity U and the term which is due to the TAYLOR transform.

The spectral decomposition of a moving point vortex can therefore be regarded as an infinite sum of harmonic 'vorticity waves' with frequency ω and locally varying wave speed U. Since a single moving point vortex is the basic element of each vorticity field in the time domain, these 'vorticity waves' are in turn taken as the basic source pattern in the frequency domain for the treatment of inflow-turbulence noise. Furthermore, the amplitude Γ_0 of the wave is taken as a frequency dependent function $\Gamma(\omega)$.

2.4 Relation to the AMIET model

Now consider the prediction model by AMIET.[3] He treated the sound generation by convected sinusoidal gusts of the form

$$u_2(x_1,t)=A_1\, e^{ik_1(x_1-Ut)}=A_1\, e^{i(k_1x_1-\omega t)} \tag{12}$$

where the convection velocity U, the wave number k_1 and the frequency ω are related by

$$U=\frac{\omega}{k_1} \tag{13}$$

According to HOWE, the vorticity is considered as the basic source element as it induces the whole flow, the incompressible turbulent fluctuations and the acoustic field which is radiated as sound.[5] Therefore, in order to compare the present approach to AMIETS, the basic case of a point vortex moving in a uniform flow is considered. The spectral decomposition as shown above yields then a uniform vorticity wave (see Figure 5). The incompressible velocity field induced by this vorticity wave is given by

$$\mathbf{u}(\mathbf{x},t)=\frac{A_2}{2U}e^{i(k_1x_1-\omega t)}e^{-|k_1x_2|}\begin{pmatrix}-\mathrm{sign}(x_2)\\ -i\end{pmatrix}. \tag{14}$$

Now consider two vorticity waves of equal strength the first at $x_2=\varepsilon$ the second at $x_2=-\varepsilon$. The velocity on the centerline between the two waves ($x_2=0$) is given by

$$u_2(x_1,0,t)=-\frac{iA_2}{U}e^{i(k_1x_1-\omega t)}e^{-|k_1\varepsilon|}. \tag{15}$$

The velocity in the x_1-direction cancels to zero. In order to have the same vertical velocity fluctuation of amplitude A_1 like in Eq. (12), the amplitude A_2 must be equal

$$A_2=iA_1Ue^{|k_1\varepsilon|}. \tag{16}$$

Then the vorticity wave has the same effect on a flat plate airfoil at $x_2=0$ like the AMIET source term. This is illustrated in Figure 6.

In view of this identity the basic approach for modeling inflow-turbulence noise on arbitrary airfoils is easily found: Two vorticity waves of same strength have a distance of 2ε far ahead the airfoil. The strength is given by Eq. (16) in order to have a determined vertical velocity fluctuation. When the vorticity waves approach the airfoil they follow the streamlines of the steady potential flow as shown in Figure 7. The incompressible velocity field that they induce especially on the airfoil surface differs from the one proposed by AMIET. Figure 8 shows an example for the velocity field which is affected by the presence of an airfoil.

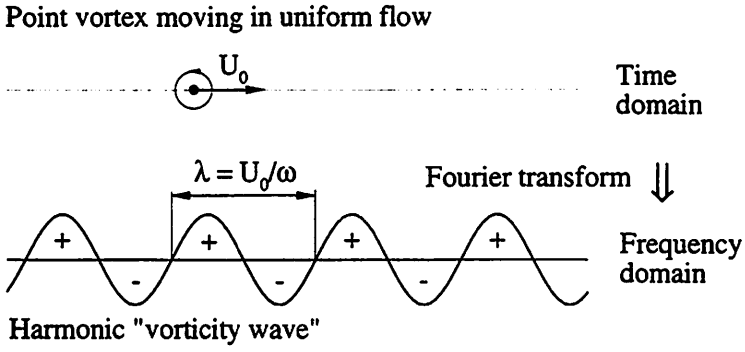

Figure 5: Spectral decomposition of a point vortex in a uniform flow to a uniform harmonic vorticity wave.

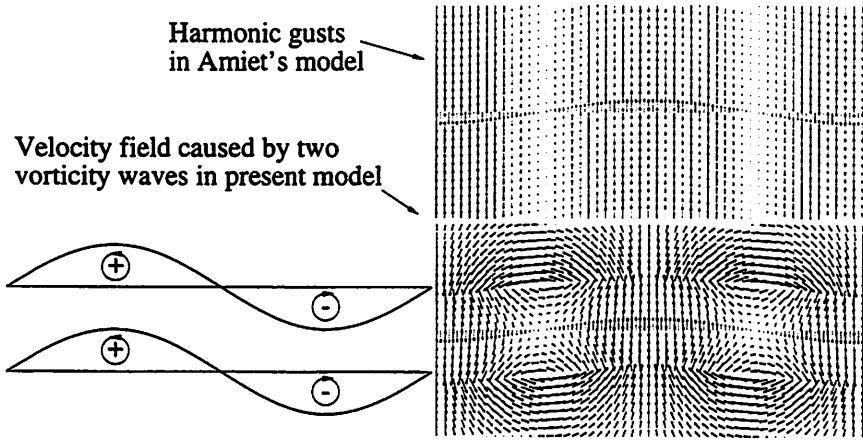

Figure 6: Incompressible velocity field of two vorticity waves in comparison with the harmonic gusts of AMIETS model.

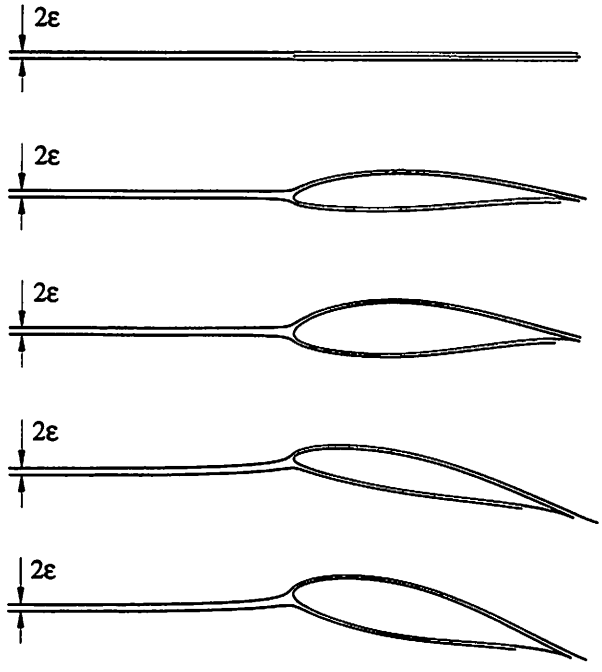

Figure 7: Examples for vorticity waves for different airfoils at different incidence angles.

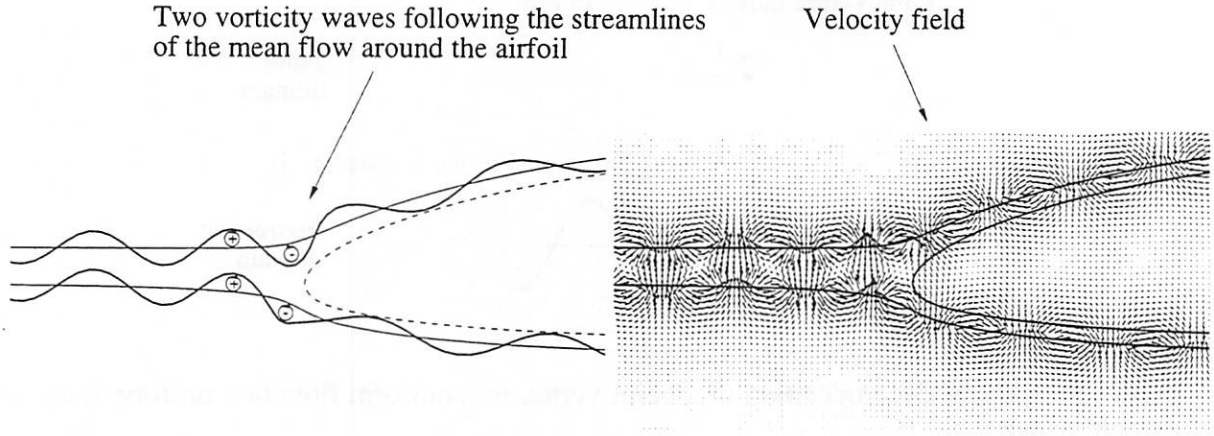

Figure 8: Extension of the present approach to the case of an arbitrary airfoil shape.

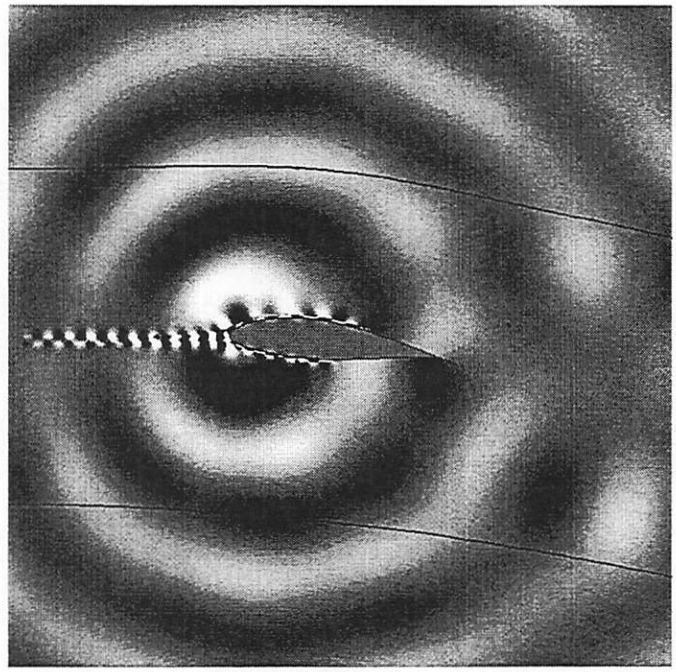

Figure 9: Instantaneous picture of sound pressure for a NACA–63618 airfoil.

3 NUMERICAL IMPLEMENTATION

The integral equations (14) and (16) are solved with the boundary element method. The surface of the airfoil, the wake and the shear layers which bound the open jet are split up into straight panels of linearly varying strength. Thus, the unknown continuous distribution of $\mathcal{B}_{\mathrm{I}}$, $\mathcal{B}_{\mathrm{I}}^{n}$, $\mathcal{B}_{\mathrm{II}}$, and $\mathcal{B}_{\mathrm{II}}^{n}$ is reduced to a limited number of unknowns on the edges of each panel. A set of linear equations is obtained by evaluating the integral equation at these corner points. This gives together with the boundary conditions the acoustic influence matrix. The right-hand side of the equation is given by the incident wave $\mathcal{B}^{\sigma}$ which is due to the source term described in the preceding section.

The line integral in Eq. (11) is solved numerically by employing a 4th-order RUNGE-KUTTA algorithm with variable stepsize. This procedure is less time consuming because the

number of evaluations of the integrand is automatically adapted to the frequency. For practical reasons, the strength of the vorticity wave smoothly increases from zero upstream of the airfoil. Furthermore, the strength fades out at approx. 70 % of the airfoil chord. Figure 9 shows an example of the instantaneous pressure field around a NACA–63612 airfoil.

4 MEASUREMENT OF INFLOW-TURBULENCE NOISE

4.1 Test set-up

The experimental program of the DRAW project was carried out in the Low Speed Wind Tunnel (LST) and the Small Anechoic Wind Tunnel (KAT) of the National Aerospace Laboratory. For the topic addressed in this paper only the KAT measurements are relevant and will be discussed.

The KAT is a open circuit wind tunnel with a test section which consists of an open jet surrounded by a 4×5 m^2 anechoic room. For airfoil self-noise tests a 0.4×0.5 m^2 rectangular exhaust nozzle is used, allowing for jet flow speeds up to 80 m/s. With the aim to vary the turbulence of the tunnel flow, a grid can be mounted onto the exhaust nozzle. A sketch of the KAT test set-up is given in Figure 10. Descriptions of the set-up as it was used for previous studies on airfoil self-noise have been given by DASSEN ET AL.[1,10]

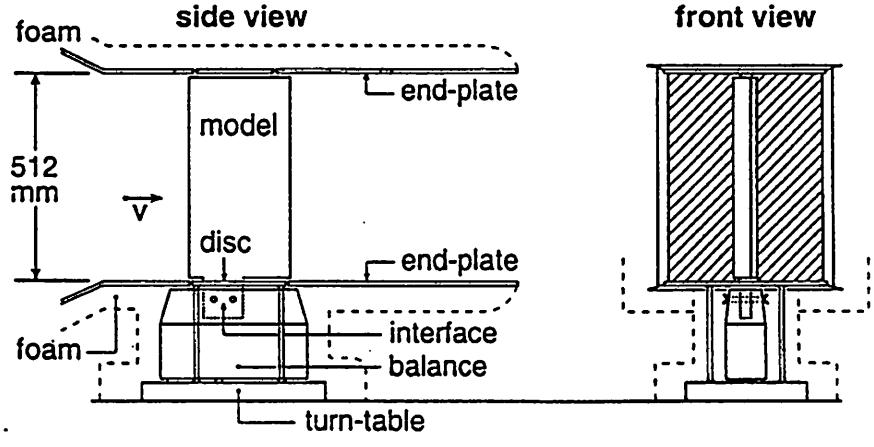

Figure 10: Side and front view of KAT set-up for airfoil self-noise measurements.

As a consequence of the relatively low levels of noise emanating from aerodynamic bodies (such as airfoils are in particular), a directional noise measuring technique had to be used. First of all to filter off the tunnel background noise, and secondly to enable the separate measuring of noise radiated from different parts of a model.

For this purpose, an acoustic antenna was used which consists of a cross of 36 microphones in total; a horizontal array of 22 microphones and a vertical array of 14 microphones. Each array consists of two subarrays of 15 (horizontal) microphones and 9 and 14 (vertical) microphones. The spacing of the microphones in these subarrays is 4 cm and 8 cm respectively and enables measurements in the frequency range from 750 Hz to 6 kHz. The antenna was placed 50 cm from the center line of the test section yielding a spatial resolution of approximately 20 cm in the frequency range up to 1500 Hz and approximately 10 cm for higher frequencies. Figure 11 shows the antenna (left) as it was placed just out of the flow of the KAT. On the right hand side the turbulence grid can be seen.

The antenna beamforming is carried out in the frequency domain and is obtained from multiplying all cross power spectra by weighting functions. These weighting functions

account for amplitude and phase differences resulting from the differences in distance from all individual microphones to a large number of scan points in the plane of the model. The reader interested in more details of this sum-and-delay beamforming is referred to one of the many textbooks on array signal processing. [11,12]

4.2 Measurements in DRAW

In the framework of DRAW, a large series of models with various chord lengths were used. For the investigations on inflow-turbulence noise only three, 25 cm chord models were tested: a NACA–63612, a NACA–63618, and a modified NACA–63612 airfoil. The selection of these models was partially based on insights obtained from previous investigation which had revealed that the thickness may have a significant influence on the radiated inflow-turbulence noise[13]. The modified airfoil was designed to yield minimal inflow-turbulence noise *without* increasing the airfoil thickness, using a computational code which is based on the model described in this paper.

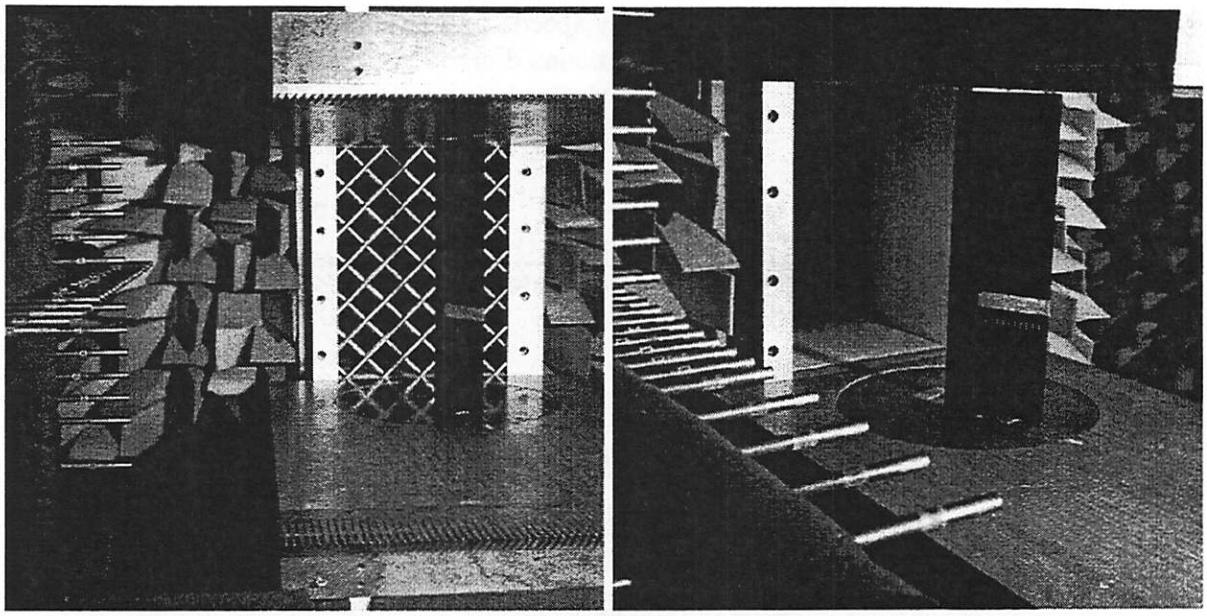

Figure 11: Airfoil self-noise measurements using the cross antenna; with (left) and without turbulence grid mounted onto the tunnel exhaust nozzle.

A typical acoustic image resulting from the antenna beamforming is shown in Figure 12. These images can be obtained in different frequency bandwidths and show the locations and contributions of the dominant sources. In the figure the noise as radiated from the leading and the trailing edge can be recognized as well as some influence of reflection from the end-plates. The spectra of leading and trailing-edge noise are obtained by taking the maxima at the tunnel center line. It has been proven by previous calibrations that this procedure leads to a reliable (± 3 dB) absolute value for the noise radiated from different parts of the models.[14]

The final step consists of a comparison of these levels with the tunnel background noise levels (with and without grid) at these positions. As it turned out that the grid may generate high levels of noise, i.e. broad peaks which overlap the leading edge peak, it is sometimes impossible to correct for this noise, despite the use of an antenna. Therefore, no spectral value was determined in case the difference in level with and without models was less than 2 dB. In case this difference was more than 2 dB, the tunnel background noise level was subtracted from the airfoil noise level to obtain the spectrum of airfoil noise. The results of this procedure are shown in the next section.

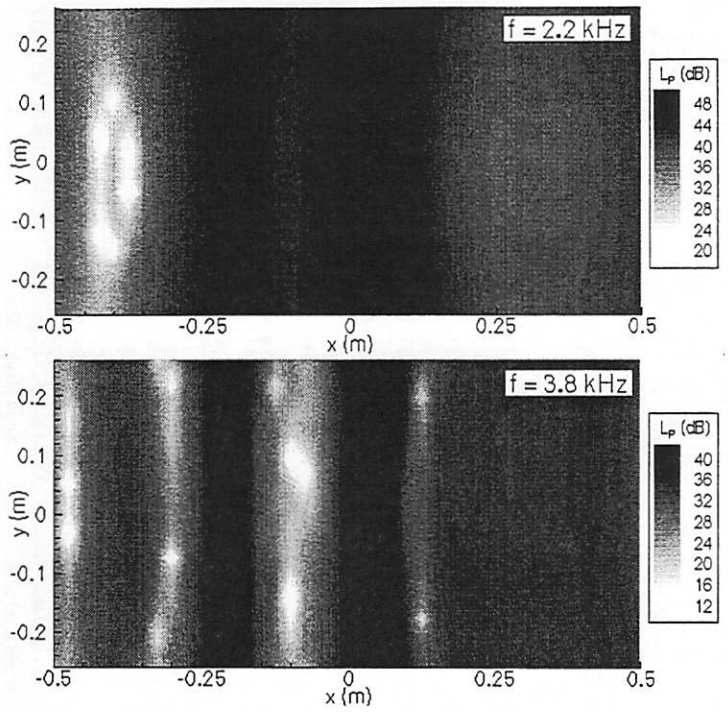

Figure 12: Typical acoustic image resulting from antenna measurement (modified NACA–63612, $M_0 = 0.15$, $c_l = 0.0$).

5 VALIDATION OF PREDICTION MODEL

In the following, the predictions which are based on the model described in Section 2 are compared to the results of the measurements. This comparison is shown for three airfoils, two MACH numbers, and four lift coefficients (see Table 1). All results are presented in 1/3rd octave bands and normalized by the sound levels found for the NACA–63612 airfoil at c_l = 0.25. In the predictions the beam-forming algorithm used in the measurements is modeled and the peak of the acoustic image at the leading edge is taken as the source strength.

Table 1: Overview of conditions.

Model	NACA–63612 NACA–63618 modified NACA–63612
MACH number M_0	0.15, 0.18
Lift coefficient c_l	0.0, 0.25, 0.5, 0.75

Figure 13 shows the results for M_0 = 0.15 and M_0 = 0.18 (left side: prediction, right side: measurement). It can be seen that the trend of the measurements is clearly reproduced, i.e. the NACA–63618 airfoil radiates less noise than the NACA–63612 airfoil. Furthermore the new airfoil which was designed to reduce inflow-turbulence noise *without* increasing the relative thickness shows a reduction in sound level of 2–5 dB.

Figure 14 shows the difference in sound level between the normalized measurements and the normalized predictions. For most conditions the three curves collapse in a satisfactory way. Thus, the model is able to predict the *difference* between the airfoils for a given MACH number and incidence angle. However, there is a trend that the prediction underestimates the sound level at the highest lift coefficient.

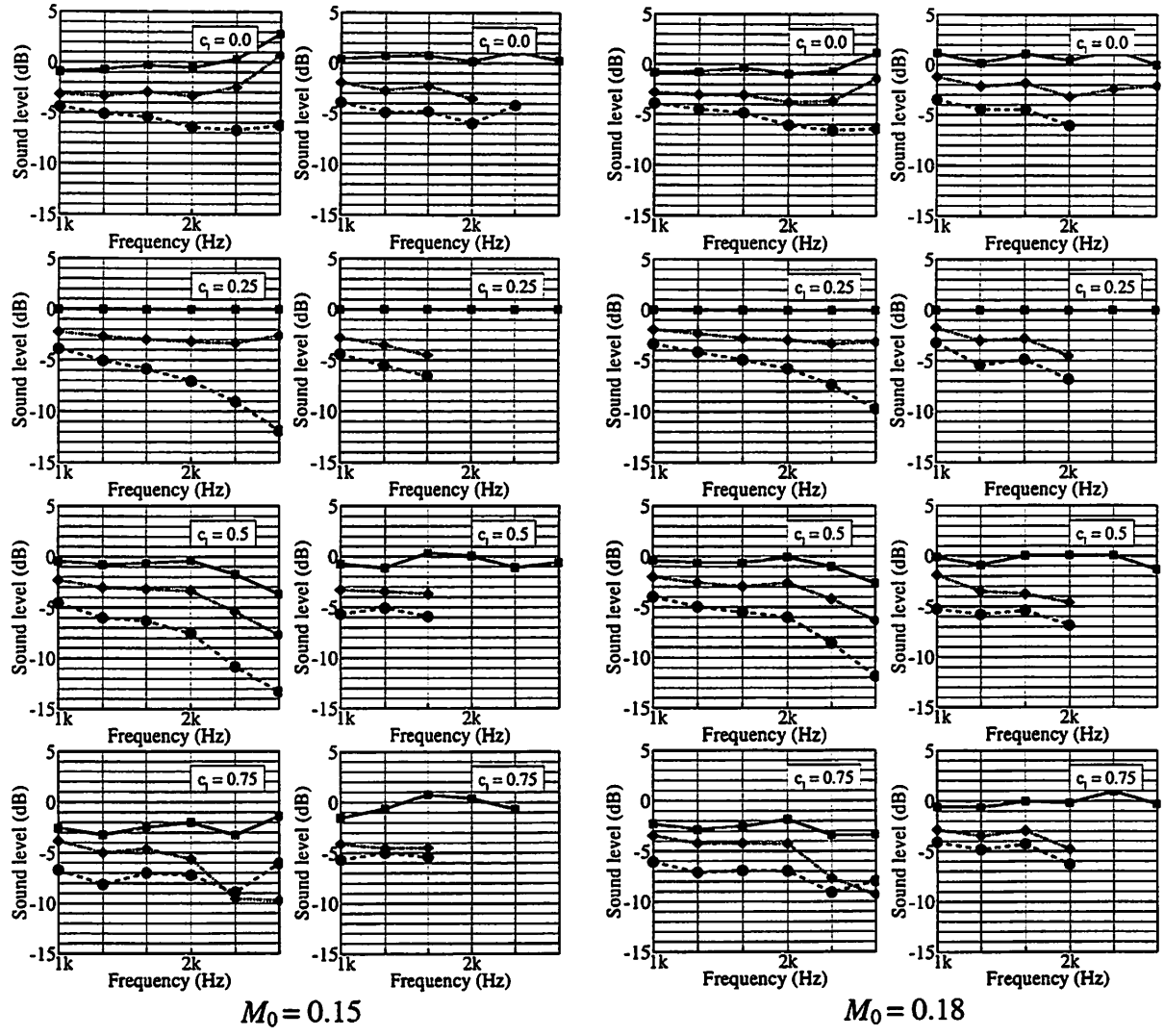

Figure 13: Normalized prediction (left) and measurement (right), NACA–63612 —■—, NACA–63618 --●--, modified NACA–63612 ---◆---

6 CONCLUSIONS

The investigations presented in this paper have shown that the airfoil shape can have a major influence on the generation of inflow-turbulence noise. While former experiments revealed that an increased airfoil *thickness* leads to a reduction of inflow-turbulence noise, it turned out now that the noise is strongly dependent also on the airfoil *shape*, i.e. a noise reduction can be obtained *without* increasing the thickness.

These experimental findings are confirmed by the new model presented in this paper, which is able to predict the differences in noise level between airfoils with a reasonable accuracy, although more work is needed in order to obtain a reliable prediction of the absolute noise level.

In view of the fact that the computer program based on this model runs only a few minutes on a small workstation, it may be possible in the near future to design acoustically optimized airfoils for the application on fans, propellers, or wind turbines.

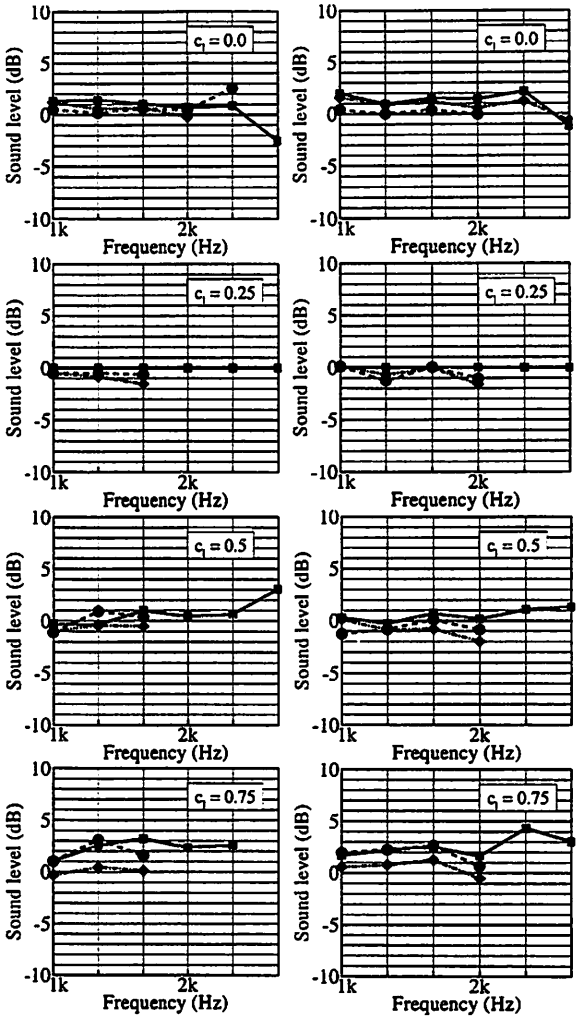

Figure 14: Difference between the normalized measurement and the normalized prediction for M_0 = 0.15 (left) and M_0 = 0.18 (right), NACA–63612 —■—, NACA–63618 - -●- -, modified NACA–63612 ---◆---

ACKNOWLEDGMENTS

This work was sponsored by the European Commission under the JOULE-Contract No. JOR3-CT95-0083.

REFERENCES

1 DASSEN, T.; PARCHEN, R.; BRUGGEMAN, J.C.: *Wind tunnel measurements of the aerodynamic noise of blade sections.* Proceedings of the European Wind Energy Conference and Exhibition, Thessaloniki, pp. 791-798, 1993.

2 GUIDATI, G.; BAREIß, R.; WAGNER, S. ET AL.: *Development of Design Tools for Reduced Aerodynamic Noise Wind Turbines (DRAW).* Proceedings of the European Union Wind Energy Conference and Exhibition, Göteborg, pp. 778-781, 1996.

3 AMIET, R. K.: *Acoustic Radiation From an Airfoil in a Turbulent Stream.* Journal of Sound and Vibration. Vol. **41** (4), pp. 407-420, 1975.

[4] GUIDATI, G.; DASSEN, T.; PARCHEN, R.; BAREIß, R.; WAGNER, S.: *Simulation and measurement of inflow-turbulence noise on airfoils.* AIAA Paper No. 97-1698, 1997.

[5] HOWE, M. S.: *Contributions to the Theory of Aerodynamic Sound, with Applications to Excess Jet Noise and the Theory of the Flute.* Journal of Fluid Mechanics, Vol. **71** (4), pp. 625-673, 1975.

[6] TAYLOR, K.: *A transformation of the acoustic equation with implications for wind-tunnel and low-speed flight tests.* Proceedings of the Royal Society of London, **A 363**, pp. 271-281, 1978.

[7] ASTLEY, R.J.; BAIN, J.G.: *A three-dimensional boundary element scheme for acoustic radiation in low mach number flows.* Journal of Sound and Vibration, Vol. **109** (3), pp. 445-465, 1986.

[8] RIBNER, H.S.: *Reflection, Transmission, and Amplification of Sound by a Mowing Medium.* Journal of the Acoustical Society of America, Vol. **29** (2), pp. 435-441, 1957.

[9] MILES, J.W.: *On the reflection of Sound at an Interface of Relative Motion.* Journal of the Acoustical Society of America, Vol. **29** (2), pp. 226-228, 1957.

[10] DASSEN, A.G.M.; PARCHEN, R.; BRUGGEMAN, J.C; HAGG, F.: *Results of a Wind Tunnel Study on the Reduction of Airfoil Self-Noise by the Application of Serrated Blade Trailing Edges.* Proceedings of the European Wind Energy Conference and Exhibition, Göteborg, pp. 800-803, 1996.

[11] HAYKIN, S.: *Array signal processing.* Englewood Cliffs, N.J., Prentice Hall, 1985.

[12] JOHNSON, D.H.; DUDGEON, D.E.: *Array Signal Processing, concepts and techniques.* Englewood Cliffs, N.J., Prentice Hall, 1993.

[13] HAGG, F.; DASSEN, A.G.M.; PARCHEN, R.; BRUGGEMAN, J.C: *Influence of the airfoil shape and thickness on the emission of turbulence inflow noise as measured in the wind tunnel.* Proceedings of the European Wind Energy Conference and Exhibition, Göteborg, pp. 785-788, 1996.

[14] DASSEN, A.G.M.: *Calibration of an acoustic antenna.* NLR report TR 95270 L, 1995.

Experimental And Theoretical Characterization Of Acoustic Noise From A 7.6m Diameter Yaw Controlled Teetered Rotor Wind Turbine

Emil Moroz
(emil@wind.me.utep.edu)
Department of Mechanical and Industrial Engineering
University of Texas at El Paso
El Paso, TX 79968, USA

Abstract

An experimental investigation into the acoustic noise from a small (7.6m diameter) teetered rotor wind turbine, set at various yaw angles up to 90 degrees of yaw, was conducted. The results revealed a 1/3 octave spectra which was dominated by a broad peak in the higher frequency range, at all yaw angles investigated. This prompted a theoretical investigation to reveal the mechanisms producing the dominant feature in the experimentally obtained noise spectra and resulted in the development of a wind turbine aerodynamic noise prediction code, WTNOISE.

The location near busy roads and the relatively rough terrain of the wind test site caused difficulties in obtaining useful noise spectral information below 500Hz. However, sufficiently good data was obtained above 500Hz to clearly show a dominant "hump" in the spectrum, centered between 3000 and 4000Hz. Although the local Reynolds number for the blade elements was around 500,000 and one might expect Laminar flow over a significant portion of the blade, the data did not match the noise spectra predicted when Laminar flow was assumed. Given the relatively poor surface quality of the rotor blades and the high turbulence of the test site it was therefore assumed that the boundary layer on the blade may have tripped relatively early and that the turbulent flow setting should be used. This assumption led to a much better correlation between experiment and predictions. The WTNOISE code indicated that the broad peak in the spectrum was most likely caused by trailing edge bluntness noise. Unfortunately time did not allow for modifications to the trailing edge to be investigated.

Introduction

An experimental investigation into the acoustic noise from a small (7.6m diameter) teetered rotor wind turbine, set at various yaw angles up to 90 degrees of yaw, was conducted. The results revealed 1/3 octave spectra which were dominated by a broad peak between 3000 Hz and 4000 Hz, at all yaw angles and wind speeds investigated. This prompted a theoretical investigation to reveal the mechanisms producing the dominant feature in the experimentally obtained noise spectra. A noise prediction code, WTNOISE, was developed at UTEP, since none were found in the public domain.

WTNOISE combines Lowson's (1993) method for predicting aerodynamic noise due to the effects of inflow turbulence upon an airfoil section with the Brooks, Pope, and Marcolini (1989) prediction schemes for airfoil self-noise. The inflow turbulence noise method is theoretical and is

dependent upon a number of factors including ground roughness, while the self-noise prediction schemes are semiempirical and are based on both theoretical studies and experimental data obtained from wind tunnel tests of two- and three- dimensional airfoil blade sections. These methods are integrated into WTNOISE which averages the noise of a two bladed rotor over one revolution and gives as output a 1/3 octave A-weighted spectra at a user selectable location. Details of the airflow at each blade element is obtained from the teetered rotor dynamics code, TEETER, developed at the University of Texas at El Paso (UTEP.) The Output spectra were predicted at a downwind location for various yaw angles and compared with the experimental data.

This paper details the work carried out to date: it documents the differences between the UTEP code, WTNOISE, and two other principal noise codes; compares experimental data for the UTEP turbine with prediction; identifies the aerodynamic mechanism responsible for the most significant noise feature in the experimental data; and suggests a solution, which could significantly quieten the rotor under investigation.

The UTEP Wind Turbine Noise Prediction Program, WTNOISE

The UTEP wind turbine noise prediction code, WTNOISE, is an attempt at calculating the noise produced by the individual blade elements of a rotor during one revolution. It is based on the NASA airfoil self-noise prediction program called PREDICT, that is documented at the end of the report by Brooks et al. (1989). The steps taken to adapt this code for use as a wind turbine noise prediction program are listed below:

1. The hardcopy of the PREDICT program was converted into MS-FORTRAN 5.1 and compiled.
2. During the debugging process a number of minor coding errors were identified, by comparing the code listing with the text in the report. The text was assumed to be correct and corrections were incorporated in the code.
3. Correct operation of the code was confirmed by comparison with the two example cases given in Brooks et al. (1989): one with a single section and one with multiple sections.
4. Transformation equations were derived so that microphone locations could be expressed in terms of distances and angles based on blade element aligned coordinate systems. The results for one revolution were placed into a file, that was used as input by WTNOISE.
5. A version of the dynamic analysis code, TEETER (Kantipudi, 1994), was modified such that it created an output file containing blade element angles of attack and relative wind for one complete revolution.
6. The PREDICT program was modified; to read the data files containing microphone geometry and aerodynamic details; to incorporate data describing the rotor, such as chord length, trailing edge thickness, twist distribution etc.; and to integrate, using 20 degree azimuth steps, the noise components from all mechanisms for two blades as they rotated through one revolution. The correct performance of these steps was established by comparing the noise averaged over one revolution with that of a stationary blade determined from the original program. The simple rotation of the blade section and integration of the resulting noise is justifiable according to Lowson (1993a), who points out that it is normal to ignore the effects

of local accelerations due to rotary motion on the noise radiation and that a blade section can be treated as equivalent to an airfoil in a uniform flow.

7. Finally Lowson's equations for the prediction of inflow turbulence were incorporated into WTNOISE.

Table 1 summarizes the differences between WTNOISE and previous work. It should be noted that WTNOISE: neglects retarded time issues; assumes that the aerodynamic noise is incoherent and that cancellation does not occur; and includes directivity in the inflow turbulence calculation to account for yawed operation but does not incorporate any method to account for blade vortex interaction, nor Doppler shift effects at high yaw angles.

Results of Experimental Investigation

A total of 55 sets of 1/3 octave spectra and average noise level data were collected from the UTEP teetered rotor wind turbine, over six days in November, 1994. These data sets were collected from four microphones located: approximately downwind of the wind turbine, at the reference position; upwind; to the left; and to the right of the turbine. The data sets comprised noise information from the reference microphone plus one of the three remaining microphones, along with wind speed and direction measured at hub height for a 25 second period. This time period being due to the necessity of integrating the noise tests with other data collection activities, being conducted in parallel with these experiments.

Figure 1 is an example of a set of raw 1/3 octave spectra for the zero yaw angle case. It is subdivided by microphone position and features a legend block that identifies the individual curves by average wind speed and the corresponding average sound level value. As the frequency analyzer indicated that spectra below 100 Hz were unreliable, these have not been plotted. Similar sets of plots were obtained for yaw angles centered on 30, 60 and 90 degrees. Eventhough the higher yaw angle spectra included data for wind speeds up to 26 mph, all spectra were of a similar shape and were dominated by a peak near 3000 Hz.

Curves representative of the average background noise for the wind turbine cases of interest were obtained from data collected with the wind turbine shut down. Following the American National Standard Institute (ANSI) S1.13-1971 scheme, background noise was subtracted from the raw wind turbine noise. ANSI S1.13-1971 specifies that if the difference in the two levels is 3 decibels or less then no figure can be estimated and the data should not used. The outcome was that none of the data below 300 Hz and near 10000 Hz were usable. However in the area of key interest, in terms of human perception, the wind turbine noise dominated the overall noise spectra and hence useful data was obtained. To obtain the free field noise levels the data was corrected for the effect of the ground board by subtracting a further 6 dB.

Comparison between Predicted and Experimental Data for the UTEP Wind Turbine Rotor

As a consequence of the difficult terrain and the changeable winds, it was difficult to maintain the ideal microphone orientation with respect to the wind and the wind turbine. Instead a directivity correction was incorporated into the prediction code to account for any misalignment. Although

data was collected at various locations around the operating wind turbine only the location nearest the downwind position is considered in this report. Four cases are shown, representing the noise generated at yaw angles of zero, 30, 60 and 90 degrees. For each of these four orientations, the modified TEETER code and the geometry code were run to obtain input files for WTNOISE. The physical details of the wind turbine geometry and the choice of prediction mechanisms to be used were included as data statements.

Although the local Reynolds number for the blade elements was around 500,000 and one might expect Laminar flow over a significant portion of the blade, the data did not match the noise spectra predicted when Laminar flow was assumed. Given the relatively poor surface quality of the rotor blades, the fact that the dominant noise feature seemed insensitive to wind speed and yaw angle, and the high turbulence of the test site it was, therefore, assumed that the boundary layer on the blade may have tripped relatively early and that the turbulent flow setting should be used. This assumption, which is used in the comparisons that follow, led to a much better correlation between experiment and predictions, than was found if the Laminar flow equations were used.

Figures 2 to 5 show comparisons between the current prediction scheme and experimental data obtained for the UTEP rotor. In each case the corrected experimental data points, which could be separated from the background noise, are plotted against the overall predicted noise level and the relevant constituent noise components. In all cases there is an overprediction of the noise levels at frequencies above 7000 Hz. Although the exact cause for this was not determined, dips in the background noise levels centered on 6000 Hz may be an indication of limitations of the frequency analyzer over this range.

Figure 2, which depicts the zero Yaw angle case, compares well with the code except for a slight over prediction of the frequency of the peak sound pressure level. This is a direct consequence of the values input for the trailing edge thickness. A slightly larger value for the trailing edge may be a more appropriate input because of the poor surface finish on the actual blade, which has a small step in both upper and lower surfaces prior to the actual trailing edge. This would shift the peak down to 3150 Hz from 4000 Hz and lead to a much closer match.

Figure 3, which depicts the 30 degree Yaw angle case, also shows good agreement except for an isolated spike at 800 Hz. The 800 Hz spike could be attributed to mechanical noise or be a function of some transient background noise effects which were not subtracted in the data reduction phase.

Figures 4 and 5, show that at Yaw angles of 60 degrees and beyond, the prediction starts to break down although the location of the trailing edge bluntness feature is still well captured. Reasons for this are expected to be associated with blade wake interaction and the simplifying assumptions made about retarded time and due to neglecting the effects of Doppler shift.

Conclusions

Overall it appears that, for modest Yaw angles, the WTNOISE code does a good job of capturing the key features of the noise produced by the UTEP rotor. It accurately predicts that the noise of the rotor will be dominated by tonal noise due to the trailing edge bluntness. As shown in Figure 6, this form of noise is controllable by simply sharpening the trailing edge. Figure 7, which shows the contribution of individual blade sections to the overall noise, highlights the importance of the outer portions of the blade. It points to the fact that only the outer 40 percent of the blade needs to be sharpened in order to reduce the noise level, due to the trailing edge bluntness, to a level below that of the unavoidable turbulent boundary layer noise.

Future Work

It is hoped that time can be found to rerun some of the field tests with a reduced trailing edge thickness. This would allow us to validate the conclusions of this report and to ascertain whether the assumptions about using turbulent rather than laminar flow are valid.

References

Amiet, R.K., "Acoustic Radiation from an Airfoil in a Turbulent Stream", Journal of Sound and Vibration, Vol. 41 No.4, 1975.

Brooks, T.F., Pope, D.S., and Marcolini, M.A., "Airfoil Self Noise and Prediction", NASA Reference Publication 1218, 1989.

Grosveld, F. W., "Prediction of Broadband Noise from Horizontal Axis Wind Turbines," AIAA Journal of Propulsion and Power, Vol. 1, No. 4.

Kantipudi, S., "Improving the TEETER Code for Wind Turbines (Version 2.0)," Masters Thesis, UTEP, 1994.

Lowson, M.V., "Assessment and Prediction of Wind Turbine Noise", ETSU W/13/00284/REP, Harwell, England, 1993a.

Lowson, M.V., "Systematic Comparison of Prediction and Experiment for Wind Turbine Aerodynamic Noise", ETSU W/13/00363/REP, Harwell, England, 1993b.

Table 1. Comparison of Different Wind Turbine Noise Prediction Codes

Noise component	Grosveld (1985)	Lowson (1993a)	UTEP (1995)
Inflow Turbulence	• Based on whole rotor • Based on scaling of Mod-2 data • Wind speed inferred through power curve • Uses root mean square turbulence as a parameter	• Blade element analysis, integrated over rotor • Based on Amiet's(1975) theoretical model • Estimates blade element velocities by assuming inflow, a=1/3 • Includes turbulence scale, ground roughness length and root mean square turbulence as parameters	• Same as Lowson except for use of TEETER code to calculate the exact values of the elemental velocities seen by each blade element at each azimuthal step
Turbulent Boundary Layer Trailing Edge Interaction	• Based on earlier data set by Brooks et al. (1981)	• Based on a rework and "simplification" of the more recent Brooks et al. (1989) data	• Utilizes unmodified prediction method published by Brooks et al. (1989)
Trailing Edge Bluntness Vortex Shedding	• Based on trailing edge thickness dimension, with scaling from experimental data by Brooks et al. (1981)	• Not included	• Utilizes Brooks et al. (1989) method which incorporates effects of boundary layer thickness and blade trailing edge "included angle"
Separation Stall	• Not included	• Not included	• Not included
Laminar Boundary Layer Vortex Shedding	• Not included	• Not included	• Available option, based on Brooks et al. (1989)
Tip Vortex Formation	• Not included	• Not included	• Available option, based on Brooks et al. (1989)

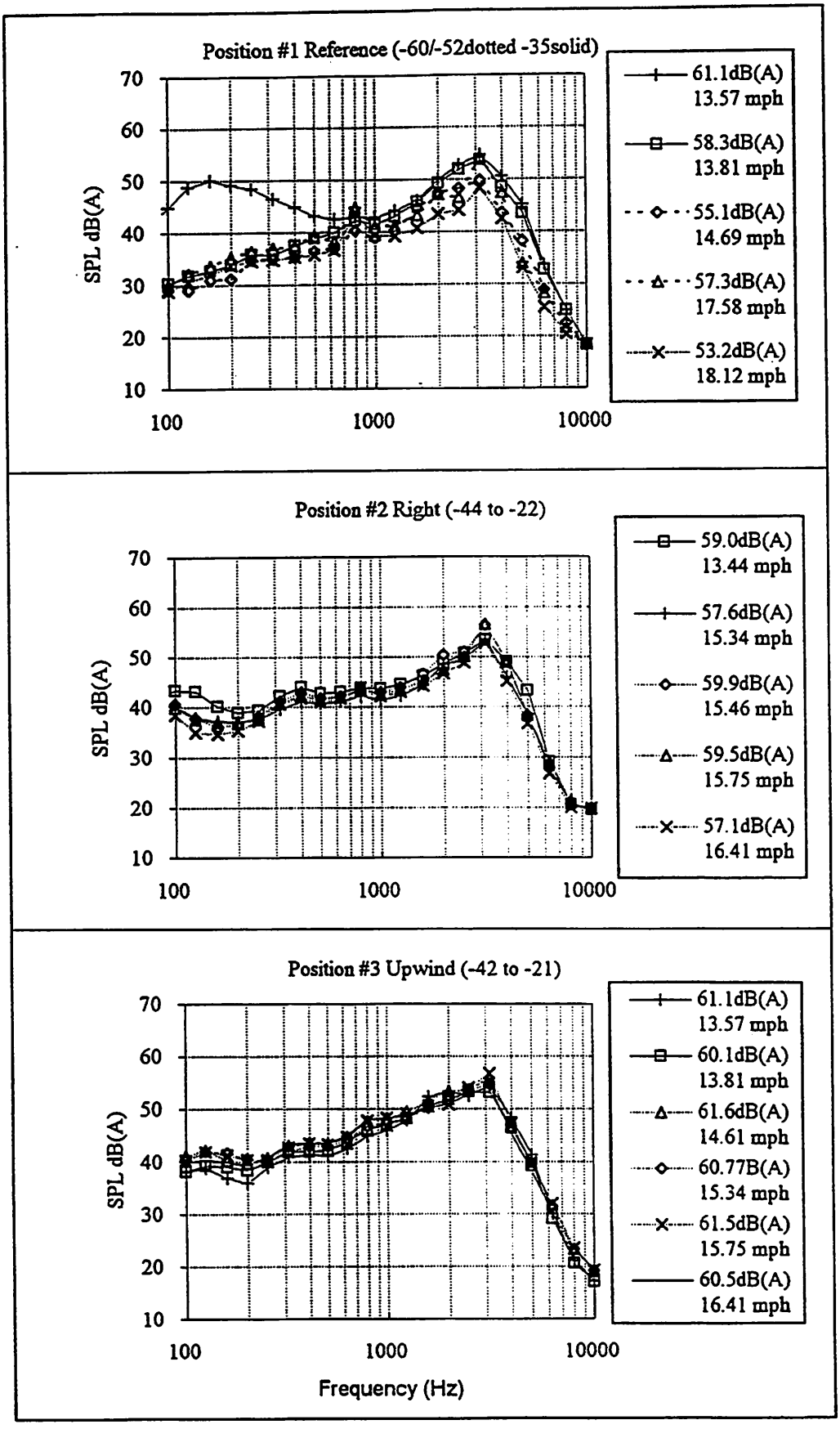

Figure 1 Zero Yaw Angle - Raw 1/3 Octave Spectra for 3 Microphone Locations

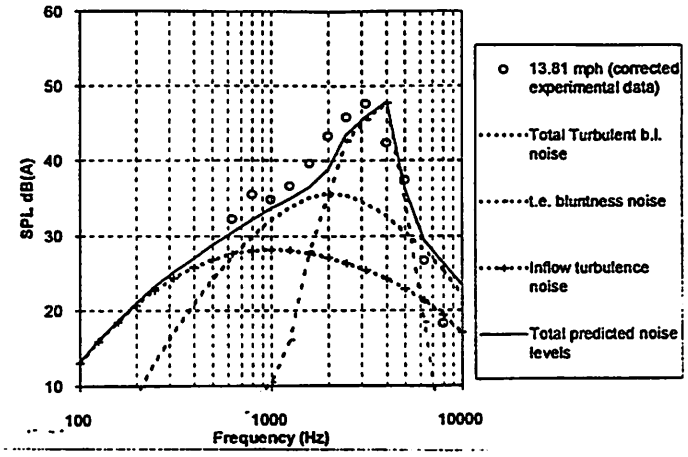

Figure 2 Comparison at zero degrees yaw

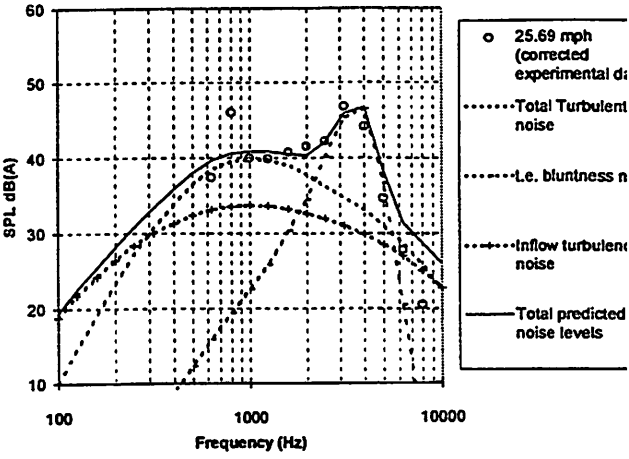

Figure 3 Comparison at 30 degrees yaw

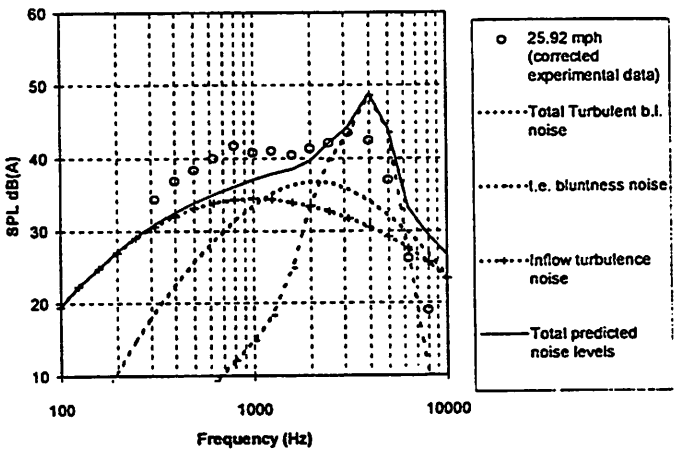

Figure 4 Comparison at 60 degrees yaw

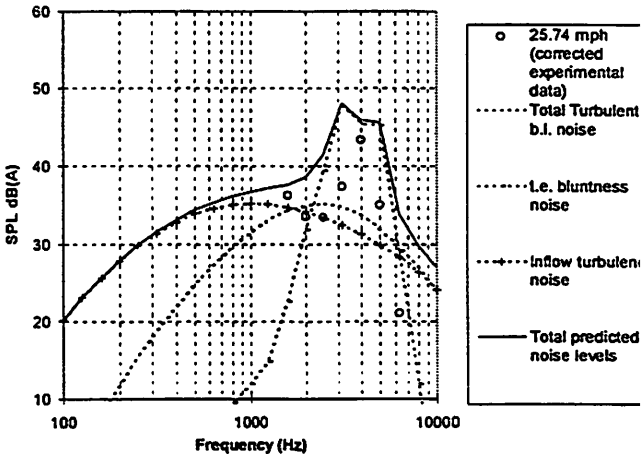

Figure 5 Comparison at 90 degrees yaw

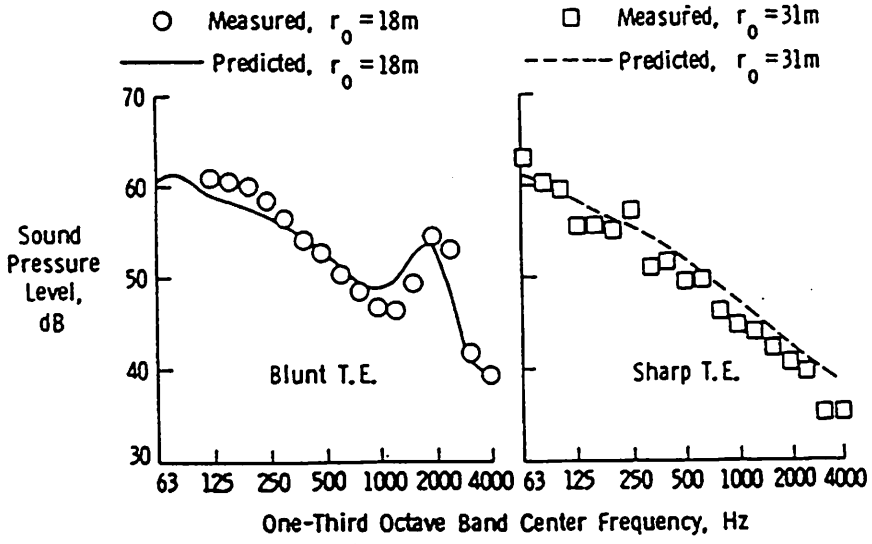

Figure 6 Measured and Predicted Noise Spectra for the US Windpower (USWP 56-50) for Blunt and Sharp Trailing Edges [Grosveld, 1985.]

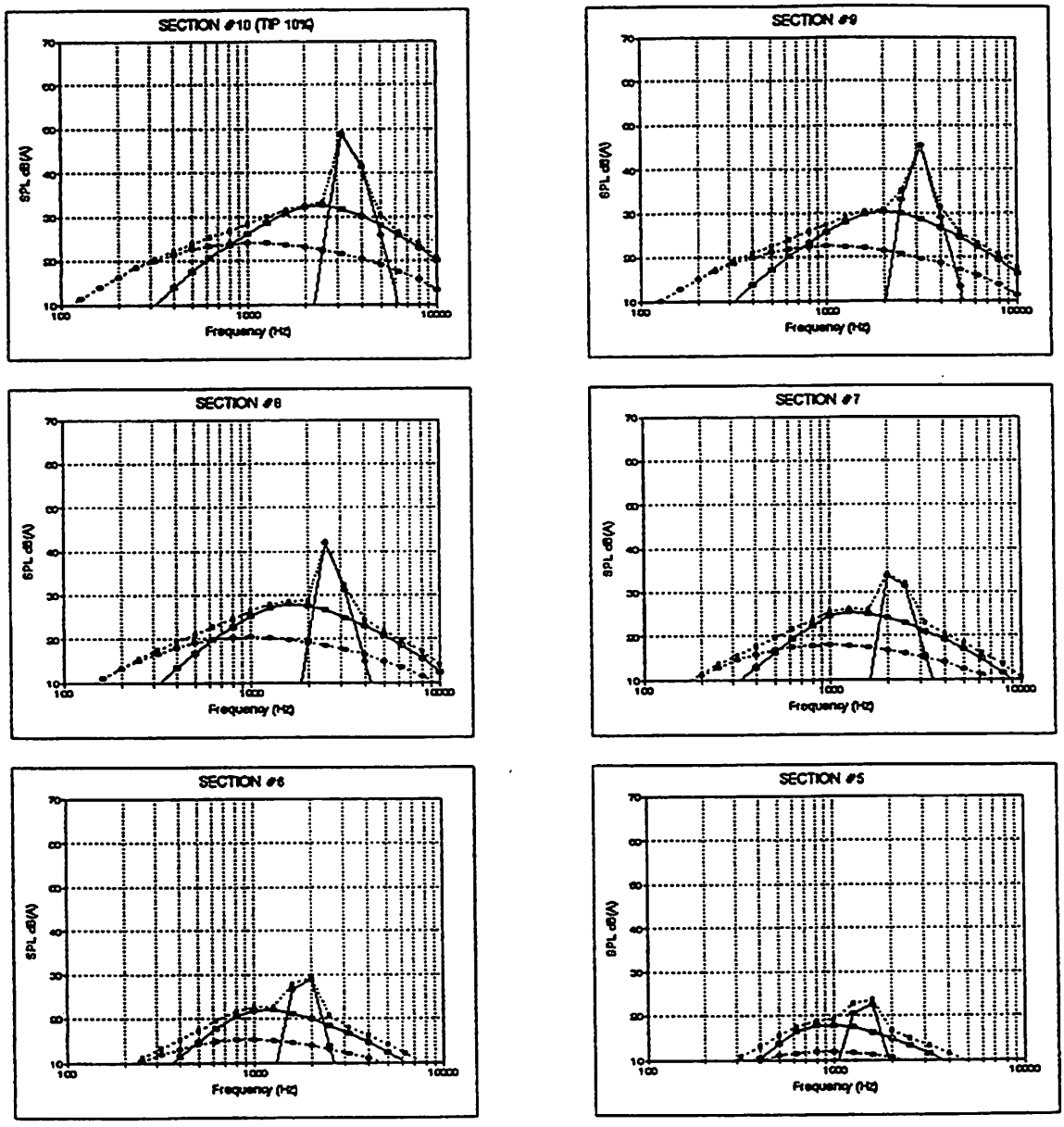

Figure 7 Contribution of Individual Blade Sections to the Overall Noise from a Wind Turbine.

NOISE ASPECTS AT AERODYNAMIC BLADE OPTIMISATION PROJECTS

J.G. Schepers
Netherlands Energy Research Foundation
P.O. Box 1, 1755 ZG Petten
Tel: +31 0224 564233
Fax: +31 0224 563214
e-mail: schepers@ecn.nl

1 Introduction

The Netherlands Energy Research Foundation, ECN, has often been involved in industrial projects, in which blade geometries are created automaticly by means of numerical optimisation, see for example [1] and [2]. Usually these projects aim at the determination of the aerodynamic optimal wind turbine blade, i.e. the goal is to design a blade which is optimal with regard to energy yield. In other cases, blades have been designed which are optimal with regard to cost of generated energy. However, it is obvious that the wind turbine blade designs which result from these optimisations, are not necessarily optimal with regard to noise emission.

This paper shows an example of an aerodynamic blade optimisation, using the ECN-program PVOPT. PVOPT calculates the optimal wind turbine blade geometry such that the maximum energy yield is obtained. Using the aerodynamic optimal blade design as a basis, the possibilities of noise reduction are investigated.

The development of PVOPT (and its successor BLADOPT) is made possible by financial support from the Dutch Organisation for Environment and Energy, NOVEM.

2 The program PVOPT

The program PVOPT (version 1.5, [3]), determines the optimal chord and twist distribution along a rotor blade of a stall or pitch regulated, constant speed turbine, such that the maximum energy yield is obtained. In PVOPT the twist is defined relative to the tip (tip twist is zero by definition), positive when it decreases the angle of attack. The angle between the tip chord and the rotor plane is called the tip angle, see figure 1.

Rotor diameter, rotor speed and aerodynamic profile coefficients should (still) be prescribed and are not optimised. In addition, the rated power should be specified. Then the energy yield is calculated under the condition that this rated power may not be exceeded.

The aerodynamic power curve is calculated by means of the blade element momentum theory, for axisymmetric, stationary conditions. The wind climate should be prescribed by a Weibull distribution through $\overline{V_{year}}$ and the k factor. Hence from the power curve and the wind speed distribution, the aerodynamic energy yield is known.

A very simple optimisation algorithm is implemented. Thereto the chords and twist angles along the blade are changed independently (with constant steps), until the optimal values are found.

The PVOPT program originates from a preliminary version which was developed by ECN for a SUN Workstation. At present the program is further developed within the BLADOPT project. This project is funded by NOVEM, the Dutch Organisation for Environment and Energy. Within the BLADOPT project, the following tasks are performed:

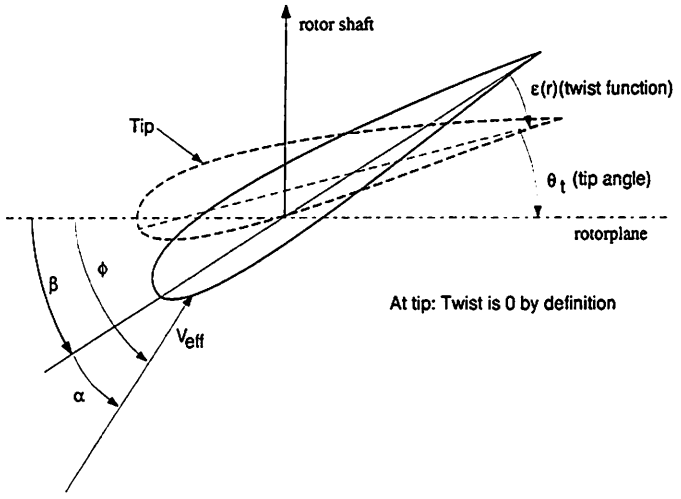

Figure 1: Twist and tip angle

1. Modification of the program such that it can operate on PC's working under WINDOWS 3.1, Windows NT or Windows 95. Furthermore a graphical user interface is added;
2. Reporting and installation of an on-line, context sensitive user's manual, [4];
3. Addition of the possibility to impose constraints on the design variables;
4. Implementation of a drive train efficiency model;
5. Addition of the possibility to optimise the diameter and rotor speed automaticly;
6. Addition of the possibility to optimise the chords and twist as function of radius by means of specified functions (for example polynomials), instead of an optimisation at discrete positions;
7. Implementation of a more efficient optimisation algorithm;
8. Implementation of a cost function;
9. Implementation of a noise algorithm.

The BLADOPT project is still running. At the time of writing this paper, the tasks 1 to 3 have been completed.
Note that after completion of the project the name of PVOPT will change to BLADOPT.

3 Optimisation Example

The optimisation example which is shown in the present paper refers to the optimisation of a hypothetical wind turbine blade. The characteristics of the turbine, for which the blade is optimised, are:

- 3 Bladed;

- Stall regulated;
- Rotor diameter = 46 m;
- Aerodynamic root at 5.4 m (21% blade span);
- Rated power = 650 kW (aerodynamic).

The blade is optimised for a wind climate with an annual average wind speed of 7 m/s. The chords and twists are optimised at 5 radial positions [r=5.4 m (aerodynamic root); r=9.37 m (r/R $\approx$ 40%); r=14 m (r/R $\approx$ 60%); r=18.75 m (r/R $\approx$ 80%); and r=23 m (r/R = 100%)]. The twist at the root is constrained to 17.5 degrees (due to start torque considerations).

3.1 Results

Figure 2 shows a (black and white) screendump of the optimisation with PVOPT. The upper panes show the chord (m) and the twist (deg) as function of radius (m). The lower panes show the energy yield (Wh) as function of iteration. The power curve is also presented. An important property for the noise production is the tip angle, which is shown at the bottom of the screen. The 'initial' values on the screen refer to the start values, where the 'current' values refer to the optimised values.

It can be observed that (starting from the arbitrary begin geometry), PVOPT increases the energy yield with $\approx$ 8% (from 1.50 GWh to 1.625 GWh). The tip angle is -3.9 degrees.

Note that the discontinuous behaviour in twists and chord distribution is a result of the optimisation at a discrete number of positions. Although it is possible to smooth the twist and chord distribution, this is not performed for the present study.

3.2 Noise reduction

The optimal configuration, presented in figure 2, is now used as a basis to derive configurations with a lower noise level. However at the same time, the loss in energy yield should remain limited. To this end a sensitivity study is conducted by applying modifications to the optimal design. Note that version 1.5 of PVOPT is not yet able to calculate the noise level from the turbine. Therefore it is only possible to make qualitative assumptions on the noise effects from the suggested modifications.

In the present study it is attempted to reduce the noise level by means of two design parameters:

- Rotor speed: A lower rotor speed leads to a reduced tip speed, which decreases the noise level;
- Tip angle. A higher tip angle generally decreases the strength of the tip vortex, which reduces the noise level. Measurements indicate as a rule of thumb that a 1 degree increase in tip angle leads to a 1dB(A) noise reduction, [5]. However, it is emphasised that these measurements are performed on blades which remain unchanged. If the tip angle is changed in an optimisation, due to a modification in blade geometry, the rule of thumb is not necessarily valid.

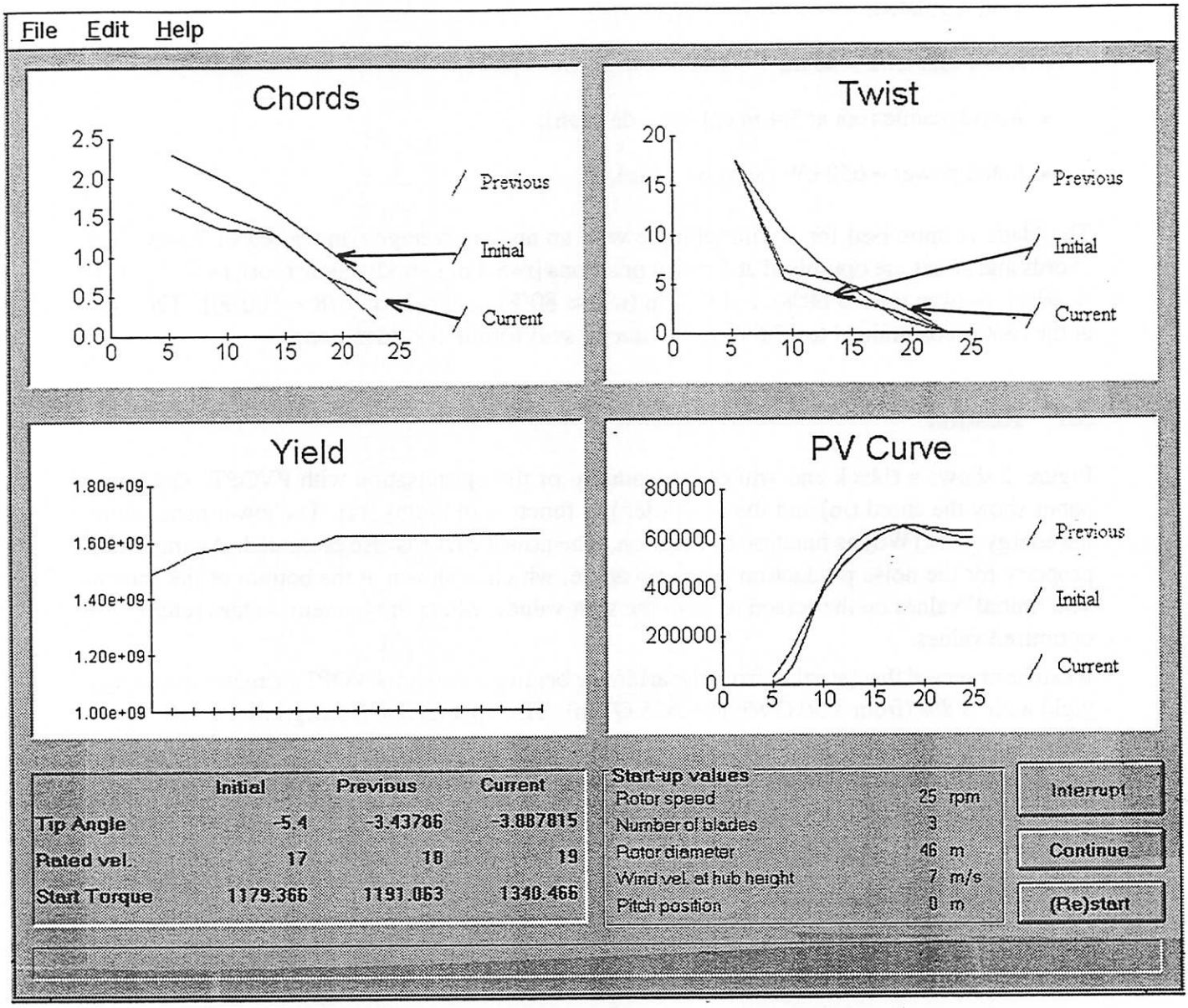

Figure 2: Optimisation: (Root twist constrained to 17.5 degrees)

3.2.1 Variation of rotor speed

In version 1.5 of PVOPT it is not yet possible to optimise the rotorspeed automaticly. However an optimisation 'by hand' indicates that the optimal rotor speed for the present configuration was in the order of 22 rpm, hence lower than the prescribed value of 25 rpm. This is shown in figure 3. This figure shows the optimisation at 22 rpm (starting from the same begin geometry as figure 2). The optimal energy yield at 22 rpm is 1.6675 GWh which is about 2.5% higher than the optimal energy yield at 25 rpm. Although this optimisation indicates that a lower rotor speed would be very advantageous, it should be noted that the rotor speed often has to be constrained to a minimum value due to costs of the drive train. In the present hypothetical example, the minimum rotor speed is assumed to be 25 rpm. Therefore the following examples are again performed at 25 rpm.

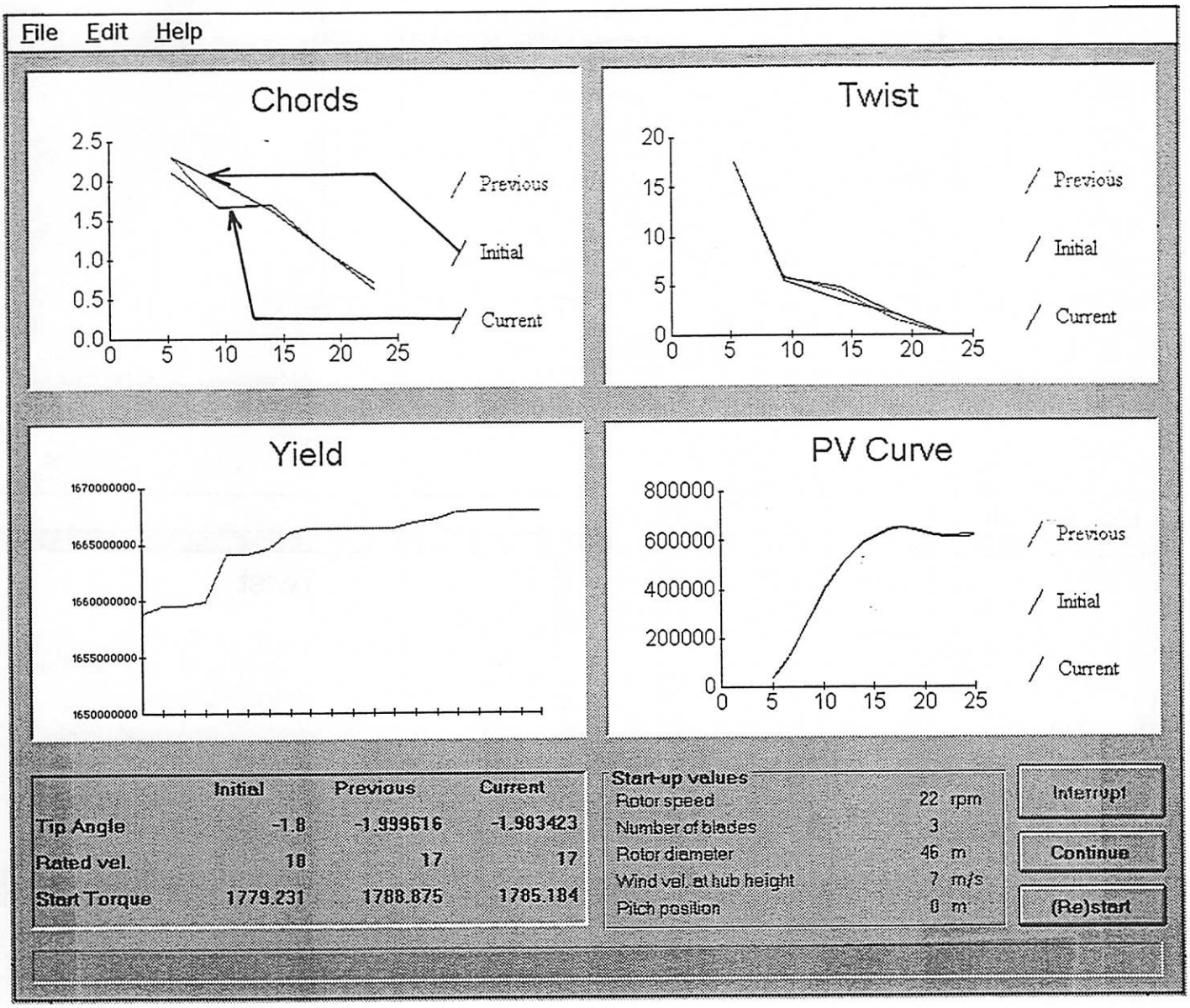

Figure 3: Optimisation at $\Omega = 22$ rpm (Root twist constrained to 17.5 degrees)

3.2.2 Variation of tip angle

Three possible strategies have been attempted which aimed at an increase of the tip angle.

1. Application of low lift profiles: A lower lift reduces the peak power level and hence the tip angle can be reduced. The sensitivity of the tip angle to the maximum lift coefficient is investigated by modifying the $c_l - \alpha$ curve. Thereto the maximum lift coefficient is decreased with 0.1. The resulting curve is presented in figure 4. It is emphasised that this $c_l - \alpha$ curve is artificial and it is only intended to investigate the sensitivity of the optimal configuration to c_l.

   The results of the optimisation with low lift profiles are shown in figure 5.

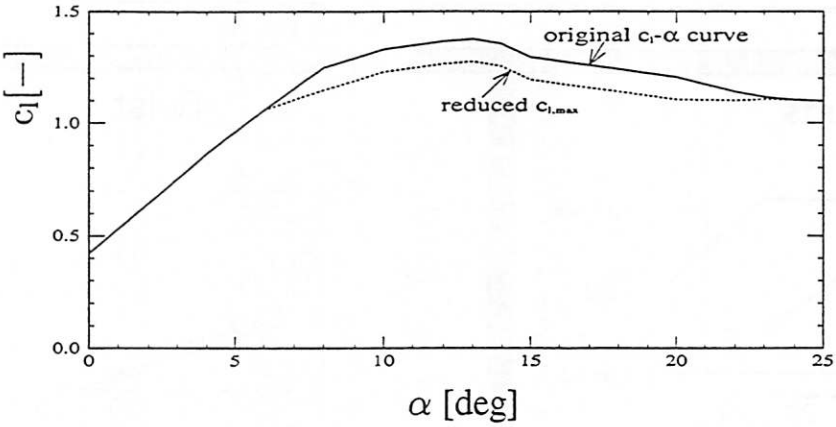

Figure 4: Artificial low lift behaviour

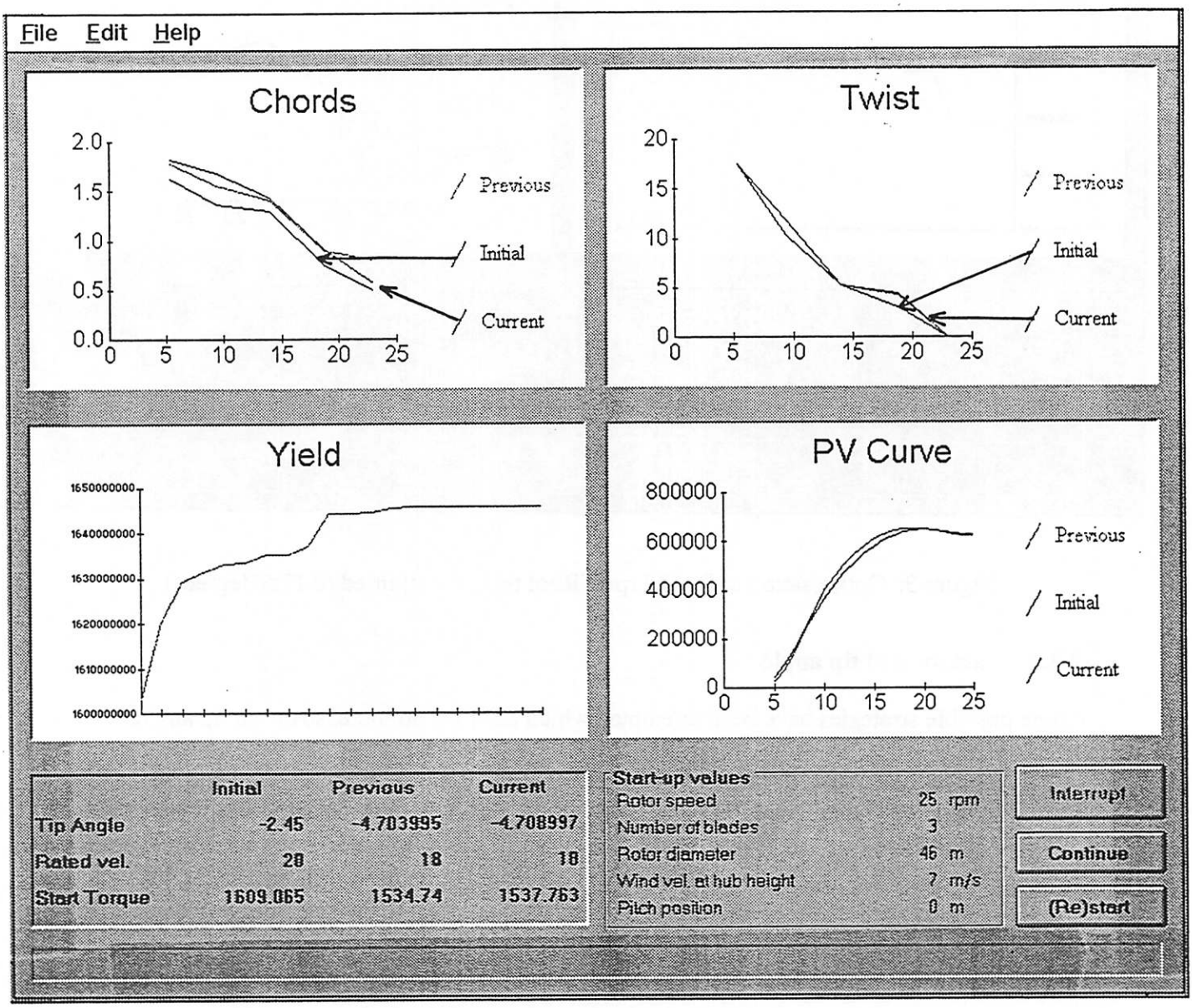

Figure 5: Optimisation: Reduced lift coefficients (Root twist constrained to 17.5 degrees)

The start geometry in this figure, is the optimised geometry which results from the optimisation with the original profiles, see figure 2. For this geometry, the initial values in figure 5 show an energy yield of 1.605 GWh and a tip angle of -2.45 degrees. When these results are compared with the values for the original profiles in figure 2, it can be concluded that by applying lower lift profiles on the geometry which is obtained after the optimisation with the original profiles, a 1.4 degrees increase in tip angle is possible. The loss in energy yield is which is associated to this tip angle increase, is 1.5 %.

Figure 5 shows that the optimal geometry with low lift profiles has a larger solidity than the optimal geometry with the original aerodynamic profiles. The energy yield is 1.645 GWh which is 1.5% higher than the yield from the original profiles. However, the tip angle decreases to -4.7 degrees. Note that the improved energy yield from a lower $c_{l,max}$ is not a generally valid result. At ECN it was found that for other cases, the energy yield can be decreased from a lower lift.

2. A second possibility to increase the tip angle, is a reduction of the chords. This results in an increased design tip speed ratio, i.e. the tip speed ratio where the power coefficient is maximum. As a rule of thumb, the design tip speed ratio is inversely proportional to the solidity, see for example [1]. The increased design tip speed ratio yields a larger inflow angle ϕ (see figure 1), from which the tip angle can be increased. The figures 6 to 8 show that for the present example the chords at r = 14 m, r=18.75 m and r = 23 m are constrained. The chords at the inboard stations remained unchanged. The optimisation is presented in figure 9. In this figure the start geometry is the optimised (unconstrained) geometry from figure 2. It can be seen that the energy yield is decreased considerably (approximately 4%). Although the tip angle is increased with 1 degree, it must be noted that the angle of attack at the tip (V=7m/s) changes only from 6.79 degrees to 6.75 degrees. Hence a reduction in strength of tip vortex is only possible from the reduced chords and not from the angle of attack.

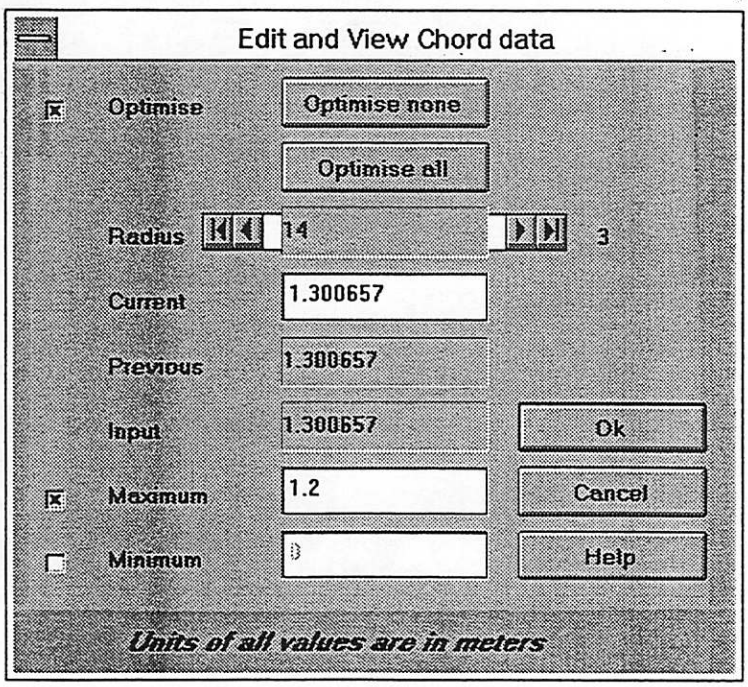

Figure 6: Maximum value of chord at r = 14 m

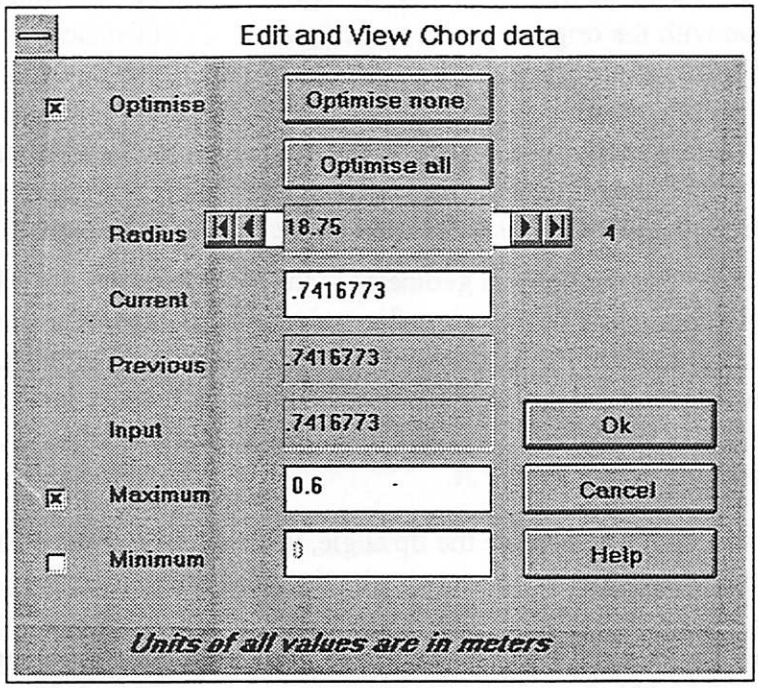

Figure 7: Maximum value of chord at r = 18.75 m

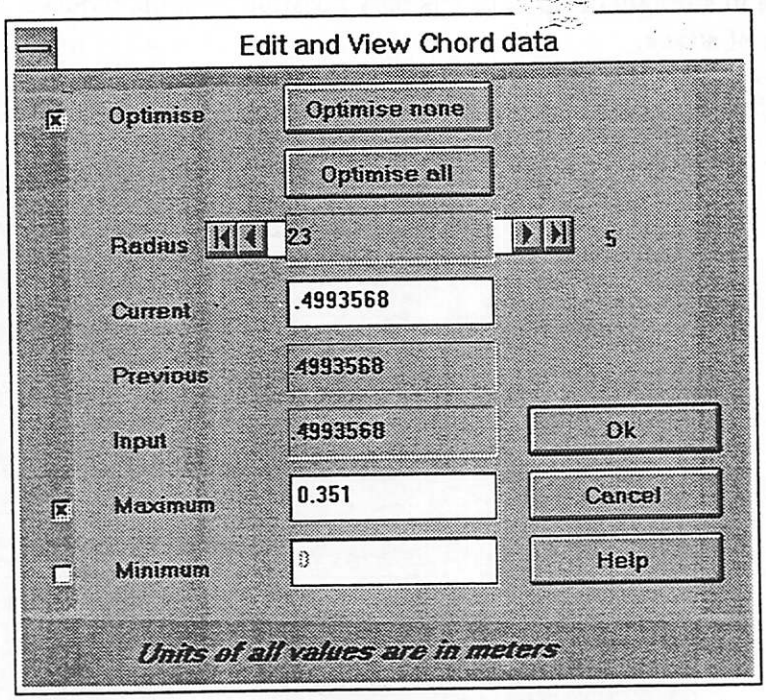

Figure 8: Maximum value of chord at r = 23 m

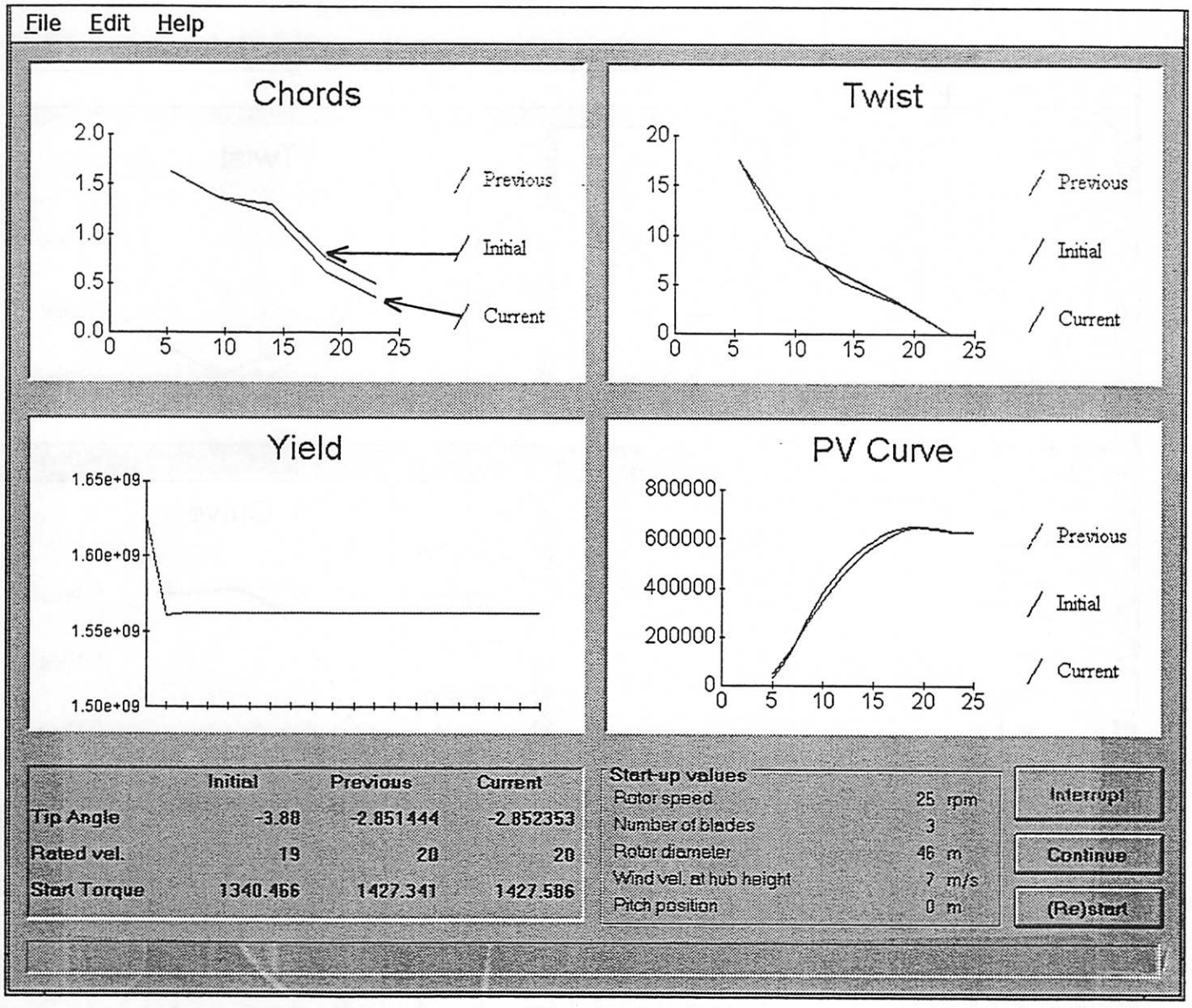

Figure 9: Optimisation: Chords constrained

3. A third possibility to increase the tip angle is the reduction of the twist at the outboard stations. This tends to increase the angle of attack which can be compensated by an increased tip angle. In order to investigate this, the twist at r=18.75 is constrained to 0 degrees, see figure 11 (note that the twist at the tip is zero by definition). The result is shown in figure 10. In this figure, the start geometry is the optimised (unconstrained) geometry from figure 2. It can be observed that the tip angle is increased with 1.3 degrees. The loss in energy yield is negligible: Although there is a (small) initial loss in energy yield, this is almost completely recovered after the optimisation.

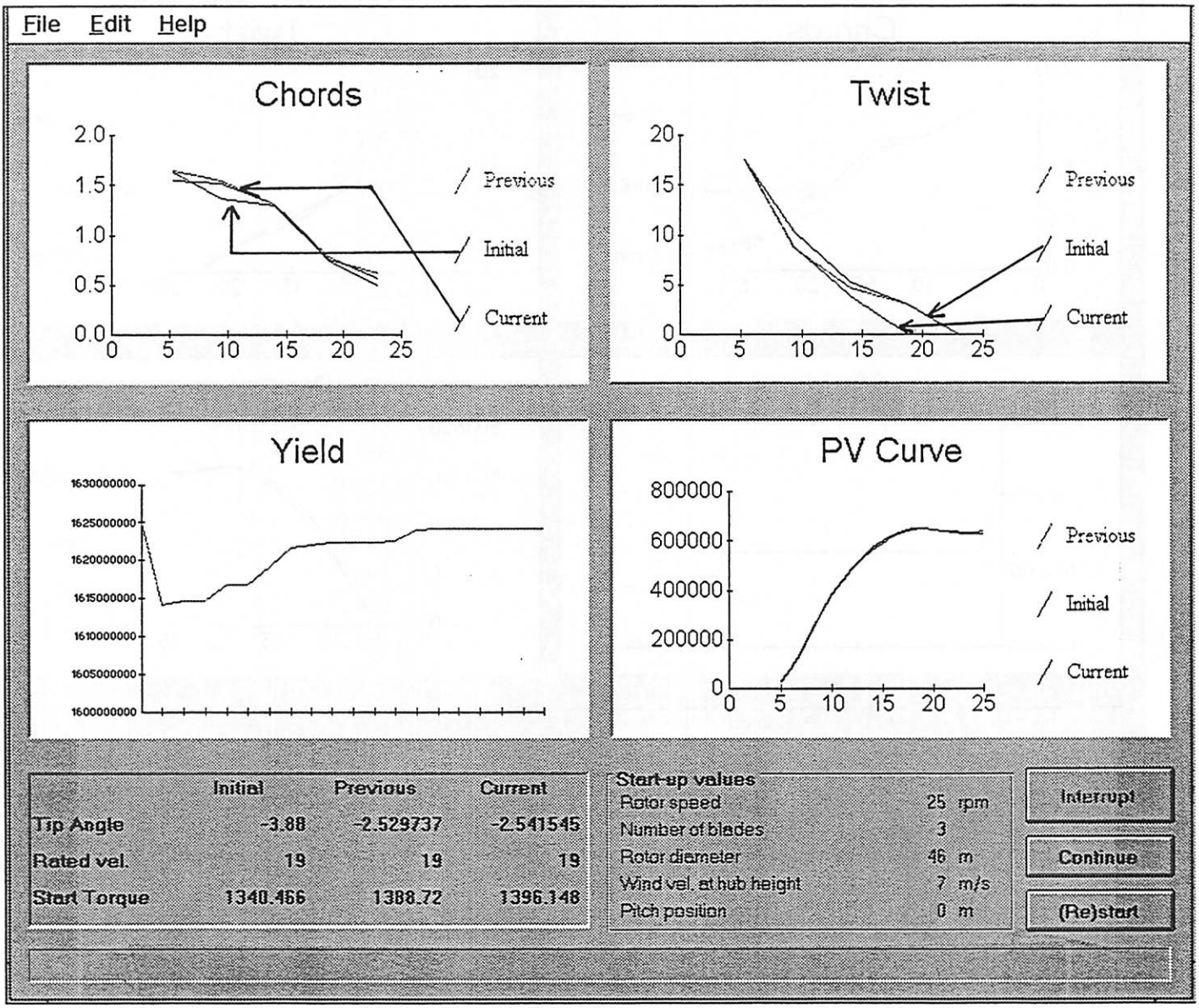

Figure 10: Optimisation: Twist constrained

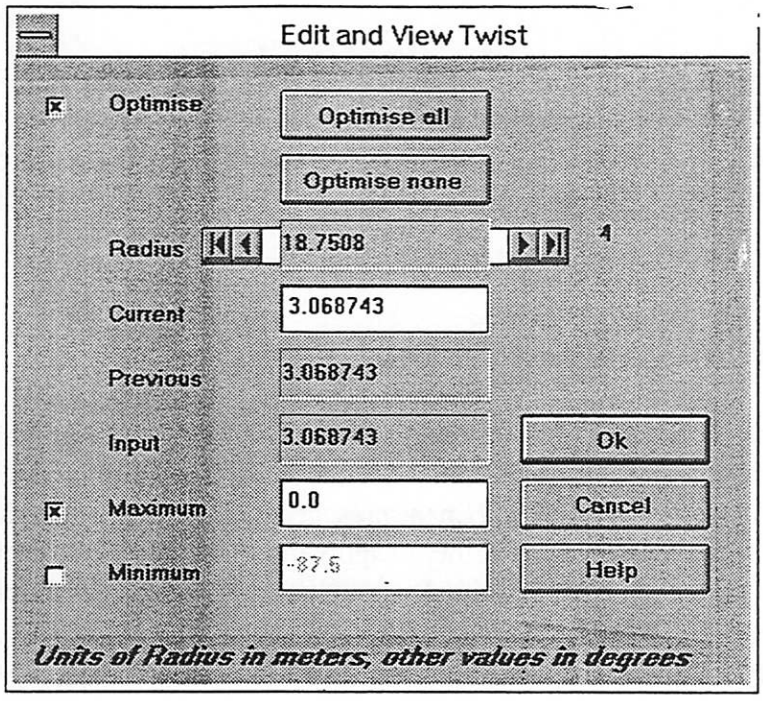

Figure 11: Maximum value of twist at r = 18.75 m

4 Future developments

In section 2, the improvements are listed which are at present implemented within the BLADOPT project. One of the improvements, is the addition of a noise model. This is a very important addition, since this makes it possible to confirm and quantify the noise reduction, which are expected from the modifications, suggested in the previous sections.

The noise prediction model which will be implemented in BLADOPT, is the SILANT program [6]. This program is developed within a NOVEM project by Stork Product Engineeering (SPE), the Dutch National Aerospace Laboratory (NLR) and the Netherlands Organisation for Applied Scientific Research (TNO). It calculates the inflow and trailing noise. No model is available for the tip noise.

In an optimisation procedure there are two different ways for the inclusion of noise level results:

1. The noise level can be included as a constraint;
2. The noise level can be included in the objective function (The function to be optimised).

In BLADOPT the objective function will be the cost of generated energy. If the second option is selected, this implies that a relation between costs and noise should be available. Due to the fact that such a relation will probably be rather arbitrary, a general optimisation may be difficult.

It is not known yet how the inaccuracy which results from the missing tip noise model will effect the optimisation results. It must be noted that in optimisations, the requirements on the accuracy of the noise calculation may be less strict than for most other applications: For optimisations, it is mainly the relative differences in noise level between various configuration which should be predicted well. It may be that even without a tip noise model, the relative differences are predicted sufficiently accurate.

However if the noise level is treated as a constraint, an accurate prediction of the absolute value is required, since it is not allowed that the resulting design exceeds a specified, absolute value, of the noise level. At present, ECN considers the addition of the tip noise model from [7] to BLADOPT, similar to the tip noise model which is applied by RISØ in their optimisation design tool, [8].

5 Conclusions

The aerodynamic optimised geometry from PVOPT is the 'real' optimum (up to the latest decimal). The most important conclusion from this study is, that it is worthwhile to investigate the behaviour of the objective function (in the present case the energy yield) around the optimum: If the optimum is flat, there is a possibility to apply modifications to the optimum configuration with only a limited loss in energy yield. It is obvious that the modified configurations emits a different (and possibly lower) noise level.

In the BLADOPT program (the successor of PVOPT) it will be possible to quantify the noise level and hence to assess the reduced noise emission more thoroughly. At present the most promising approaches for noise reduction are believed to be a reduction of the rotor speed (if at all possible), and a reduction of the tip angle by means of low lift profiles, or decreased twist at the outboard stations. These modifications were possible without a significant loss in energy yield.

References

[1] J.G. Schepers and H. Snel. "Aerodynamic redesign NedWind 40 rotor (in Dutch) ". ECN-C –95-055, Netherlands Energy Research Foundation, ECN, August 1994.

[2] B.H. Hendriks J.G. Schepers T.G. van Engelen A.J. Stern and G.K. Boerstra. "Aeroelastically Optimised Cost Efficient Wind Turbine ". In *Proceedings of the EUWEC 1996 Conference held at Gotheborg*, pages 116–119, May 1996.

[3] J.G. Schepers. "PVOPT, Theory and test cases, " ECN-C–96-057, January 1996.

[4] Seignette P.F.A.B. "On-line PVOPT user's manual, version 1.2 " Netherlands Energy Research Foundation, ECN, March 1996.

[5] N.J.C.M van der Borg and P.W. Vink. "Acoustic Noise Measurements on Wind Turbines Performed in the frame of JOU2-CT92-0233 ". ECN-C –95-112, Netherlands Energy Research Foundation, ECN, November 1995.

[6] "User's documents SILANT (in Dutch) ". SPE- report, Stork Product Engineering, SPE, December 1996.

[7] T.F. Brooks and M.A. Marcolini. "Airfoil Tip Vortex Formation Noise". *AIAA Journal*, 24(2):246–252, 1986.

[8] P. Fuglsang and H.A. Madsen. "Implementation and Verification of an Aeroacoustic Noise Prediction Model for Wind Turbines ". RISØ R-867(EN), RISØ, National Laboratory, March 1996.

Application of aeroacoustic models to design of wind turbine rotors

Peter Fuglsang Helge A. Madsen
Wind Energy and Atmospheric Physics Dept.
Risø National Laboratory
P.O. Box 49
DK-4000 Roskilde, Denmark
e-mail: peter.fuglsang@risoe.dk

Abstract

A design method is presented for wind turbine rotors. The design process is split into overall design of the rotor and detailed design of the blade tip. A numerical optimization tool is used together with a semi-empirical noise prediction code for overall rotor design. The noise prediction code is validated with measurements and good agreement is obtained both on the total noise emission and on the sensitivity to wind speed, tip pitch angle and tip speed. A design study for minimum noise emission for a 300 kW rotor shows that the total sound power level can be reduced by 3 dB(A) without loss in energy production and the energy production can be increased by 2% without increase in the total noise. Detailed CFD calculations are subsequently done to resolve the blade tip flow. The characteristics of the general flow and the tip vortex are found, and the relevant parameters for the aeroacoustic models are derived for a sharp rectangular tip.

1 Introduction

The radiation of noise is an important issue at the erection of wind turbines near residential areas. Although noise radiation from a wind turbine is not large by ordinary standards, it can still be of significance compared to the low background levels that exist in much of the countryside. The radiation of noise is a sales parameter and much effort is going into the design of a new generation of efficient, less noisy wind turbines. There is a need for accurate prediction of the radiated noise and a need for design tools, that incorporate noise considerations directly into the design process.

The noise is divided into two principal sources: Mechanical noise and aerodynamic noise. Aerodynamic noise is further divided into airfoil self noise and turbulent inflow noise. Whereas mechanical noise is well understood, the understanding of aerodynamic noise is still limited. Several semi-empirical models for noise prediction are available, Grosveld (1985), Brooks et al. (1989) and Lowson (1993,1994), based on work by Ffowcs Williams et al. (1970) and Amiet (1975). The models have only included the overall parameters of the rotor blade shape. A model including a detailed description of the airfoil sections was not yet established.

A large effort has recently gone into further development of the understanding of noise sources and the modelling of the noise. Both experimental and theoretical investigations are carried out under the JOULE II and JOULE III research programs, Wagner et al. (1996). However, except for rules of thump the incorporation of noise considerations directly in the design process has received less interest.

The subject of the present work is to develop a method for design of rotors for wind turbines with noise considerations, based on state of the art semi-empirical noise prediction, rotor optimization and computational fluids dynamics (CFD) calculations for detailed flow analysis of the tip flow. Even though the semi-empirical noise prediction models are still at an early stage we found that they can be effectively used together with rotor shape optimization to trade off energy production and total noise emission. Furthermore we found that CFD is well suited to understand the complex tip flow.

2 Method

The design method is divided into two stages:

1. Overall design of the rotor by use of the optimization tool for rotor design, "ROTOR", Fuglsang et al. (1995, 1996). Noise considerations are introduced by use of a semi-empirical noise prediction model. We apply the Brooks et al. (1989) model for airfoil self noise, extended for wind turbine use. Noise from turbulent inflow is included following Lowson (1993, 1994).
2. Detail design of the blade tips by CFD calculations of the tip near flow, to determine the tip aerodynamic parameters used for prediction of tip noise. The commercial CFD-code, 'FIDAP' is used and results are compared to measurements used by George et al. (1984) and Brooks et al. (1986).

2.1 Rotor design optimization method

Figure 1 illustrates the design process with the numerical optimization tool, Fuglsang et al. (1996).

A mathematical optimization algorithm is used together with calculation models for the rotor aerodynamics, blade structure, extreme/fatigue loads, manufacturing costs and aerodynamic noise. The calculation models are those that are normally used at rotor design and include aeroelastic time simulations of

the unsteady wind field acting on the wind turbine structure.

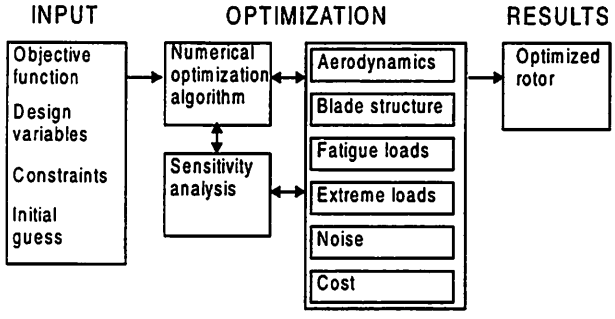

Figure 1 Use of the numerical optimization algorithm with calculation sub models.

The designer specifies an initial guess on a rotor design and the objective function, which is the aim of the optimization. This could be maximum energy production, minimum noise radiation or minimum cost of energy. In addition, a number of design variables are specified. The design variables are the rotor shape, such as chord, twist and the operational conditions, such as tip pitch and tip speed. Finally constraints are added. The constraints bound the possible solution into a feasible region. Constraints can be applied to loads, generator power, blade strains, noise and so on.

The optimization algorithm finds an optimum design in a systematic and automatic way by use of the different calculation models. In this process, the design variables are changed within the bounds from the constraints to yield a minimum of the objective function. After the optimization, the designer performs calculations on the result. Eventually adjusting the result or defining a new optimization problem.

The most significant advantages by use of systematic optimization instead of the "manual" changes by the designer are, that a large number of parameters (design variables) can be varied simultaneously. Furthermore, an unlimited number of constraints are automatically being fulfilled by the optimization algorithm. For a given problem set-up, the optimum solution is automatically found.

2.2 Blade tip design method

After the optimization of the rotor, the detailed design of the blade tip is left to the designer. The lifting line analysis that is used for rotor design is insensitive to different tip shapes, since it does not resolve the flow field near the tip, but only the far field. It is therefore necessary to do experiments or additional CFD calculations to resolve the tip flow and subsequently to design the tip from requirements to power production and tip noise using the following approach:

1. Blade design by rotor optimization
2. Detailed tip flow analysis with CFD
3. Determination of the aerodynamic characteristics for noise prediction
4. Shaping of the tip region with considerations on power and noise
5. Eventual wind tunnel or full scale experiments

3 Aeroacoustic model

The aeroacoustic model is limited to the rotor aerodynamic noise, since this is the object of interest. Therefore, noise contributions from tower shadow, tower and nacelle are not included. It is assumed that the noise radiation for any 2-d blade section on the wind turbine is identical to that for an equivalent airfoil section. Summation of the sound pressure from a number of blade elements leads to the total sound power level radiated from the rotor.

3.1 Airfoil self noise sources

Airfoil self noise is due to the interaction between the airfoil and the flow. The interaction produces turbulence in the airfoil boundary layer and near wake. Noise is especially radiated at the interaction of the flow with the trailing edge. Airfoil self noise is mainly broadband.

Brooks et al. (1989) divide the total noise into the following different noise sources:

- Turbulent boundary layer trailing edge noise
- Separation noise
- Tip vortex formation noise
- Laminar boundary layer vortex shedding
- Trailing edge bluntness vortex shedding noise

Brooks et al. establish scaling laws, partially based on the fundamentals work of Ffowcs Williams (1970), for the different noise sources. The scaling law prediction equations are fitted to measured noise spectra for the NACA 0012 airfoil. In addition, the airfoil boundary layer velocity profiles are measured and boundary layer parameters are determined as function of angle of attack and Reynolds number. In this way, the sound pressure level can be is estimated by simple knowledge of the airfoil gross flow.

A considerable part of the experimental data relates to low Reynolds numbers and low incidence. Furthermore, the majority of the data used, refer to boundary layer cases where the flow is tripped. The calibration with the scaling parameters should therefore be looked upon with caution, especially at high incidence and high Reynolds numbers, which are typical for wind turbine use.

For the present study we decided to include only turbulent boundary layer trailing edge noise, separation noise and tip noise, since we believe, that the remaining noise sources can be avoided by proper design and high blade manufacturing quality.

3.2 Turbulent inflow noise

Turbulence is a part of the natural wind environment. The passage of turbulence causes unsteady pressures on the blades, leading to radiation of noise. Since the wind has a wide range of natural wavelengths, the generated noise is broadband, except for low frequency harmonics of the rotational frequency from blade to blade

interaction. The mechanism for noise radiation from turbulent inflow for an entire rotor is complex and a universal theory has not yet been developed.

We used the model of Lowson (1993, 1994), based on Amiet (1975), for an airfoil section under turbulent inflow. The turbulence spectrum shape is constructed from an approximate formula for a Sears function. The blade is divided into blade sections and the sound power level is calculated for a low- and a high-frequency regime.

3.3 Coupling to aerodynamic calculation code

The semi-empirical noise prediction model is interfaced with the aerodynamic code in "Rotor", Fuglsang et al. 1996. The aerodynamic calculation is based on standard blade element/momentum theory, including wind shear and yawed flow. The total noise is calculated by dividing the blades into blade elements. The aerodynamics for each blade element is found and the total sound pressure level is summed from the different noise sources. The tip noise contribution is only calculated for the tip blade segment.

In total, the necessary aerodynamic parameters for each blade section are:

- The angle of attack for the oncoming flow
- The free stream velocity for the oncoming flow
- The section chord
- The section spanwise length
- The retarded distance to the observer
- The directivity angles

In addition the following overall parameters are needed:

- A representative geometric angle of attack for the tip noise calculation.
- The shape of the rectangular tip, rounded/ sharp
- The leading edge flow condition, tripped/ untripped
- Viscosity of air
- Density of air
- The length scale of the oncoming turbulence
- The oncoming turbulence intensity

To find the total noise emission from the entire rotor, the noise from one blade is calculated at different azimuth angles and an average sound power level is found by taking into account the actual number of blades.

The total sound pressure level from a blade section is related to an observer position by taking into account the directivity together with the coordinate transformation from the blade segment to the observer, Figure 2.

The total sound power level experienced by the observer is then transformed into an equivalent sound power level, L_W, from a single source at hub height:

$$L_W = (L_P)_{TOTAL,c} - 6 + 10\log\left(\frac{4\pi R^2}{S_0}\right) \qquad (1)$$

Where $(L_P)_{TOTAL,c}$ is the total sound pressure level corrected for background noise, -6 dB(A) is a correction for reflection from the reflection of the hard board, R is the distance from the measurement observer point to the rotor centre and $S_o = 1$ m^2 is a reference area.

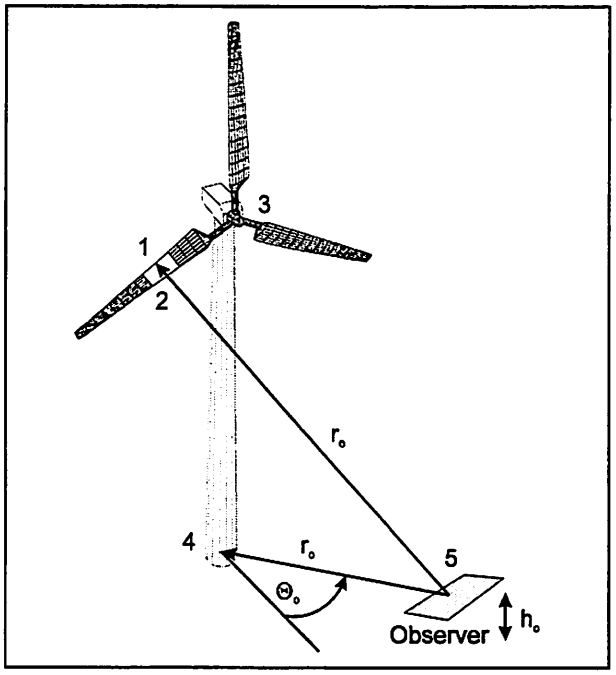

Figure 2 The relation between a blade segment and the observer.

3.4 Tip flow aerodynamics

The calculation of tip flow noise requires detailed knowledge of the tip flow. George et al. (1984) and Brooks et al. (1986) describe the flow by the spanwise extension of the tip vortex, l, and the maximum velocity in the vicinity of the tip vortex, U_{max}.

George et al. (1984) propose the following for l and U_{max}:

$$\begin{aligned} \frac{l}{c} &= 0.023 + 0.0089\alpha_{tip} \quad (Sharp) \\ \frac{l}{c} &= 0.074 + (\alpha_{tip} - 2) \quad (Round) \\ \frac{U_{max}}{U} &= 1 + 0.0359\alpha_{tip} \end{aligned} \qquad (2)$$

Where c is the airfoil chord and α_{tip} is the angle of attack at the tip.

Brooks et al. (1986) use almost identical expressions:

$$\begin{aligned} \frac{l}{c} &= 0.023 + 0.008\alpha_{tip} \\ \frac{U_{max}}{U} &= 1 + 0.036\alpha_{tip} \end{aligned} \qquad (3)$$

These expressions are however only valid for a rectangular tip with either round or sharp edge. More general shaping of the tip with tapering from the trailing and leading edges requires CFD calculations to estimate l and U_{max}.

4 Validation of aeroacoustic model

The predictions from the semi-empirical aeroacoustic model was compared to measurements. The total sound power level should be calculated within the uncertainty from measurements, around 1.5 - 2 dB(A). Furthermore the relative change in sound power level with wind speed, tip pitch angle and tip speed should be comparable to measurements.

We compared predictions to measurements for the Danish wind turbines, Vestas V27 225 kW and the Bonus Combi 300 kW. The measurements were performed by Jacobsen and Andersen (1993, 1995). The predictions were calculated with a turbulent length scale of 100 m, the observer position was 40 m downstream from the rotor on the ground level. Resulting pressure levels were converted to the equivalent sound power level by eq. (1).

4.1 Total sound power level

Figure 3 shows predictions and measurements for the Bonus Combi 300. Good overall agreement is found. The measurement reveal two tonal areas. A peak at 250 Hz, which Jacobsen et al. (1993) found to originate from machinery noise. There is a minor irregularity in the spectrum shape at 2000 Hz. This could be either due to tip noise or trailing edge bluntness noise. The dominating noise source at low and high frequencies is turbulent inflow noise, whereas airfoil self noise is dominant at intermediate frequencies from 400 Hz to 1600 Hz.

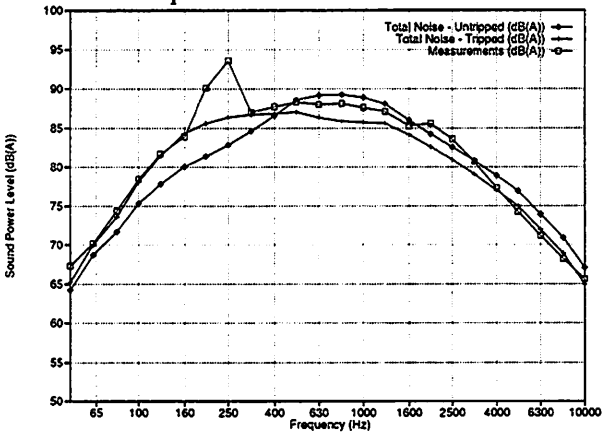

Figure 3 Total noise at V = 8 m/s for the Bonus Combi 300 with untripped/tripped boundary layer compared to measurements.

The difference between untripped and tripped flow is seen to shift the spectrum towards left for tripped flow. At low frequencies, the untripped prediction seems to fit best, whereas the tripped prediction is better suited at the higher frequencies. The total sound power level is found to 98.0 dB(A) for the untripped prediction and 97.1 dB(A) for the tripped prediction compared to 99.1 dB(A) for the measurements without the tonal contribution from machinery. Even better agreement on the spectrum shape could be obtained by including the turbulent trailing edge noise and fitting the turbulent inflow noise to the measurements, this was however not the purpose of the present work.

4.2 Model sensitivity analysis

We tested the variation of the predicted noise spectra from changes in the input parameters to investigate the sensitivity of the different noise sources.

The difference between tripped and untripped flow is a shift toward lower frequencies for the peak frequency as seen in Figure 3. The operational conditions for wind turbines are very different, and the design stage should therefore contain noise calculations at both tripped and untripped flow.

The predicted noise spectrum from turbulent inflow is very dependent on the chosen turbulence length scale and correct turbulence properties are crucial to the prediction of the total noise. The shape of the spectrum is nearly unaffected, but the sound power level is increased with higher length scales. The turbulence length scale is however complex to determine, since it depends on the specific site and the climate. At the design stage, the total noise should always be split into turbulent inflow noise and airfoil self noise, so that the airfoil self noise is not overseen because of too high noise from turbulent inflow.

The prediction of the sound pressure level is related to the distance between the observer and the radiating noise sources. When results from different measurements/ predictions are compared, the influence from the distance is accounted for by eq. (1). We found the variation of the equivalent sound power level with the observer distance to be less than 1 dB(A).

4.3 Design sensitivity analysis

The change of the predicted noise from changes in wind speed, tip pitch angle and tip speed is important to the rotor optimization results, since the noise emission and the power should be properly dependent on the design variables (rotor shape and regulation).

4.3.1 Wind speed variation

The noise was predicted at different wind speeds for the Bonus Combi 300. The variation of the noise spectrum is large for low frequencies, whereas higher frequencies are almost unaltered.

Figure 4 shows the predicted sound power level versus wind speed compared to measurements. The measurements are mainly from around 8 m/s and are less accurate at low and high wind speeds. The total sound power level is increased with wind speed. Despite the offset, there is good agreement at low wind speeds, whereas the prediction tend to bend off at higher wind speeds. The total predicted noise is divided into noise from turbulent inflow and airfoil self noise. It can be seen, that noise from turbulent inflow is dominating the total noise especially at low wind speeds, hence changes in the airfoil self noise will have only little effect on the total noise.

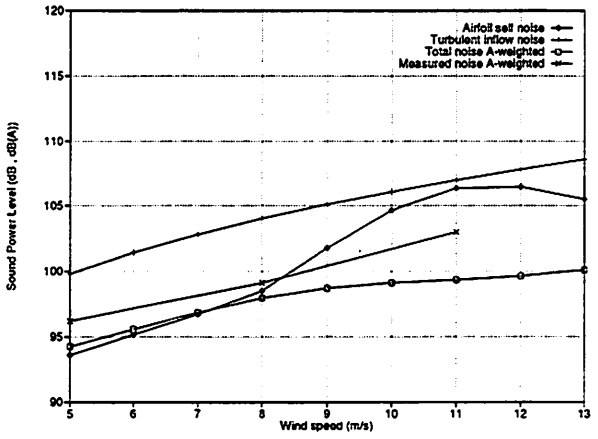

Figure 4 Total sound power level at different wind speeds for the Bonus Combi 300.

4.3.2 Tip pitch angle variation

The noise was predicted for different tip pitch angles for the Vestas V27. The noise spectrum is only different at intermediate frequencies around 400 - 1600 Hz, since the noise from turbulent inflow remains constant. Figure 5 shows the total predicted sound power level versus tip pitch angle together with measurements. The measurements show a slightly steeper reduction in noise with increase of the tip pitch angle, but in general there is good agreement. Even though the dominating noise from turbulent inflow remains constant, the total noise is reduced with increase in the tip pitch angle. This is because the airfoil self noise is reduced in the intermediate frequency range where the A-weighting is minor. This validates the relation between the noise from turbulent inflow and airfoil self noise.

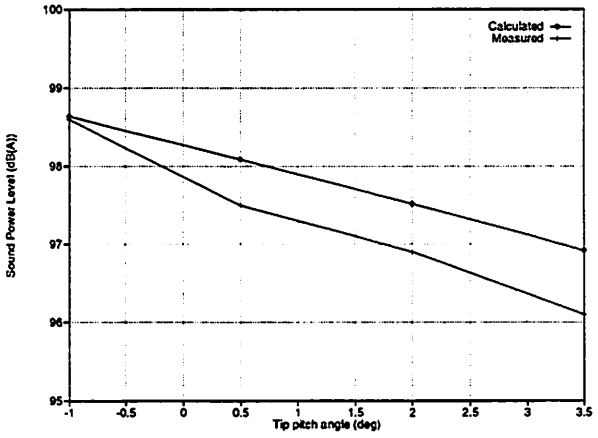

Figure 5 Total sound power level at 8 m/s at different tip pitch angles for the Vestas V27.

4.3.3 Tip speed variation

The noise was predicted for the Bonus Combi 300 kW at different tip speeds. Measurements have not been available, and an empirical expression reported in Wagner (1996) was instead used for comparison:

$$L_W = 10\log D + 50\log V_{tip} - 4 \qquad (4)$$

Where D is the rotor diameter and V_{tip} is the tip speed.

The frequency spectrum is different over the entire frequency range. Turbulent inflow noise and airfoil self noise are in general increased with tip speed. The total sound power level is in good agreement with eq. (4), Figure 6. There is a linear increase in the noise from turbulent inflow, whereas the airfoil self noise tend to increase mainly at lower tip speeds. Even though the total sound power level is dominated by the noise from turbulent inflow, airfoil self noise is again seen to be an important contribution.

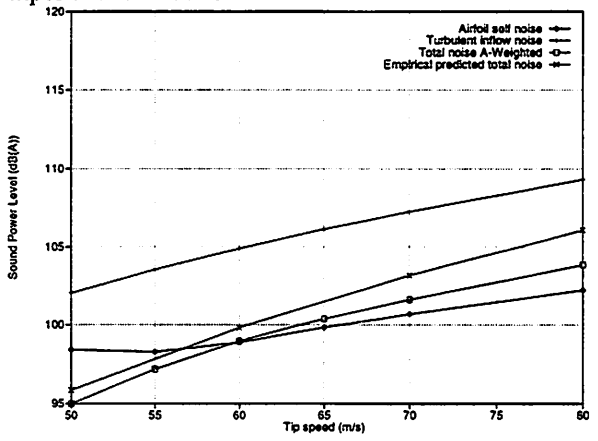

Figure 6 Total sound power level at 8 m/s at different rpm for the Bonus Combi 300.

5 Results

We performed a design study for optimization of the Bonus Combi 300. The aim was to demonstrate control of both the total noise and the power production and to use CFD to identify the aerodynamic parameters for noise prediction from the blade tip.

5.1 Rotor optimization

Three different optimizations studies were performed according to the following problem set-up:

1. A rotor with minimum aerodynamic noise subject to constraints on the minimum allowable energy production.
2. A rotor with maximum energy production subject to constraints on the total noise.
3. A rotor with maximum energy production with no constraints on noise.

The maximum generator power together with constraints are in all cases set equal to predicted values for the Bonus Combi 300. The rotor shape except the airfoils is optimized together with the tip pitch angle and the tip speed. For simplicity reasons, there was no constraints on loads and cost. When comparing sound power levels with the Bonus Combi 300, the predicted value will be used to avoid the offset on the absolute value.

Key results are shown in Table 1. The resulting chord and twist distributions are shown in Figure 7 and Figure 8 and the power curves are shown in Figure 9.

Table 1 Overall results for three different optimized rotors, compared to the Bonus Combi 300.

	Bonus Combi 300	Optimum 1	Optimum 2	Optimum 3
Noise		Minimum	Constrained	
Production		Constrained	Maximum	Maximum
Production (MWh)	838	838	855	860
Noise (dB(A))	98.0	94.9	98.0	101.2
Tip speed (m/s)	56.8	50.1	57.0	65.2
Tip pitch (°)	-1.8	1.2	0.8	0.6

Optimization 1 results in a rotor of equal peak power and energy production as the Bonus Combi 300, but the total sound power level is reduced by 3.1 dB(A). Important for the reduction in noise is the drop in tip speed to 50.1 m/s and the increase in tip pitch angle to 1.2°. The chord is increased on most of the blade to maintain peak power, Figure 7, and energy production, since the tip speed is reduced. The twist is reduced on a large part of the blade, resulting in an increase in the angle of attack, Figure 8. However, at the tip this increase is counter balanced by the increase in tip pitch angle. On the power curve in Figure 9, it can be seen, that the power is reduced just before rated power. This is counter balanced by an increase at wind speeds around 10 - 13 m/s, so that the energy production is maintained. Because of the increased chord, the resulting blade will be more expensive and wind loads will be increased. The reduction in tip speed will increase the drive train torque. All in all, the wind turbine with the optimized rotor will be more costly.

Optimization 2 results in a rotor of equal noise emission and rated power as the Bonus Combi 300, but with the energy production increased by 2.0%. This is a very common value from realistic aerodynamic optimization of an already existing blade, when the swept area and the airfoils are fixed, Fuglsang et al. (1995). The tip speed is slightly increased to 57.0 m/s and the tip pitch angle is increased to 0.8°. The increase in tip speed is counter balanced by the increase in tip pitch angle and the change in blade shape to avoid an increase in the total noise. The chord is slightly increased, Figure 7, whereas the twist is reduced, Figure 8.

The power curve shows an increased power before the wind speed of maximum power, Figure 9. The resulting blade is very similar to Bonus Combi 300 kW, but fine adjustment of the blade chord and twist have resulted in a controlled increase of the energy production. The cost of the optimized blade is probably not very different from the starting point.

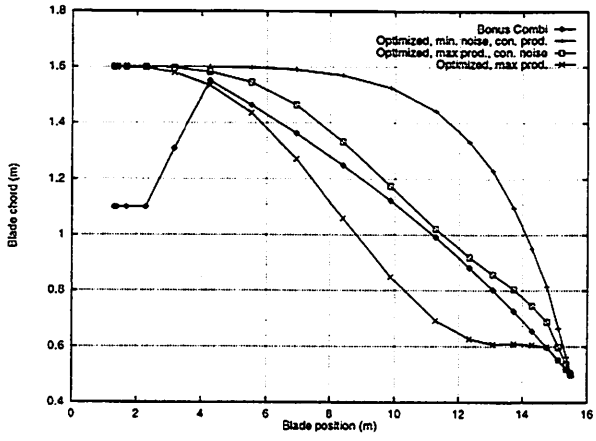

Figure 7 Chord distributions for the Bonus Combi 300 and the optimized rotors.

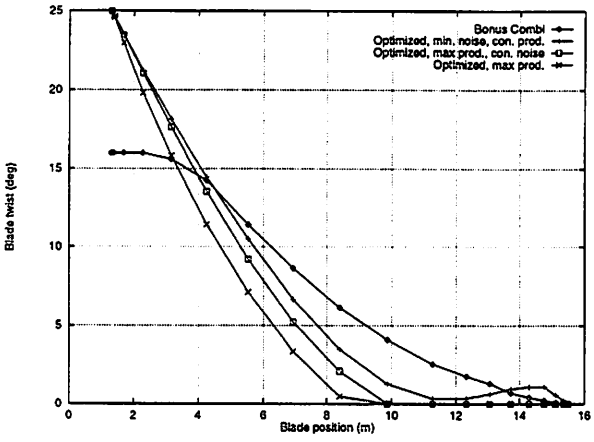

Figure 8 Twist distributions for the Bonus Combi 300 and the optimized rotors.

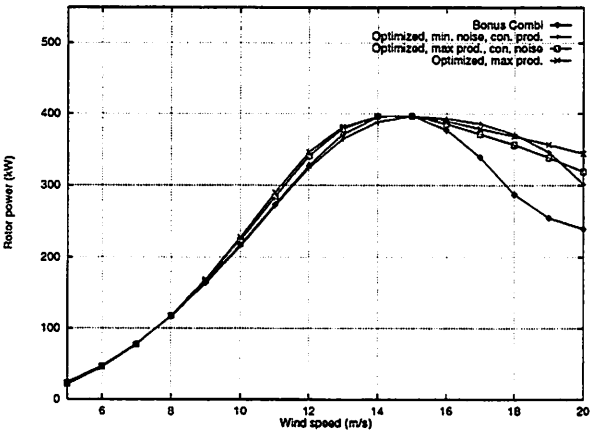

Figure 9 Power curves for the Bonus Combi 300 and the optimized rotors.

Optimization 3 is performed mainly for reference, since it does not contain any noise concerns. The energy production is increased by 2.6% compared to the Bonus Combi 300. The noise is increased by 3.2 dB(A), because of the increase in the tip speed to 65.2 m/s. The chord is substantially reduced, so that the rated power is not exceeded, since tip speed is increased, Figure 7. The twist is also reduced, Figure 8. There is only a small increase in the energy production compared to the second

optimization. From the large increase in the sound power level, it can be concluded, that the aerodynamic optimum is very expensive with concern to additional noise emission. This means, that the noise should always be constrained in the design process, either by application of the noise prediction model or by rules of thumb for the tip speed.

Figure 10 shows the total predicted noise spectra for the different optimized rotors together with the Bonus Combi 300, calculated for untripped flow. The shape of the spectrum is similar for the different rotors. The peak level frequency varies from 400 Hz to 1600 Hz. The rotor optimized for minimum noise is below the other rotors for all frequencies, and the optimized rotor for maximum production without noise concerns has the highest sound power levels. The rotor optimized for maximum production with constraint on the noise has an almost equal spectrum as the Bonus Combi 300.

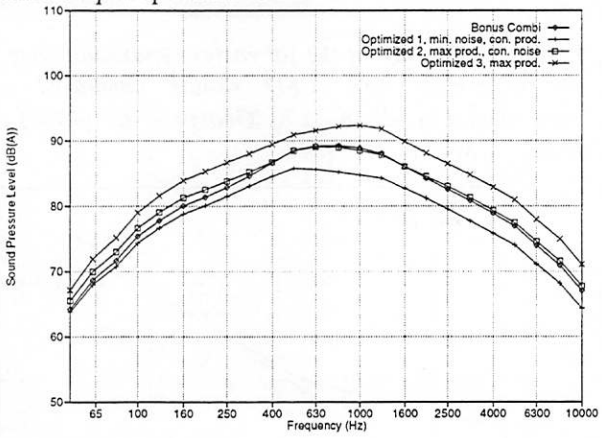

Figure 10 Total noise at 8 m/s for the Bonus Combi 300 and the optimized rotors.

5.2 Blade tip aerodynamics

We did CFD calculations of the tip flow with the 'FIDAP' code, Madsen et al. (1996). The governing equations were the time averaged Navier-Stokes equations without rotational effects, with the RNG k-ε model by Yakhot et al. (1992). The finite element method was used with structured and unstructured grids. The flow around the outer 4 chord lengths of the tip were modelled by 78000 elements. The Reynolds number was $2 \cdot 10^6$ corresponding to free air flow.

The general flow picture was investigated at three different angles of attack with focus on the formation of the tip vortex. An example of the tip vortex flow is shown in Figure 11, where the particle trace from the suction side flow just outside the boundary layer is visualised at angle of attack = 10°.

To obtain the necessary input for an aeroacoustic calculation, the characteristic length of the tip vortex, l, and the maximum velocity in the vicinity of the vortex core, U_{max}, should be determined. It is important, that the relationship with the angle of attack is correct, whereas an eventual offset is removed by the scaling of the prediction formula.

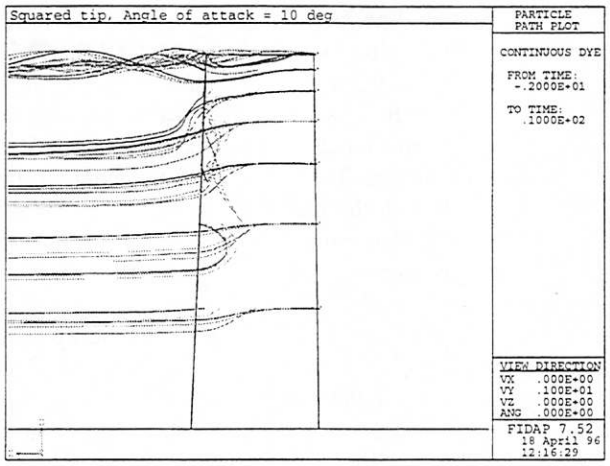

Figure 11 Particle trace of the fluid motion from the suction side, downstream from the blade for the rectangular tip at an angle of attack = 10° .

The determination of the characteristic length of the separation zone depends on a number of factors. Brooks et al. (1986) used a turbulence intensity of 5% as criteria. The characteristic length is difficult to determine from a CFD calculation because separation is in general poor predicted and the solution is steady and probably mesh dependent. The turbulent kinetic energy is related to the turbulence intensity and we chose to determine l from the turbulent kinetic energy, k:

$$k = \tfrac{1}{2}\overline{u_i u_i} \qquad (5)$$

Where $\overline{u_i u_i}$ is the mean-square fluctuating components of the velocity vector.

The contour lines of the turbulent kinetic energy in the plane perpendicular to the flow just downstream of the blade tip is shown for angle of attack = 10° in Figure 12. The contour lines are somewhat distorted by the changes in the mesh resolution. An area of higher turbulent kinetic energy exists at the suction side of the tip.

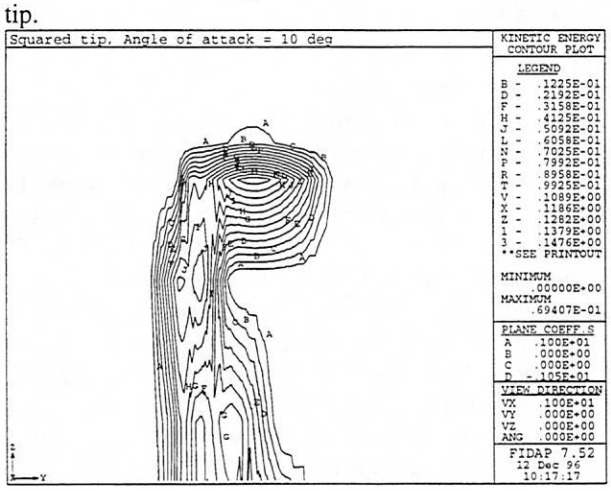

Figure 12 Contour plot of the turbulent kinetic energy for a rectangular tip at 10° in the plane perpendicular to the flow and the span just downstream from the trailing edge.

The contour line equal to k = 0.05 was chosen as criteria from the solution at the angle of attack = 10°. The vertical extent of this area was found to be about the same for all angles, whereas the maximum turbulent kinetic energy and the horizontal extent increased with the angle of attack. The picture of the contour lines compares well with the pictures of turbulence intensities from Brooks & Marcolini, (1986). They also found, that the vertical extension of the area of contour lines was about the same for all angles.

The maximum speed in the vicinity of the tip vortex was found by plotting contour lines of the speed. Figure 13 show the corresponding contour lines of the speed at the angle of attack = 10°. It can be seen that the maximum speed is found just outside the vortex core in the area below the tip region. This is in the area of low turbulent kinetic energy and it compares well with George et al. (1984). It appears that additional secondary areas of high speed are located around the vortex core, especially for higher angles of attack.

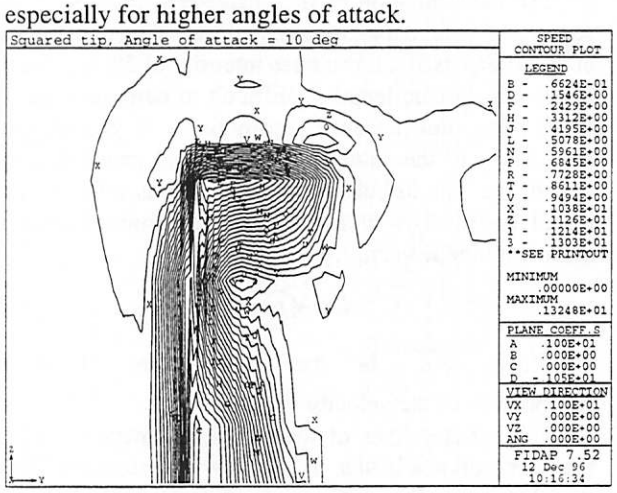

Figure 13 Contour plot of the flow speed for the rectangular tip at 10° in the plane perpendicular to the span and to the flow, 0.05 chord downstream from the trailing edge.

Before the predicted values can be plotted as a function of the angle of attack at the tip, α_{tip}, this was corrected from vortex theory to compensate for the finite span. Figure 14 shows the separation length versus the angle of attack. It is compared with the expressions from George et al. (1984) eq. (2) and Brooks et al. (1986) eq. (3). It appears that the separation size from the CFD solution is somewhat overestimated. This deviation is expected since we used a different parameter for determining l and the value of k = 0.05 was chosen rather arbitrarily. However, it is important that the slope of the curve is in fair agreement with the experiments.

Figure 15 shows the maximum velocity, U_{max} versus the angle of attack. This is compared to George et al. (1984), Brooks et al. (1986) used the same expression. Again a fair agreement is obtained. The deviation between the two curves is below 10% at low angles of attack and almost zero at higher angles of attack.

It would be straight forward to change the tip shape and determine the change in l and U_{max}, however the model for tip noise is only valid for rectangular tips, and it should be further developed or re-scaled to cover other tip shapes.

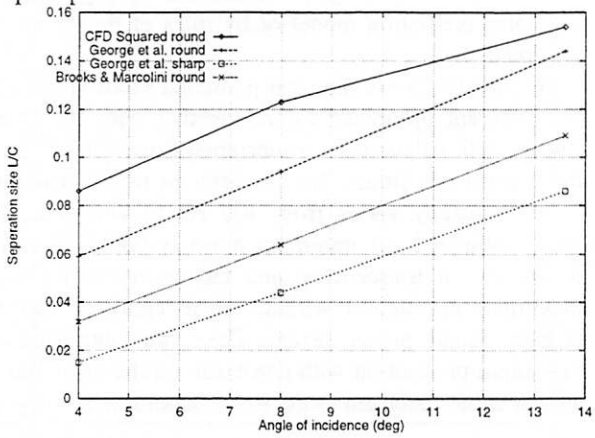

Figure 14 The size of the tip vortex separation zone for the rectangular tip, CFD results compared with experimental results used by George et al. (1980) and Brooks & Marcolini (1984).

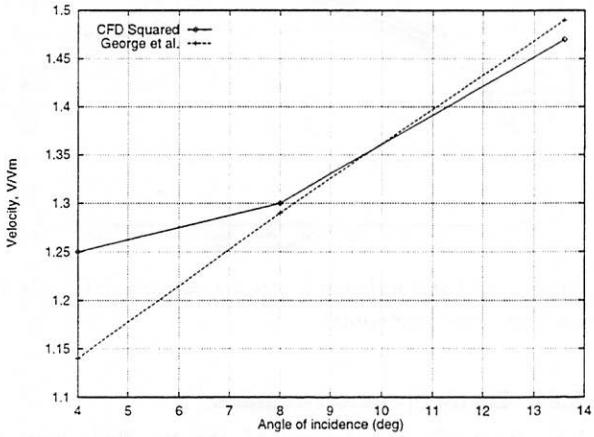

Figure 15 The maximum speed in the vicinity of the tip vortex for the rectangular tip, CFD results compared with experimental results used by George et al. (1980) and Brooks & Marcolini (1984).

6 Conclusions

We presented a design method for design of wind turbine rotors with numerical optimization together with a semi-empirical noise prediction model and subsequent detailed CFD calculations of the tip flow.

The semi-empirical noise prediction yields sufficiently accurate results for the total sound power level and the relative variation of important parameters.

A design study for the optimum rotor concerning minimum noise emission and maximum energy production showed a possible reduction in the total sound power level of 3 dB(A) to the same energy production or an increased energy production of 2% to the same sound power level.

It was clearly demonstrated, that noise concerns can be included in the design process, to control tip speed, tip pitch angle and blade shape, however in order to further include noise aspects, the economic value of noise reduction should be settled or the maximum allowable noise emission should be constrained according to departmental orders. This, demands a further increase in the degree of detail for the prediction model, to ensure a correct absolute level of the sound power level.

Detailed CFD calculations of the tip flow revealed the nature of the tip vortex. By calculation of the turbulent kinetic energy and the speed in the vicinity of the vortex we estimated the characteristic parameters for tip noise. Compared to measurements, fair agreement was found, though there was an offset, the variation with angle of attack was captured.

Future work should include further development of the semi-empirical noise prediction model, especially the model for tip noise to cover other tip shapes and the turbulent inflow noise model. A key point is the lack of sensitivity to the applied airfoils, where an airfoil prediction code should be used.

Acknowledgements

The present work was funded by the Danish Ministry of Energy under the contracts, ENS-1364/93-0006, ENS-1364/93-0001, ENS-1363/95-0001.

References

Amiet, R.K., 1975, Acoustic Radiation from an Airfoil in a Turbulent Stream, J. Sound Vibration, 41[4] pp. 407-420.

Brooks, T.F. and Marcolini, M.A., 1986, Airfoil Tip Vortex Formation Noise, AIAA Journal Vol 24[2], pp. 246 - 252.

Brooks, T.F., Pope, D. S. and Marcolini, M.A., 1989, Airfoil Self-Noise and Prediction, NASA Reference Publication 1218, USA.

Committee Draft for an IEC standard, 1995, Wind turbine generator systems - Part 10: Acoustic noise measurement techniques. Ref. 88/48/CDV.

Ffowcs Williams, J. E. and Hall, L.H., 1970, Aerodynamic Sound Generation by Turbulent Flow in the vicinity of a Scattering Half-Plane, J. Fluid Mechanics 40, pp. 657-670.

Fuglsang, P. and Madsen, H.A., 1995, A Design Study of a 1 MW Stall Regulated Rotor, Risø-R-799(EN), Risø National Laboratory, Denmark.

Fuglsang, P. and Madsen, H.A., 1996, Implementation and Verification of an Aeroacoustic Noise Prediction Model for Wind Turbines, Risø-R-867(EN), Risø National Laboratory, Denmark.

Fuglsang, P. and Madsen, H.A., 1996, Numerical Optimization of Wind Turbine Rotors, *Proc. EUWEC'96*, Göteborg, Sweden.

Grosveld, F.W., 1985, Prediction of Broadband Noise from Horizontal Axis Wind Turbines, J. Propulsion, 1[4], pp. 292-299.

Jakobsen, J. and Andersen, B., 1993, Aerodynamical Noise from Wind turbine Generators, Danish Acoustical Institute. 1993-06-04, LI 464/93 D/70.89-464.1

Jakobsen, J. and Andersen, B., 1995, Aerodynamical Noise from Wind Turbines - Experiments with full scale rotors, change of pitch, trailing edges, and tip shapes, Delta Acoustics & Vibration. AV 590/95.

Lowson, M.V., 1993, Assessment and Prediction of Wind Turbine Noise, ETSU W/13/00284/REP.

Lowson, M.V. and Fiddes, S.P., 1994, Design Prediction Model for Wind Turbine Noise, ETSU W/13/00317/REP.

Madsen, H.A. and Fuglsang, P., 1996, Numerical investigation of different tip shapes for wind turbine blades - Aerodynamic and aeroacoustic aspects, Risø-R-891(EN), Risø National Laboratory, Denmark.

Yakhot, V., et al., 1992, Development of Turbulence Models for Shear Flows by a Double Expansion Technique, Physics of Fluids, A 4 (7), 1510 - 1520

Wagner, S., Bareiss, R. and Guidati, G., 1996, Wind Turbine Noise, Springer-Verlag Berlin Heidelberg, Germany.

Several Rotor Noise Sources and Treatments

James Tangler

National Renewable Energy Laboratory
1617 Cole Boulevard
Golden, CO 80401

Abstract

Noise has been a design consideration in the development of advanced blades and turbines at the National Renewable Energy Laboratory. During atmospheric testing associated with these efforts various types of aeroacoustic noise have been encountered. This presentation discusses several of these noise sources and treatments used to mitigate or eliminate the noise. Tonal noise resulting from tip-vortex/trailing-edge interaction and laminar separation bubbles was found to be easily eliminated. Impulsive noise resulting from blade/vortex interaction for rotors that furl and that due to tower shadow can be mitigated by various means.

Tip-Vortex/Trailing-Edge Interaction

This pure tone noise, which occurs over a wide wind speed range, results from the interaction of the discrete tip vortex with the local trailing edge (Figure 1). This noise source was identified and discussed by George, 1980 and Brooks, 1986. It can be eliminated in one of several ways. The most straightforward means of eliminating the noise is to sharpen the trailing edge in the tip region. Another method is to diffuse or displace the tip vortex in order to minimize or eliminate its interaction with the trailing edge. A combination of both methods can also be used.

A classic example of this noise was observed while testing a Micon 108 with a set of NREL 9.7 meter thick airfoil blades (Figure 2). During testing of these blades a 3-per-rev pure tone 2000 Hz whistle was emitted from the tip region of the blades at medium wind speeds. Measurements of this noise, shown in Figure 3, were taken at ground level one rotor radius upwind of the turbine. The noise was thought to be due to either trailing edge thickness or airfoil laminar separation bubbles. The trailing edge thickness of one blade was reduced from 0.476 cm (0.188 in.) to 0.159 cm (0.063 in.) over the last 15% of span to determine if it was the influencing factor. This was accomplished by gluing a balsa wood strip to the trailing edge which decreased the thickness over a 0.635 cm. (0.25 in.) chordwise length as seen in Figure 4. The thin trailing edge eliminated the pure tone whistle from one blade such that only a 2-per-rev whistle was detected. A similar treatment to the other two blades totally eliminated the pure tone whistle. The length of the sharp trailing edge was then reduced from 15% of span to the outer 6% of span. The absence of the noise with the shorter trailing edge strips indicated that the noise was a result of the tip vortex interacting with the 0.476 cm. (0.188 in.) blunt trailing edge. Measurements of the noise with the sharp tip region trailing edge are shown in Figure 5. No trace of the pure tone 2000 Hz whistle can be detected at all wind speeds. It was encouraging to note that this noise can be eliminated by using a sharp trailing edge over only the last 6% of the blade. A sharp trailing edge over the whole blade would easily be damaged from the sling used for moving and installing the blade.

Laminar Separation Bubble Noise

During testing of the Micon 108 discussed in the previous section, laminar separation bubbles were also suspected as being the source of the 2000 Hz whistle. The bubbles were eliminated as a possible noise source by placing serrated trip strips in front of the upper and lower surface boundary layer transition locations in the tip region of one blade as seen in Figure 6. The purpose of the trip strips was to break the bubbles. If the bubbles were significant, breaking the bubbles with trip strips should eliminate the whistle. If the bubbles were weak the trip strips would be expected to have no effect. No significant difference was noted in the noise source from the blade with the trip strips relative to the other two blade. Consequently, both the upper and lower surface laminar separation bubbles on the tip region NREL S813 airfoil were considered insignificant and quiet.

A significant encounter with tonal noise from laminar separation occurred during atmospheric testing of the UTRC 8 kW machine at the Rocky Flats site during the mid 1980s. This tonal noise was found to be wind speed sensitive. The pultruded blades on this machine used a NACA 23012 airfoil (Figure 7) which has a reflexed trailing edge to produce a zero pitching moment. At low Reynolds number this results in a strong adverse pressure gradient or laminar separation bubble on the airfoil's pressure surface back around 65% chord. To eliminate the tonal noise a strip of tape was placed in front of the suspected bubbles. The tape broke the bubbles and eliminated the tonal noise. This example of tonal noise from laminar separation bubbles pointed to the need to use airfoils that do not have significant bubbles at their operating Reynolds number. This requires not moving the airfoil's thickness too far aft which results in an excessive adverse pressure gradient and corresponding strong laminar separation bubbles. It also requires avoiding airfoils with reflexed trailing edges.

Blade/Vortex Interaction

Impulsive noise due to blade/vortex interaction is largely associated with small machines that furl in either a vertical or horizontal plane. Furling the rotor decreases the projected rotor area for the purpose of controlling peak power in high winds. Impulsive noise results from the tip vortex from a blade intersecting a following blade and inducing a large local velocity on the blade as seen in Figure 8. Blade/vortex interaction noise can be reduced through the use of lower tip speeds, more blades for a given rotor solidity, and through the use of vorticity shedding tip shapes (Klug 1995) or vortex diffusion tip shapes (Tangler 1975). An example of two vorticity shedding tip shapes are seen in Figure 9. The Ogee tip sweeps the trailing edge rapidly forward into a slender finger to shed the vorticity. This tip geometry originated in the helicopter industry in the 1970s. Although it rapidly sheds the vorticity it has poor aerodynamic performance. The more promising sword tip shape also rapidly sheds the tip vorticity and has been found to result in lower noise levels. Further testing of this tip is desired to quantify its effect on rotor performance. This tip also has the qualities to help mitigate tip-vortex/trailing-edge noise.

An alternative approach to reduce blade/vortex interaction noise is by dividing and diffusing the tip vortex as shown in Figure 10. A conventional square tip sheds a strong discrete vortex having peak rotational velocities around one-half the tip speed. The tip vortex can be divided into two smaller discrete vorticies that revolve about one another. As this occurs the opposing velocity gradient between the two vorticies results in a rapid diffusion of the vorticity. The result of this interaction is one large diffused vortex with relatively low peak rotational velocities. Interaction of this diffused vortex with a following blade will result in a less intense impulsive noise. Figure 11 from reference X shows two tip shapes designed to generate twin vorticies.

AWT-26 Noise Mitigation

In the design of the AWT-26 (Figure 12) a conscious effort was made to minimizing the noise signature. With any downwind, two-bladed rotor the impulsive noise generated by the passage of the blade through the tower wake is always a concern. This noise source was minimized through the use of a helical strake on the tower which breaks up the Karman vortices typically shed from a circular tower cross section. The use of geometrically optimizes tip plates for overspeed control also eliminates noise generated from the tip-vortex interacting with a thick trailing edge. Tip plates prevent the formation of a discrete tip vortex that interacts with the trailing edge. The tip vorticity is effectively displaced by the tip plates away from the trailing edge.

Conclusions

° A sharp trailing edge is only needed in the tip region of the blade to eliminate pure tone tip-vortex/trailing-edge noise.

° Properly designed airfoils with weak laminar separation bubbles don't appear to have a noise problem.

° Blade/vortex interaction, impulsive noise can be somewhat reduced by diffusing the tip vortex.

° Tip plates eliminate tip-vortex/trailing-edge noise and the use of a helical strake reduces tower shadow noise.

References

Brooks, T.F., and Marcolini, M.A., "Airfoil Tip Vortex Formation Noise," AIAA Journal, February 1986.

George, A.R., Najjar, F.E., and Kim, Y.N., "Noise Due to Tip Vortex Formation on Lifting Rotors," AIAA Paper 80-1010, June 1980.

Klug, H., Osten, T., Jakobsen, J., Anderson, B., et al., "Aerodynamic Noise from Wind Turbines and Rotor Blade Modifications," JOULE II, Project JOU2-CT92-0233, Final Report, DEWI-V-950006, November 1995.

Tangler, J.L., "The Design and Testing of a Tip to Reduce Blade Slap," 31st Annual National Forum of the American Helicopter Society, May 1975.

NREL National Renewable Energy Laboratory

Figure 1. Tip Vortex Induced Trailing Edge Noise

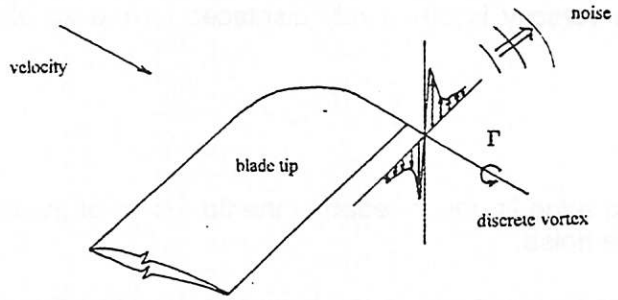

National Wind Technology Center

NREL National Renewable Energy Laboratory

Figure 2. Micon 108 with NREL 9.7 Meter Thick Airfoil Blades

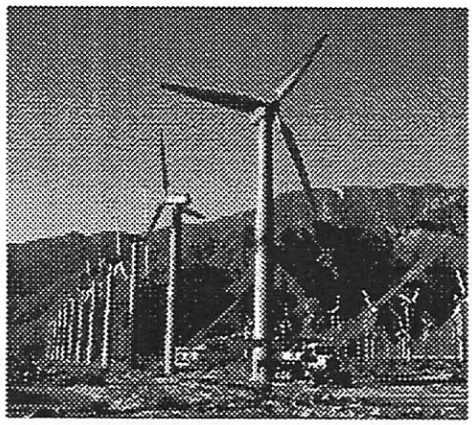

National Wind Technology Center

Figure 3. Thick Trailing Edge Noise Measurement

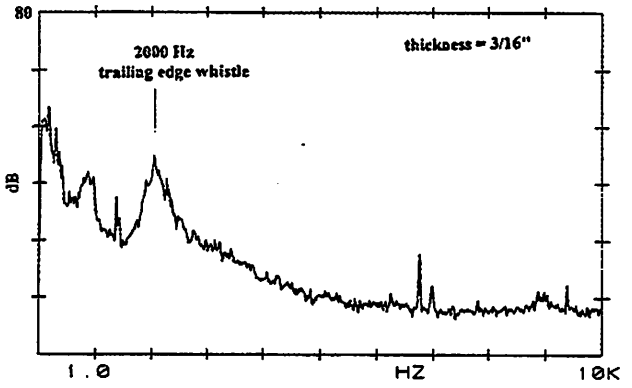

National Renewable Energy Laboratory

Figure 4. Trailing Edge Thickness

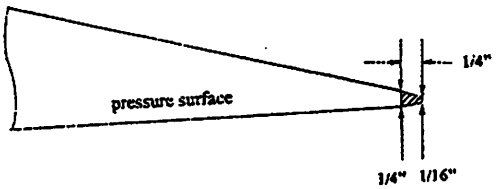

National Wind Technology Center

Figure 5. Sharp Trailing edge Noise Measurement

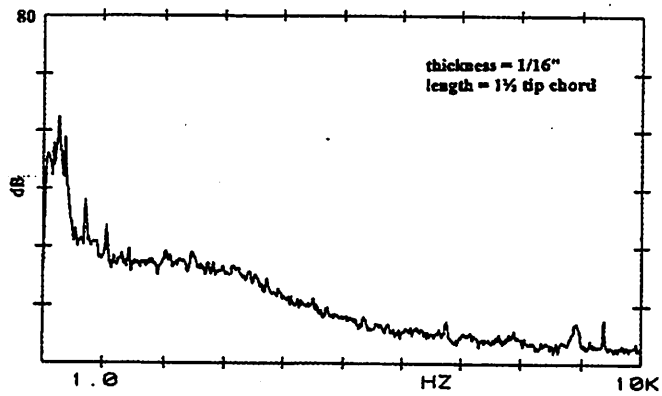

Figure 6. Laminar Separation Bubble Noise

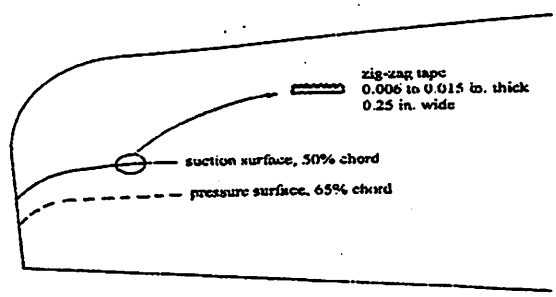

If tape results in noise reduction remove pressure surface tape to determine if upper or lower surface tape caused noise reduction.

Figure 7. Lower Surface Laminar Separation Bubble Noise

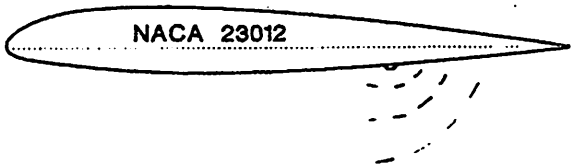

National Renewable Energy Laboratory

Figure 8. Blade /Vortex Interaction Noise

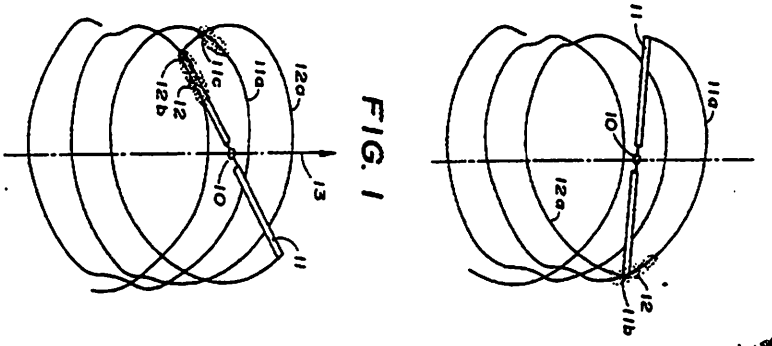

Figure 9. Vorticity Shedding Tip Shapes

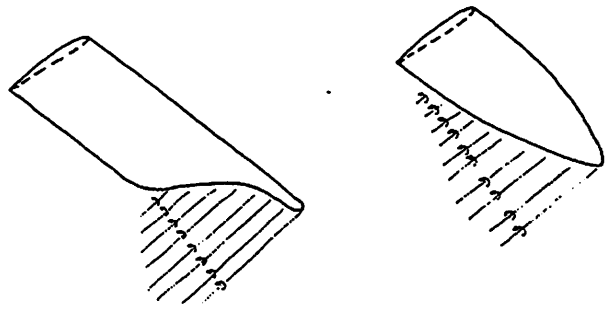

National Renewable Energy Laboratory

Figure 10. Vortex Diffusion

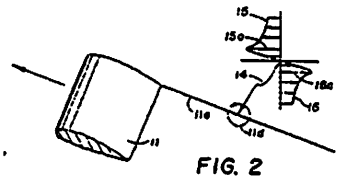

FIG. 2

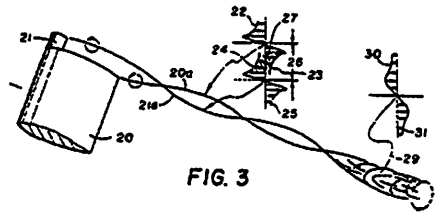

FIG. 3

Figure 11. Twin Vortex Tip Shapes

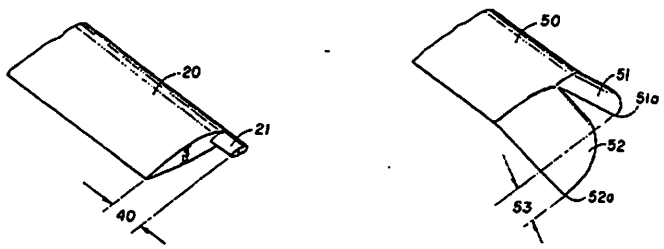

National Renewable Energy Laboratory

Figure 12. AWT-26 300 kW Utility Turbine

ANALYSIS OF BROADBAND AERODYNAMIC NOISE FROM VS45 PAPER PRESENTED AT IEA MEETING ON WIND TURBINE NOISE, MILAN 17th MARCH 1997

P. Dunbabin,
Renewable Energy Systems Ltd.,
11 Elmbank St.,
Glasgow
G11 5AY,
Scotland,
UK

CONTENTS

FIGURES

ANALYSIS OF BROADBAND AERODYNAMIC NOISE FROM VS45

1.0 INTRODUCTION AND OBJECTIVES

This paper describes the analysis of acoustic data taken from the VS45 at Kaiser-Wilhelm-Koog, as part of JOULE project W/45/00504/00/00. The aim was to investigate the dependence of aerodynamic noise on tip speed and angle of attack. In particular, the dependence of noise in individual third octave bands on these variables is examined.

The analysis is divided into 3 sections:

- data selection
- data checks and analysis of broadband nacelle noise
- analysis of broadband aerodynamic noise and its sensitivity to tip speed and angle of attack

These are described in sections 2-4.

2.0 DATA SELECTION

Only certain portions of data were suitable for analysis. In particular, conditions of constant rotational speed, and yaw positions were required. Two sets of data were selected, corresponding to normal operation and manual control. Full details of data selection are described in detail in references [1,2], but a summary is reproduced here

2.1 Normal Operation

The criteria for data selection under normal operation were:

i. data aligned to within $\pm$ 3 degrees of one of the microphones;
ii. power constant to within $\pm$ 5 kW;
iii. constant pitch angle.

Most data samples lasted between 20 and 90 seconds. This provided data over the range 20 - 600 kW, but the data were fairly sparse. Additional data samples for which the power was constant only to within 10 kW were also included.

2.2 Manual Operation

The experiments covered two kinds of manual control:

i. constant pitch angle;
ii. constant rotational speed.

Data were selected if the rotor was aligned to within $\pm$ 3 degrees of one of the microphones Where possible, samples were chosen for comparison with those taken under normal operation.

2.3 Background Noise

In addition to the above, a series of samples was taken with the turbine off, to assess the strength of background noise. The wind speed range for these samples was 5 - 11 m/s.

3.0 DATA CHECKS

The data were checked to ensure suitability for analysis. Full details are given in reference [3], and a summary is given below.

3.1 Listening

Each microphone recording for each sample was replayed and comments on the data quality were made. Some samples were rejected, owing to high background noise (for example wind noise or birds), and some rejected owing to exceptionally high electromagnetic interference. A total of 22 data samples, each comprising 13 microphone signals were chosen.

3.2 Filtering of Electromagnetic Noise

Some of the data collected was affected by electromagnetic noise from the inverter and underground electric cables. The magnitude of the interference varied strongly from one microphone to the next, but the frequencies affected were the same for all samples. It was decided to filter out all data at frequencies above 7079 Hz (upper limit of 6300 Hz third octave band), and also all data from 2750 to 3250 Hz and 5600 to 6500 Hz. There is a broadband peak at 3400 Hz, which remains included in the results. The data were filtered by linear interpolation between the 50 points either side of each frequency band omitted.

3.3 Calibration

Calibrations were performed at the start and end of each day. Each calibration signal lasted for 30 seconds. A moving 65536 point transform and hanning window were used to calculate the power spectral density of the calibration signals, and each spectrum was inspected to check that it was uncorrupted by noise. Calibration factors for each microphone on each day of testing were compared to see if there were any discrepancies. For the outdoor microphones, the average standard deviation was 0.17 dB(A); for the nacelle microphone, it was 0.46 dB(A). This indicates that the calibrations were reliable throughout.

3.4 Background Noise

The background noise samples were analysed into third octave bands and compared with data taken in similar wind speeds with the turbine operational. It was noticeable that background noise levels were also affected by electromagnetic noise and so were filtered in the same manner as the other samples.

Background noise levels at different microphones were more variable than the levels recorded when the turbine was generating. Some microphones showed increased noise levels in the frequency range 100-400 Hz.

A comparison of background noise levels and signal noise levels was made for a selection of samples and microphones, and has been reported in reference [3]. At frequencies below 100 Hz, the turbine noise and background noise were similar. At frequencies between 100 and 200 Hz, the background and turbine noise levels were sometimes similar. Over the frequency range 250 - 2000 Hz, the noise levels with the turbine operating exceeded background noise levels by between 5 and 37 dB(A), depending on the sample and the frequency, providing a good signal to noise ratio. For frequencies in excess of 3150 Hz, the background noise was invariably as loud as the noise with the turbine on (even though all recordings had been filtered for electromagnetic noise). Noise in the 2500 Hz third octave band was sometimes louder than the background noise, but not always. Graphs are given in reference [3].

3.5 Tonal Analysis

The tonal content of the noise has been examined using RES's tonal analysis program. This identifies the tones using the method recommended by the Noise Working Group, and classifies each as inaudible, audible, or prominent.

Each tone has been filtered from the broadband data, so that the resulting spectrum represents aerodynamic noise only. Although the tones contribute little to the overall sound power level, they may affect individual third octave bands.

The tonal analysis is of interest in its own right, but is not reported here.

3.6 Calculation of Mechanical Noise Radiated from the Nacelle

An assessment was made to see if mechanical noise from the nacelle affects the noise levels recorded outside the turbine. This is reported in detail in reference [4], and summarised below.

Noise levels in the nacelle were monitored by two microphones, the first just above the generator, and the second at the mouth of an air vent about 1 metre away from the generator. Unfortunately, the second meter stopped working during the experiments, and so a complete record is available only for the meter near the generator.

The recorded SPL's (in the third octave bands 63 - 2500 Hz) ranged between 79 and 90 dB(A), and were closely correlated with rotational speed.

The radiated sound power levels are calculated using a method given in reference [5]. For the purposes of these calculations, the sound in the nacelle has been assumed to be reverberant. This is a simplification; in practice, it is likely to be only semi-reverberant. The radiated sound power levels have been calculated and are presented in reference. Also included are estimates of the mechanical noise level that might be expected at the microphones, if spherical spreading of the sound were assumed. These estimates were between 20 and 27 dB(A) lower than the overall noise levels measured on the ground. (See Figure 3.01).

Some measurements of the noise level at the base of the nacelle were made. The principal noise sources were: noise from the nacelle, being transmitted down the inside of the tower, and noise from the cooling fan. The overall noise level was high: 78.7 dB(A). Using standard sound reduction indices for steel, the radiated sound power from the base of the turbine was estimated to be 56 dB(A). Assuming hemi-spherical spreading of sound, the sound pressure level at the observer is estimated at 31 dB(A), well below the measured noise levels at the microphones.

Note that these estimates do not include any structurally transmitted noise from the nacelle. Experiments on other turbines have confirmed that some noise may be transmitted down the blades or the tower. Analysis of the variation of noise with blade position would help to clarify whether tones are in fact transmitted structurally.

4.0 ANALYSIS OF BROADBAND NOISE

4.1 Procedure

In view of the results of sections 2-3, it can safely be assumed that the majority of the noise recorded by the microphones is due to aerodynamic noise emission from the blades. The next stage was to assess the broadband noise and its variation with tip speed and angle of attack.

Each recording was divided into a segment of data representing a whole number of blade rotations (generally 3-4), and then fourier analysed using a 65536 point moving transform, with a hanning window. Each power spectral density overlapped the previous one by 65408 points. A mean Doppler shift of 1 was assumed throughout. The resulting power spectral density was filtered to remove electromagnetic noise and tones, and converted into third octave bands. A representative background noise level, taken at a similar wind speed, was subtracted logarithmically from each third octave band.

A second set of analyses has been started, to investigate the variation of noise with blade position. In this case, short period samples are used to calculate the power spectral densities, and each is corrected for the Doppler shift.

4.2 Results

4.2.1 Measured Data

Table 4.01 shows the mean rotational speed, 50m wind speed, pitch and power for each sample used for this analysis. The final column shows the number of the microphone directly upwind of the turbine. For the remainder of the analysis, results will be presented for the upwind, downwind and crosswind microphones for each sample.

4.2.2 Overall Sound Power Level as a Function of Tip Speed

Table 5.02 shows the measured SPL's for each sample, as recorded by the upwind, downwind and crosswind microphones, as a function of tip speed. Estimated angles of attack over the last 10% of the blade have also been included in this Table. These are described in more detail in section 4.2.4.

Plots of the overall A-weighted sound power levels against the logarithm of tip speed have been produced (Figures 4.01 - 4.02). The sound power levels have been estimated from recordings made at four positions: upwind, 90 degrees, downwind and at 270 degrees. The tip speed range is from 45.6 - 74.3 m/s. All four trend lines show good correlation and similar dependence of the noise with tip speed, the mean square regression coefficient being 0.94. Correlation coefficients, slopes and intercepts for each of the four directions are listed in Table 4.03.

The mean dependence of noise of tip speed can be calculated from the regression, by:

$$L_{WA} = 10\log(U)^x$$

where L_{WA} is the overall sound power level, U the tip speed in m/s and x is the gradient of Figures 4.01-4.02, divided by a factor of 10 to convert from Bels to decibels. The equation can be rewritten as:

$$L_{WA} \propto U^{5.7\pm0.26}$$

This is in very good agreement with theory.

4.2.3 Spectrum as a Function of Tip Speed

The data were divided into third octave bands, and the regression of SPL versus $\log_{10}$(tip speed) was calculated for each frequency band. See Figure 4.03.

In broad terms, good correlations ($R^2 >= 0.8$) were found for frequencies between 500 and 3150 Hz, although correlations were slightly lower in the crosswind directions than up or downwind. Poor correlations were found in the frequency range 63-125 Hz, and variable values were found between 160 and 400 Hz. All four traces showed a high correlation at 50 Hz, which was almost certainly due to mains interference.

Gradients for the SPL versus log10(tip speed) in each third octave band are presented in Figure 4.04. Gradients are generally higher for noise in higher frequency bands, implying that noise in high frequency noise is more sensitive to tip speed. For example, the mean gradient at 160 Hz is 40, implying a fourth power law for noise with tip speed, while the mean gradient at 2000 Hz is 60, implying a sixth power law. Regression lines have been fitted to the graphs, and are shown in Figures 4.05-4.06. The correlation coefficients range between 0.36 and 0.65 depending on the direction of the microphone.

4.2.4 Overall SPL as a Function of Angle of Attack

The angle of attack over the outermost portion of the blade is believed to play a fundamental role in the generation of noise, although different frequencies are affected differently.

For each data sample, the angle of attack over the last 10% of the blade has been deduced using a blade element program, in conjunction with the 50m wind speed, power output, pitch angle and rotational speed as measured during the sample. Of these parameters, the wind speed is the least accurately known, as the mast was not always upwind of the turbine, and the wind speed and direction alter rapidly. It was decided to calculate the angle of attack over a range of wind speeds, within ± 1 m/s of the mean measured value. Estimated angles of attack versus tip speed are shown for each of the different samples in Figure 4.07. Samples under manual and automatic pitch control have been shown separately. Under automatic pitch, the angle of attack was found to range between 1.5 and 5.1 degrees. For the samples taken under manual pitch control, the range was -4.1 to +2.0 degrees.

Samples with similar tip speeds, but different angles of attack can be compared. The data have been normalised for the effect of tip speed, using the regression lines calculated from all the available data.

Table 4.04 shows SPL's normalised for tip speed, together with the estimated angle of attack for each sample. Figures 4.08 and 4.09 show the same information, for the upwind, downwind and crosswind directions. There is no evidence of correlation.

Two more graphs were prepared, using the absolute value of angle of attack as the abscissa (See Figures 4.10 and 4.11). Since the minimum drag coefficient for the aerofoil used occurs at 0 degrees of attack, the boundary layer thickness, and hence noise, should be lowest at this angle of attack.

In practice, it is found that correlations in the downwind and crosswind directions are negligible, but that correlations in the upwind direction improve (the new regression coefficient is 0.45, compared to 0.16 when the true value of the angle of attack is used).

Finally, two graphs have been prepared using the square of the angle of attack as the abscissa. (Figures 4.12 - 4.13) Correlations in the crosswind directions remain negligible, while correlations in the upwind and downwind directions are 0.32 and 0.13 respectively.

4.2.5 SPL in Selected Third Octave Bands as a Function of Angle of Attack

It seems reasonable to assume that noise in different frequency bands will be differently affected by angle of attack, since noise in different frequency bands is generated by different mechanisms. For example, we would expect the dominant noise source at 250 Hz to be inflow turbulence, while the dominant sources at 1000 Hz would be expected to be due to the interaction of the boundary layer with the trailing edge or to vortex shedding from a blunt trailing edge. Noise at around 2000 Hz may be influenced by separated flow region near the tip.

SPL's in third octave bands between 25 and 4000 Hz have been normalised to remove the correlation of noise with tip speed, and the residuals plotted against angle of attack. Figures 4.14 and 4.15 show typical graphs.

Pearson correlation coefficients and F-test confidence intervals have been calculated for each third octave band, as measured at each of four microphone positions (upwind, downwind and two crosswind positions).

Tables 4.04-4.07 list the calculated regression coefficients, confidence intervals and gradients for noise in each third octave band as a function of angle of attack. The following inferences can be drawn:

i. regression coefficients vary between 0.0 and 0.31, depending on frequency and microphone location;
ii. regression coefficients calculated from data measured at different positions do not agree well;
iii. confidence levels are high (>90%) for regressions in the crosswind directions, for frequencies below 400 Hz. These correlations indicate a decrease of noise with increasing angle of attack, with gradients in the range -0.5 to -1.3 dB(A) / degree;
iv. confidence levels are high (95%) in the downwind and crosswind directions for noise in the 1250 and 1600 Hz third octave bands. The corresponding regression coefficients are approximately 0.22 and 0.21;
v. in the downwind and both crosswind directions, correlations of noise with angle of attack are negligible for frequencies between 400 and 1000 Hz. In the upwind direction, the calculated regression coefficients are between 0.13 and 0.19 for this frequency range, with confidence intervals of between 82 and 93%;

vi. regression coefficients, gradients and confidence levels are low for frequencies between 400 and 1000 Hz;

vii. correlations are significant for noise in the 3150 and 4000 Hz third octave bands in the upwind and downwind directions. However, recordings at these frequencies are likely to have been affected by electromagnetic interference, despite filtering. Furthermore, noise at these frequencies is rapidly attenuated in air, and therefore contributes little to the far-field sound pressure level;

It is suggested that additional periods of data are analysed to clarify these findings, in particular, periods of data for which the modulus of the angle of attack approaches 5 or 6 degrees are required. At present, an inaccuracy of a few dB on one or two points could change the correlations significantly.

5.0 CONCLUSIONS

The main conclusions of this report are:

1. noise in frequency bands below 200 Hz may be affected by background noise, and so any trends for this noise can not be regarded as reliable;
2. the signal to noise ratio is good (5 - 37 dB) for noise in frequency bands between 200 and 2000 Hz inclusive;
3. noise in frequency bands 3150 and 4000 Hz may be affected by background or electromagnetic noise;
4. as expected, there is a clear correlation between the A-weighted sound pressure level and tip speed, with a mean regression coefficient of 0.94, and gradient $L_{WA} \propto U^{5.7\pm0.26}$;
5. regression coefficients for noise against tip speed are dependent on the frequency of the noise. For example, regression coefficients for noise in the frequency range 500 - 3150 Hz are generally over 0.8, while regressions for noise in the frequency range 32 - 400 Hz range from 0 to 0.9, depending on frequency and microphone position;
6. the gradient of noise against tip speed seems to depend on frequency. For example, noise at 1250 Hz seems to follow a sixth power law with tip speed, while noise at 200 Hz follows a fourth power law. If a regression line is drawn through the graph of gradient versus third octave band, the regression is between 0.36 and 0.65, depending on the microphone position. This suggests that the effect is real;
7. if the A-weighted sound power level is normalised for tip speed, and plotted against angle of attack, negligible correlations are found in the downwind and crosswind directions. The correlation coefficient in the upwind direction is 0.17. If the normalised levels are plotted against the absolute value of angle of attack, the correlation remains negligible for the downwind and crosswind directions, but increases to 0.45 in the upwind direction. More data would be needed to confirm this;
8. if the normalised A-weighted SPL's in each third octave band are plotted against angle of attack, the results are somewhat surprising, and depend strongly on the position of the microphone. For the crosswind microphones, correlations are significant (at the 90% level or higher) for noise at 315 Hz and below. However, it is known that some of the data below 200 Hz is affected by background noise, so this correlation should be treated with caution. Correlations and gradients are negligible in the frequency range 400-1000 Hz. The downwind and 90 degree crosswind directions show a correlation of 0.23 at 1250 - 1600 Hz, significant at the 95% level. The gradient at this frequency is -0.5 dB(A) / degree. Gradients are negligible at 2000 Hz. Data at frequencies above 2500 Hz is suspect, owing to electromagnetic interference and background noise. More data are required to clarify the variation of noise in each frequency band with angle of attack. Sufficient data have been recorded during this project, but more should be analysed.

TABLE 4.01 OPERATING CONDITIONS FOR EACH DATA SAMPLE

Sample	Mean rpm	Standard deviation rpm	Approximate 50m Wind Speed / m/s	Power	Pitch (from notes)	Upwind Microphone
1	31.73	0.04	10.25	600	84.7 deg	2
2	31.72	0.07	8.25	600	84.7 deg	2
3	25.00	0.09	7.75	230	82.3 deg	12
4	25.32	0.05	7.50	240	82.3 deg	12
5	21.85	0.08	8.00	120	82 deg, 70% full speed	2
6	20.71	0.08	7.00	80	normal operation	2
7	23.79	0.02	7.30	180	normal operation	1
8			7.25	60	60% full speed	
9	21.83	0.27	8.25	120	normal operation	2
10	21.54	0.28	10.50	120	72 deg	2
11	29.45	0.12	7.75	400	normal operation	1
12	28.81	0.12	10.00	380	79.5 deg	1
13	31.56	0.09	10.00	580	normal operation	4
14	30.13	0.07	10.00	440	normal operation	4
15	23.33	0.07	8.00	160	normal operation	4
16	25.07	0.11	8.75	200	normal operation	4
17	24.92	0.23	8.00	200	normal operation	4
18	22.08	0.18	9.95	120	normal operation	4
19	28.56	0.04	9.25	340	normal operation	4
20	19.37	0.04	7.00	60	normal operation	4
21	23.96	0.03	8.50	170	75% full speed, pitch 85 deg	3
22	20.74	0.02	7.00	90	65% full speed, 75 deg pitch	3

TABLE 4.02 TIP SPEEDS, ANGLES OF ATTACK AND SOUND PRESSURE LEVELS FOR DIFFERENT SAMPLES

sample	tip speed / m/s	α , degrees	$\delta\alpha$, degrees	SPL, as measured upwind / dB(A)	SPL, as measured at 90 degrees / dB(A)	SPL, as measured downwind / dB(A)	SPL, as measured at 270 degrees / dB(A)
1	74.77	1.28	0.32	57.51	57.24	62.70	55.75
2	74.75	0.05	0.30	57.92	57.11	59.85	55.63
3	58.91	-0.17	0.36	50.61	52.39	52.82	53.25
4	59.65	-0.42	0.35	51.17	53.39	53.80	52.39
5	51.48	-0.16	0.41	49.30	49.27	50.20	48.18
6	48.79	2.68	0.44	49.54	48.96	58.62	48.14
7	56.06	2.13	0.38	51.51	50.78	50.33	51.28
9	51.44	3.41	0.49	49.60	49.23	71.61	48.99
10	50.76	-3.72	0.36	48.99	48.70	52.66	48.81
11	69.39	1.33	0.33	57.11	56.63	56.52	56.60
12	67.88	-1.22	0.29	55.18	54.31	53.88	54.13
13	74.35	2.31	0.28	59.34	57.54	59.02	57.26
14	70.99	2.71	0.31	57.23	56.03	57.03	55.58
15	54.98	2.77	0.39	50.84	48.70	50.35	49.51
16	59.08	2.88	0.36	52.85	55.11	52.98	50.62
17	58.71	2.38	0.36	53.03	52.19	52.47	50.09
18	52.03	5.12	0.52	50.39	47.26	49.81	48.35
19	67.30	2.43	0.31	56.95	53.34	55.81	53.58
20	45.64	3.11	0.50	45.47	44.65	46.11	44.25
21	56.46	2.09	0.39	50.59	48.49	50.58	48.96
22	48.87	-4.15	0.36	48.11	49.40	50.00	46.75

TABLE 4.03 REGRESSION COEFFICIENTS, SLOPES AND INTERCEPTS FOR SOUND POWER LEVEL VERSUS LOG OF TIP SPEED

Mic Location	Regression Coefficient	Slope / dB(A)/	Intercept / dB(A)
0	0.98	59.18	-4.05
90	0.87	55.81	0.68
180	0.99	58.88	-4.05
270	0.91	52.88	5.92
mean	0.94	56.69	-0.38
standard deviation (population)	0.05	2.56	4.12

TABLE 4.04 NORMALISED SOUND PRESSURE LEVELS AS A FUNCTION OF AND ANGLE OF ATTACK

sample	tip speed m/s	α degrees	$\delta\alpha$ degrees	Normalised SPL / dB(A)			
				upwind	90 deg	downwind	270 deg
1	74.77	1.276	0.318	-1.782	-0.456	-1.470	-1.695
2	74.75	0.050	0.301	-1.358	-0.579	-1.593	-1.813
3	58.91	-0.166	0.362	-2.551	0.465	-0.231	1.278
4	59.65	-0.415	0.355	-2.314	1.168	0.455	0.132
5	51.48	-0.159	0.412	-0.405	0.612	0.096	-0.699
6	48.79	2.681	0.438	1.294	1.605	1.160	1.315
7	56.06	2.130	0.380	-0.297	1.465	-0.941	-1.692
9	51.44	3.414	0.493	0.004	-1.375	-1.890	0.824
10	50.76	-3.724	0.364	-0.345	0.384	-0.114	0.260
11	69.39	1.330	0.330	-0.262	0.739	-0.285	0.866
12	67.88	-1.218	0.294	-1.626	-1.046	-1.931	-1.099
13	74.35	2.313	0.283	0.303	-0.022	0.560	-1.438
14	70.99	2.310	0.280	0.193	-0.024	0.449	-0.059
15	54.98	2.710	0.310	-0.728	-0.414	-0.358	-0.677
16	59.08	2.882	0.363	-0.281	3.124	0.372	0.396
17	58.71	2.380	0.360	0.110	-1.057	0.041	1.389
18	52.03	5.123	0.523	0.502	0.318	0.431	0.611
19	67.30	2.434	0.313	0.464	-1.807	-0.040	-0.807
20	45.64	3.110	0.500	-1.134	-1.086	0.017	-1.862
21	56.46	2.090	0.393	-1.487	-2.408	-3.048	-2.036
22	48.87	-4.149	0.360	-0.254	2.007	1.560	-0.930

TABLE 4.05 REGRESSION COEFFICIENTS FOR SOUND PRESSURE LEVELS IN DIFFERENT FREQUENCY BANDS VERSUS ANGLE OF ATTACK (MICROPHONES UPWIND)

Third Octave Band Centre Frequency / Hz	Gradient dB(A)	Intercept / dB(A)	Regression coefficient	Significance
100	0.010	-0.012	0.00	0.03
125	0.165	-0.211	0.03	0.56
160	-0.045	0.058	0.00	0.15
200	0.011	-0.014	0.00	0.06
250	0.257	-0.328	**0.14**	**0.90**
315	0.141	-0.181	0.03	0.57
400	0.337	-0.431	**0.14**	**0.90**
500	0.368	-1.291	**0.19**	**0.95**
630	0.269	-0.699	**0.12**	**0.83**
800	0.188	-0.771	**0.14**	**0.84**
1000	0.116	-0.589	0.03	0.50
1250	0.098	-0.409	0.02	0.42
1600	-0.069	0.235	0.01	0.29
2000	0.060	-0.140	0.03	0.43
2500	0.124	-0.412	**0.09**	**0.80**
3150	0.308	-0.992	**0.25**	**0.98**
4000	0.022	-0.270	0.00	0.12

TABLE 4.06 REGRESSION COEFFICIENTS FOR SOUND PRESSURE LEVELS IN DIFFERENT FREQUENCY BANDS VERSUS ANGLE OF ATTACK (MICROPHONES DOWNWIND)

Third Octave Band Centre Frequency / Hz	Gradient dB(A)	Intercept / dB(A)	Regression coefficient	Significance
100	-0.417	0.456	0.05	0.63
1250	-0.056	0.061	0.00	0.13
160	-0.048	0.053	0.00	0.10
200	-0.086	0.093	0.00	0.17
250	-0.015	0.017	0.00	0.03
315	-0.075	0.082	0.00	0.18
400	-0.344	0.376	0.04	0.60
500	-0.080	0.087	0.01	0.27
630	0.064	-0.070	0.00	0.22
800	0.092	-0.101	0.01	0.37
1000	0.075	-0.082	0.01	0.34
1250	-0.546	0.597	**0.23**	**0.96**
1600	-0.276	0.302	**0.20**	**0.95**
2000	0.002	-0.003	0.00	0.01
2500	0.257	-0.281	**0.20**	**0.95**
3150	0.381	-0.417	**0.14**	**0.89**
4000	0.717	-0.784	**0.28**	**0.98**

TABLE 4.07 REGRESSION COEFFICIENTS FOR SOUND PRESSURE LEVELS IN DIFFERENT FREQUENCY BANDS VERSUS ANGLE OF ATTACK (MICROPHONES AT 90 DEGREES TO UPWIND)

Third Octave Band Centre Frequency / Hz	Gradient dB(A)	Intercept / dB(A)	Regression coefficient	Significance
125	-0.656	0.839	**0.25**	**0.98**
160	-0.562	0.718	**0.17**	**0.93**
200	-0.631	0.807	**0.24**	**0.98**
250	-0.527	0.674	**0.25**	**0.98**
315	-0.632	0.808	**0.30**	**0.99**
400	0.150	-0.192	0.01	0.32
500	-0.144	0.184	0.02	0.48
630	-0.174	0.223	0.04	0.63
800	0.045	-0.058	0.00	0.22
1000	-0.010	0.012	0.00	0.05
1250	-0.393	0.503	**0.22**	**0.97**
1600	-0.397	0.508	**0.22**	**0.97**
2000	-0.073	0.093	0.01	0.38
2500	-0.039	0.050	0.01	0.24
3150	0.051	-0.065	0.00	0.21
4000	-0.056	0.071	0.00	0.19

TABLE 4.08 REGRESSION COEFFICIENTS FOR SOUND PRESSURE LEVELS IN DIFFERENT FREQUENCY BANDS VERSUS ANGLE OF ATTACK (MICROPHONES AT 270 DEGREES TO UPWIND)

Third Octave Band Centre Frequency / Hz	Gradient dB(A)	Intercept / dB(A)	Regression coefficient	Significance
100	-0.383	0.489	**0.21**	**0.97**
1250	-0.269	0.345	0.04	0.60
160	-0.391	0.500	**0.22**	**0.97**
200	-0.395	0.505	**0.31**	**0.99**
250	-0.283	0.362	**0.17**	**0.94**
315	-0.233	0.298	**0.17**	**0.94**
400	0.008	-0.010	0.00	0.02
500	-0.085	0.109	0.01	0.39
630	0.033	-0.042	0.00	0.13
800	-0.028	0.036	0.00	0.14
1000	-0.025	0.032	0.00	0.19
1250	-0.047	0.060	0.00	0.23
1600	-0.166	0.213	**0.10**	**0.85**
2000	-0.150	0.192	0.08	0.78
2500	-0.066	0.085	0.01	0.35
3150	0.037	-0.048	0.00	0.12
4000	-0.028	0.035	0.00	0.08

References

[1] "Experimental Procedure for Noise Measurements made on Markham's VS45 at Kaiser-Wilhelm-Koog, Germany", P. Dunbabin, RES report 059/RES/2001, issue 1, 5/6/97

[2] "First Sixth Monthly Progress Report", P. Dunbabin, RES report 059/RES/2002, issue 1, 26/06/97

[3]"Checks made to Acoustic Data from VS45 Prior to Analysis", P. Dunbabin, RES report 059/RES/2005, issue 1, 6/1/97

[4] "Calculation of Mechanical Noise Radiated from the Nacelle of the VS45", P. Dunbabin, RES report 059/RES/2004, 31/10/96.

[5] "1 MW Horizontal Axis Wind Turbine, Acoustic Design of Nacelle", A.J. Bullmore, Hoare Lea and Partners report number DMB-AJB/6-1-94/S00059/RI, 6/01/96

Figure 3.01
Calculated Angle of Attack over Last 10% of Blade, for Different Data Samples

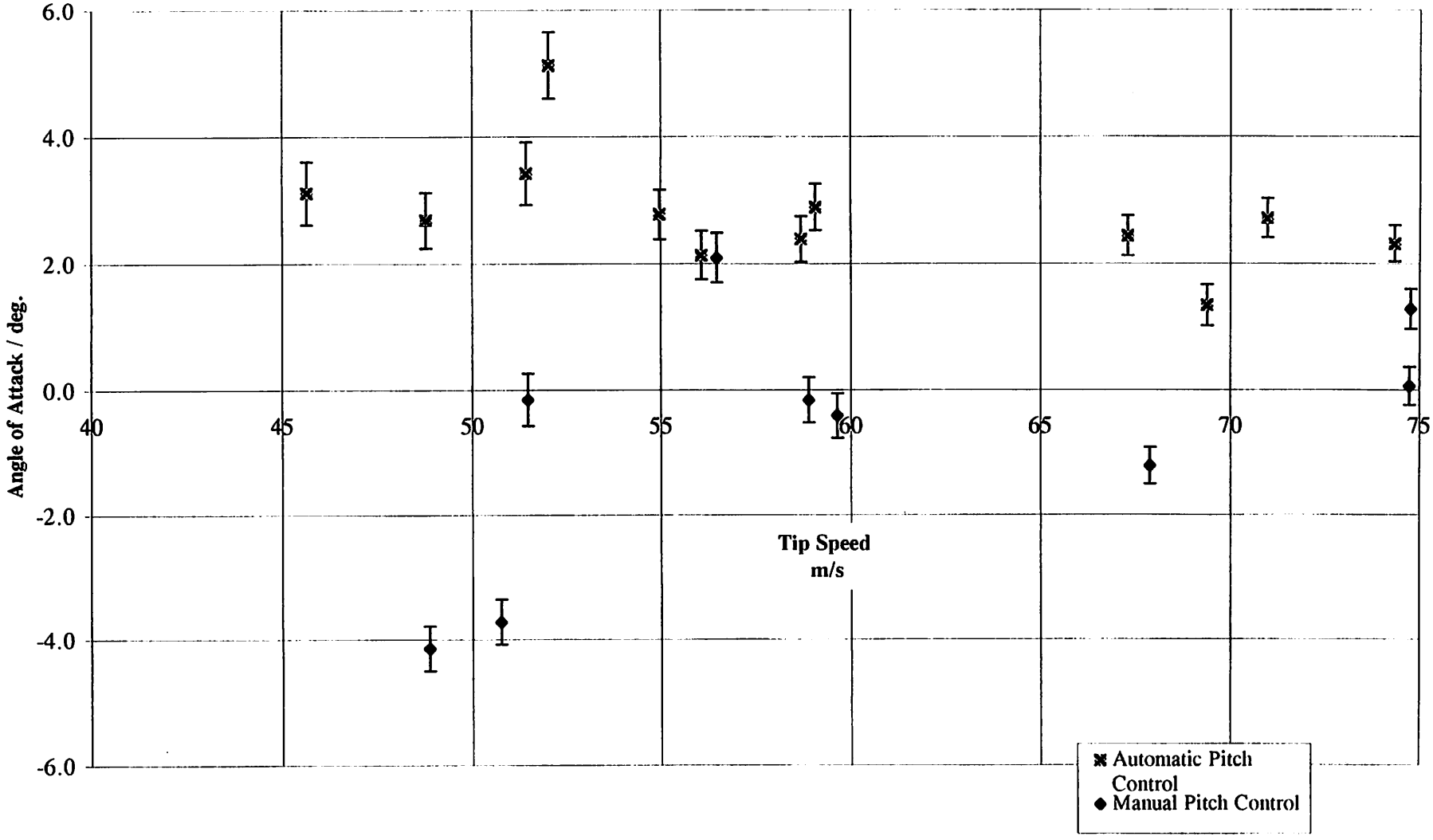

Figure 4.01
Sound Power Level , versus Log(Tip Speed)
LWA Calculated from Upwind and Downwind Measurements of Sound Pressure Level Data have been corrected for tones

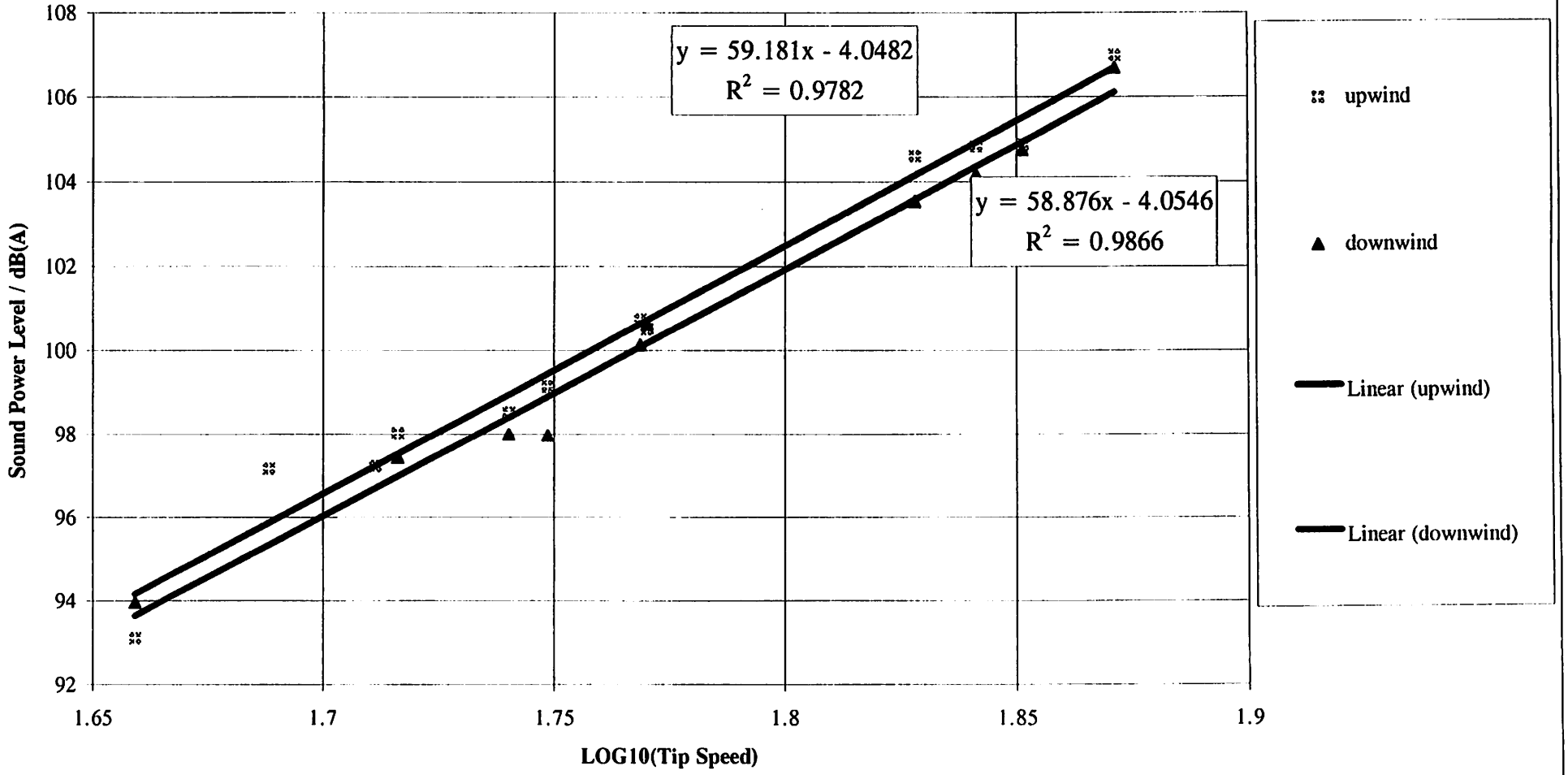

Figure 4.02
Sound Power Level , versus Log(Tip Speed)
LWA Calculated from Crosswind Measurements of Sound Pressure Level
Data have been corrected for tones

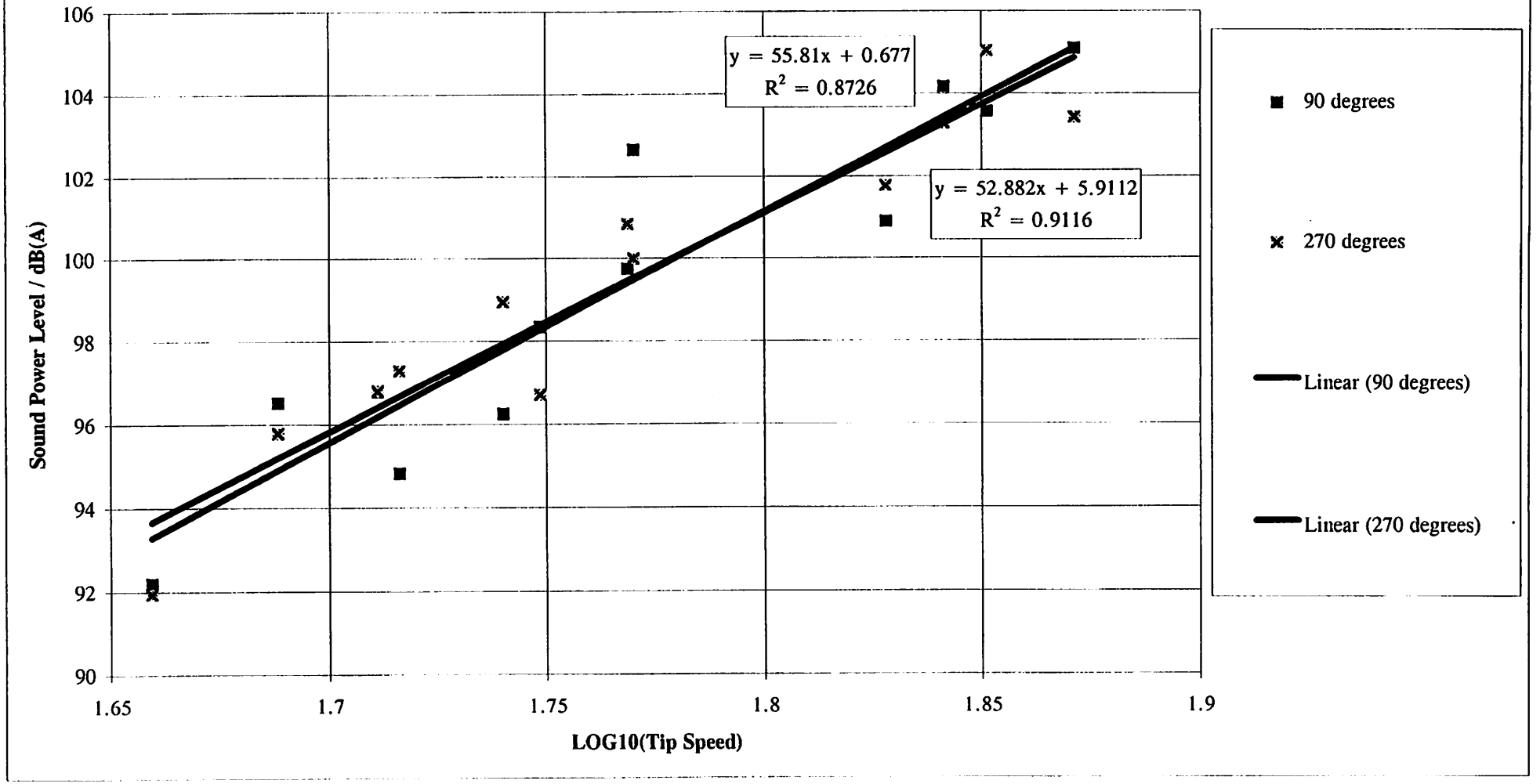

Figure 4.04
Gradients for Regression Lines (SPL versus Log(Tip Speed)), in Different Frequency Bands

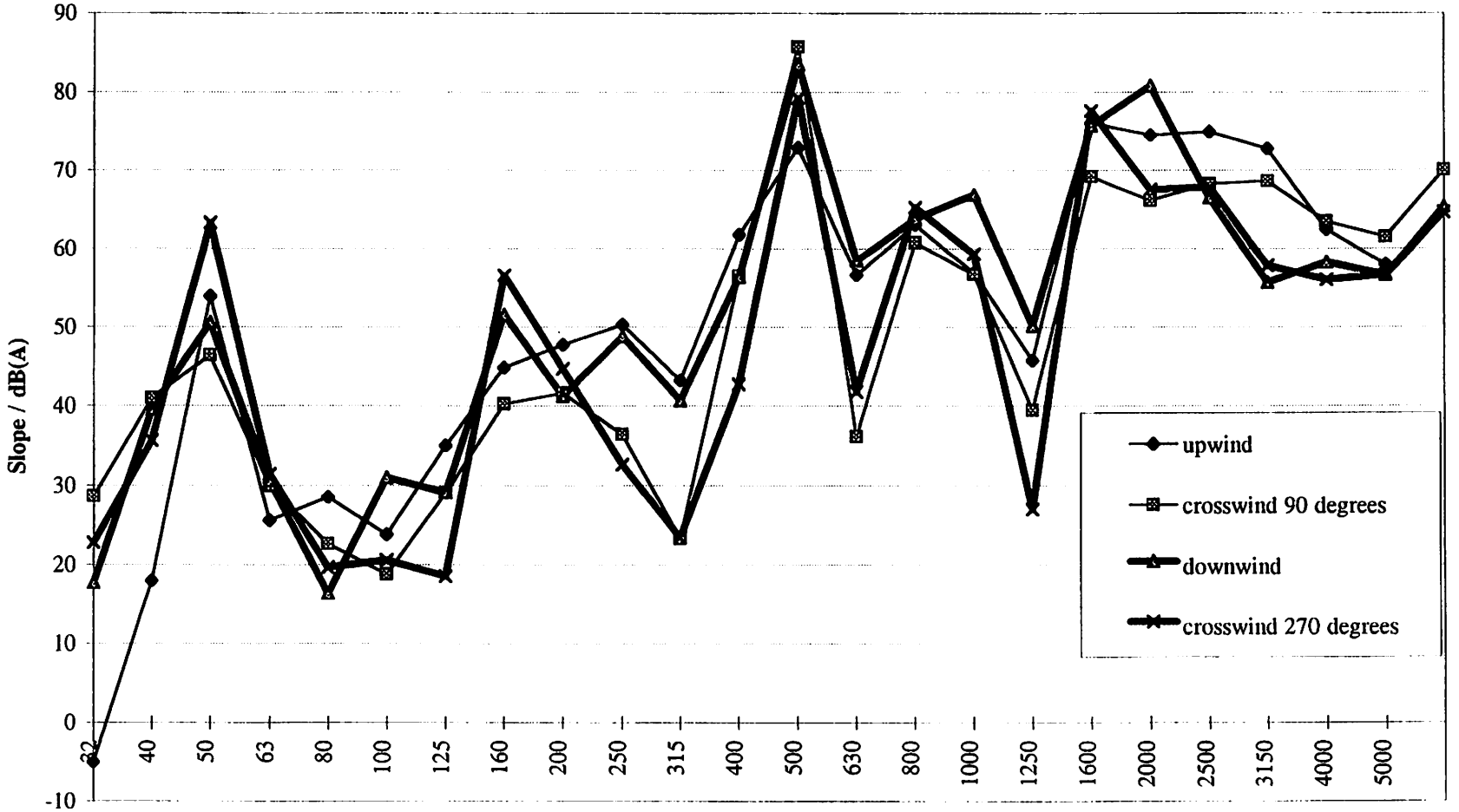

Figure 4.06
Gradients for Regression Lines (SPL versus Log(Tip Speed)), in Different Frequency Bands

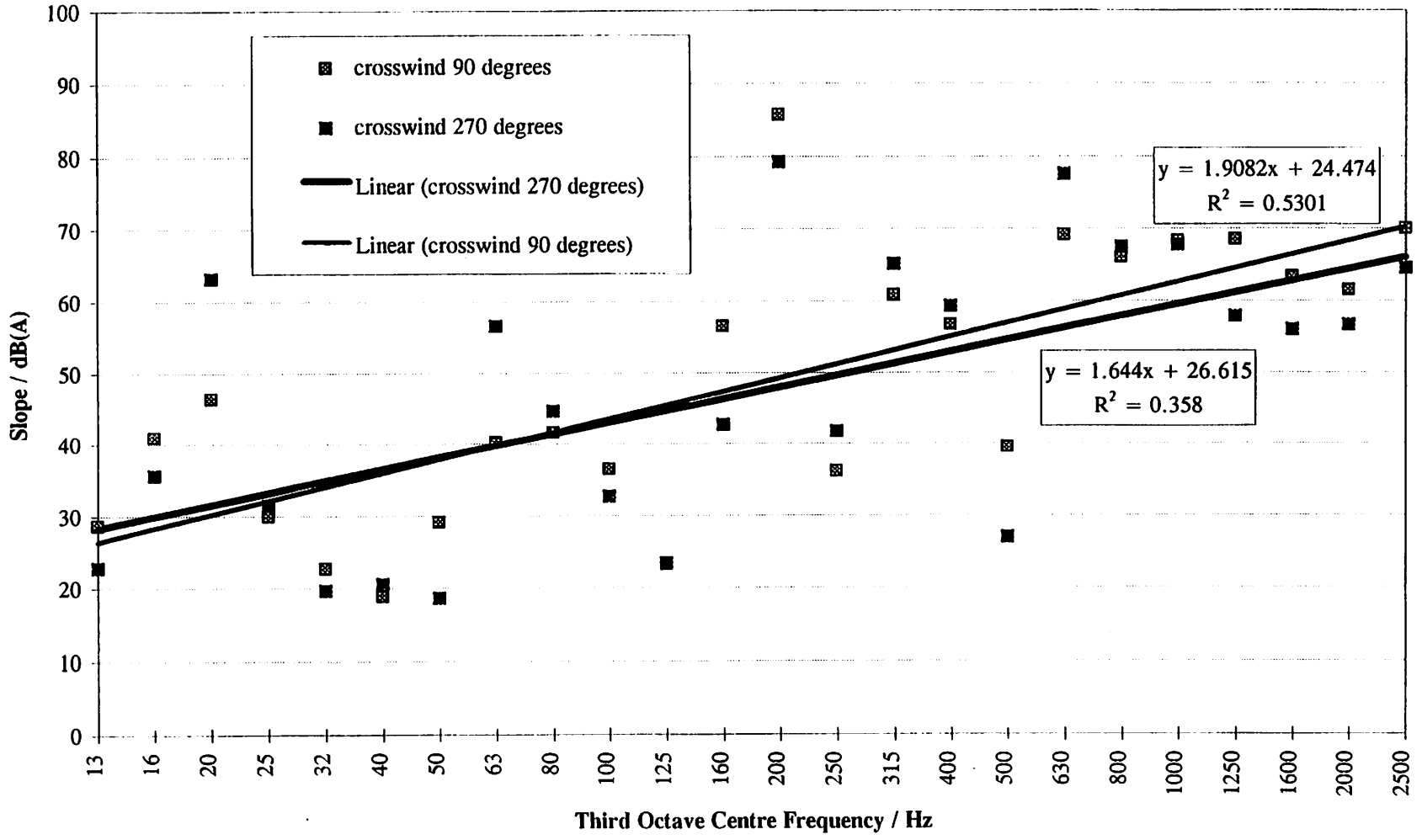

Figure 4.05
Gradients for Regression Lines (SPL versus Log(Tip Speed)), in Different Frequency Bands

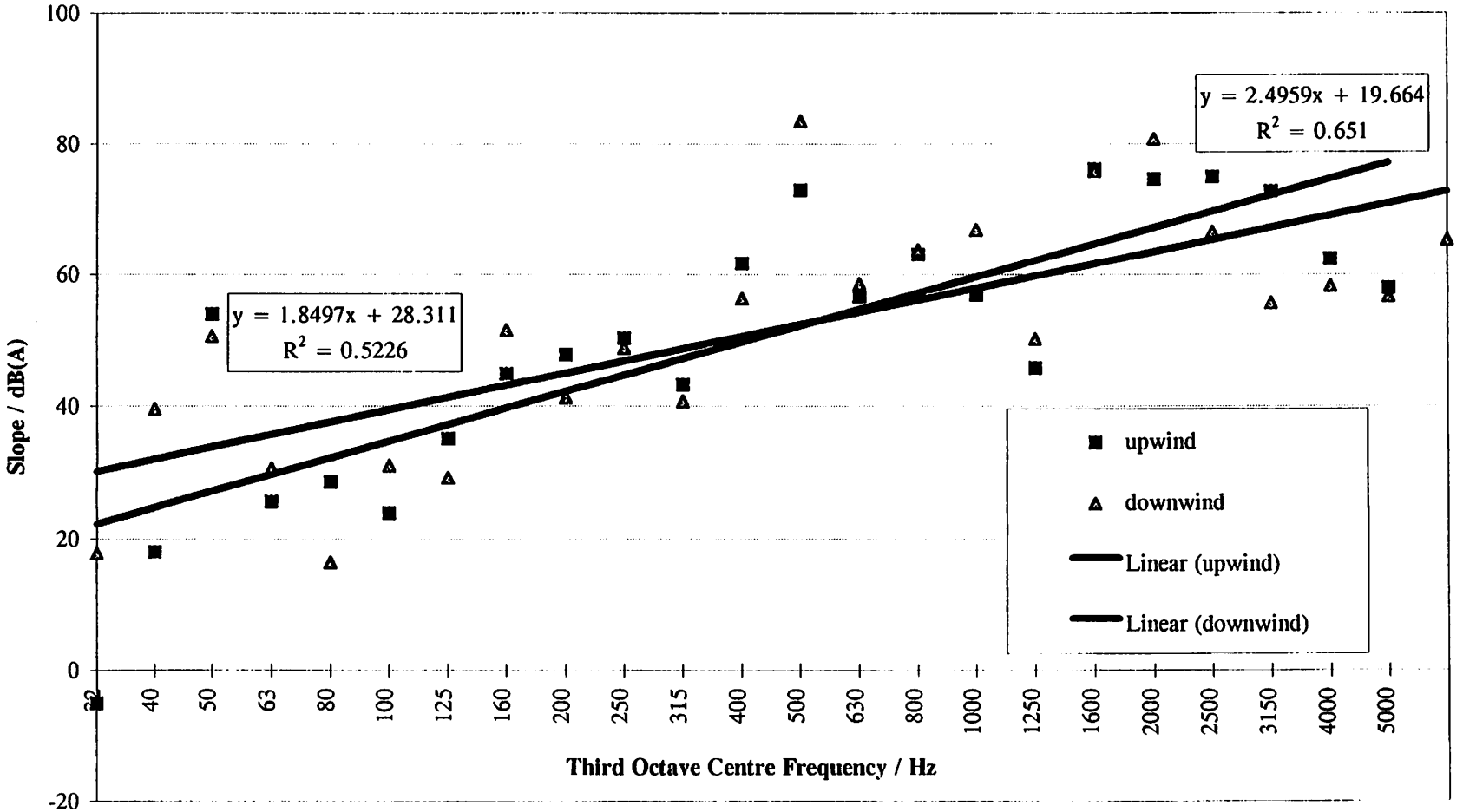

Figure 4.08
Graph of SPL (Normalised for Tip Speed) Against Angle of Attack over the Outermost 10% of the Blade

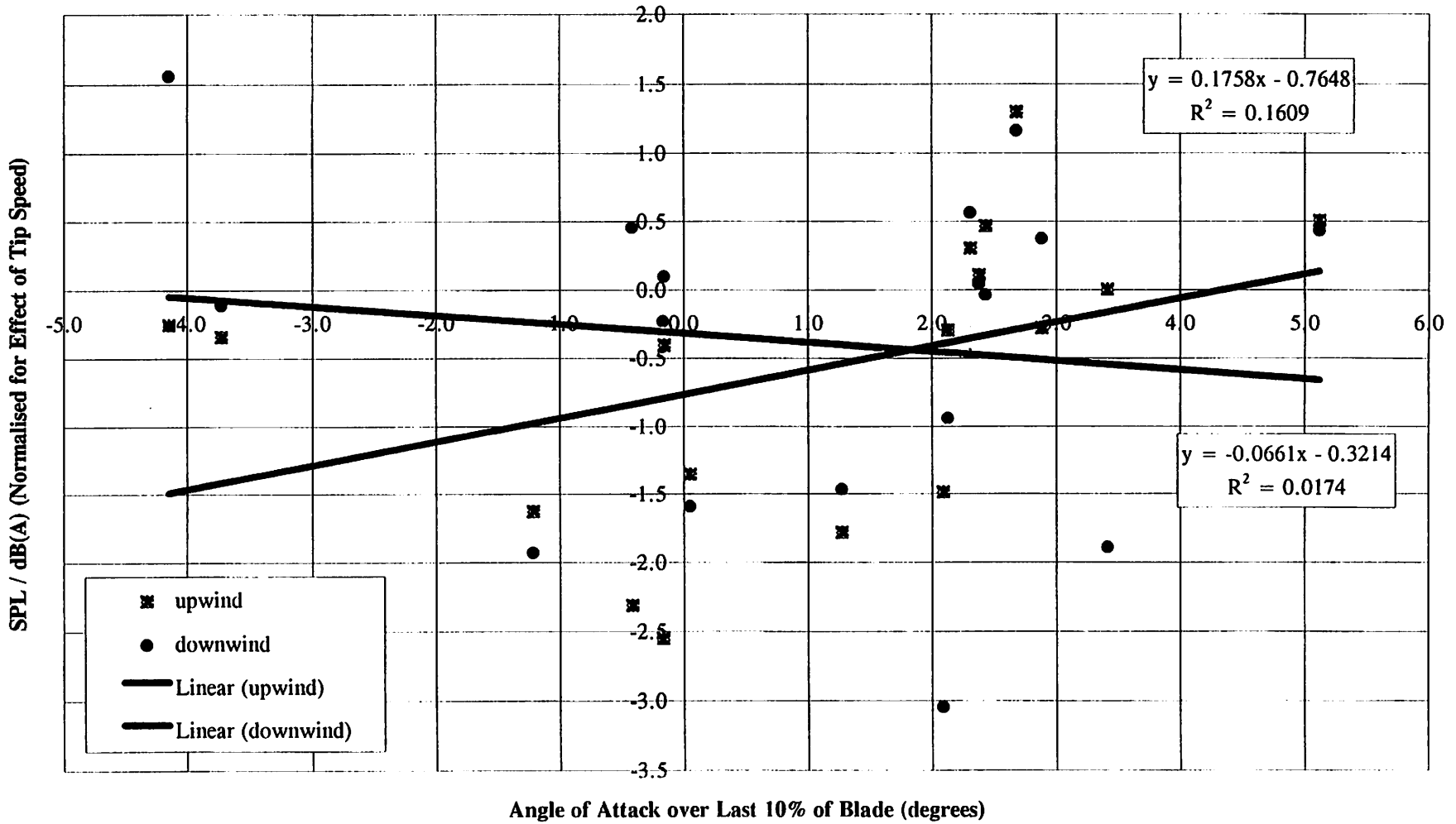

Figure 4.09
Graph of SPL (Normalised for Tip Speed) Against Angle of Attack over the Outermost 10% of the Blade

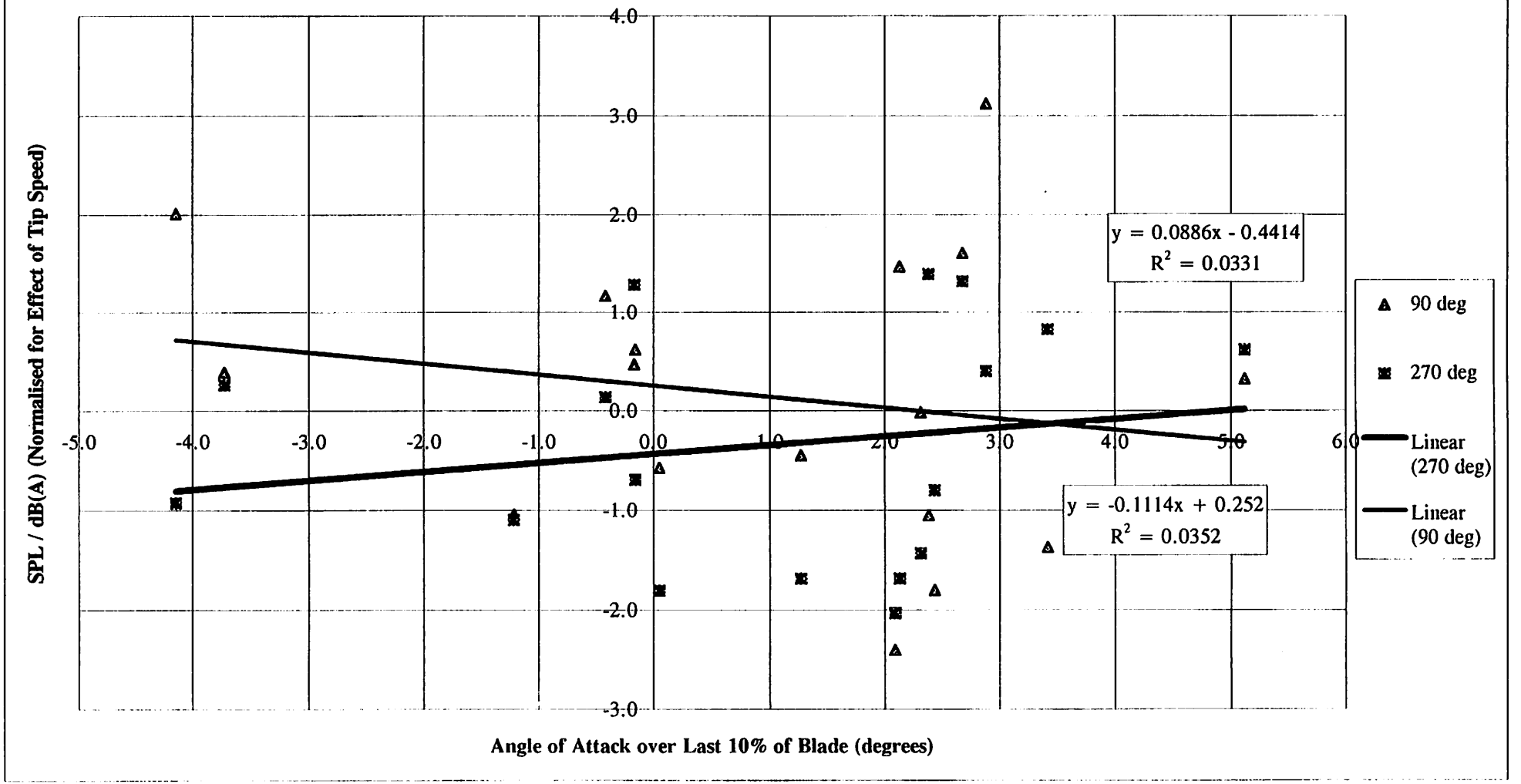

Figure 4.10
Graph of SPL (Normalised for Tip Speed) Against Modulus of Angle of Attack over the Outermost 10% of the Blade

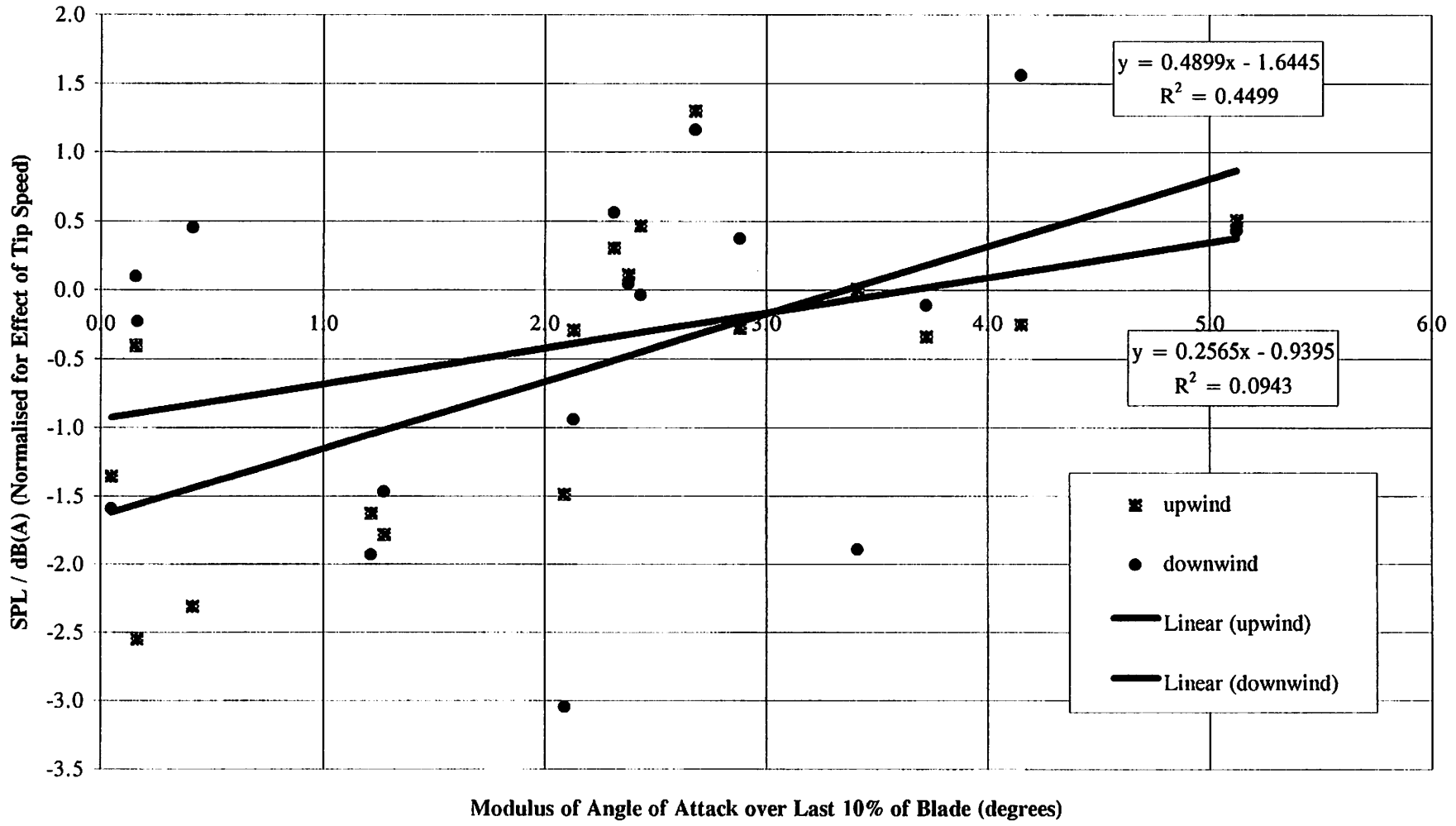

Figure 4.11
Graph of SPL (Normalised for Tip Speed) Against Modulus of Angle of Attack over the Outermost 10% of the Blade

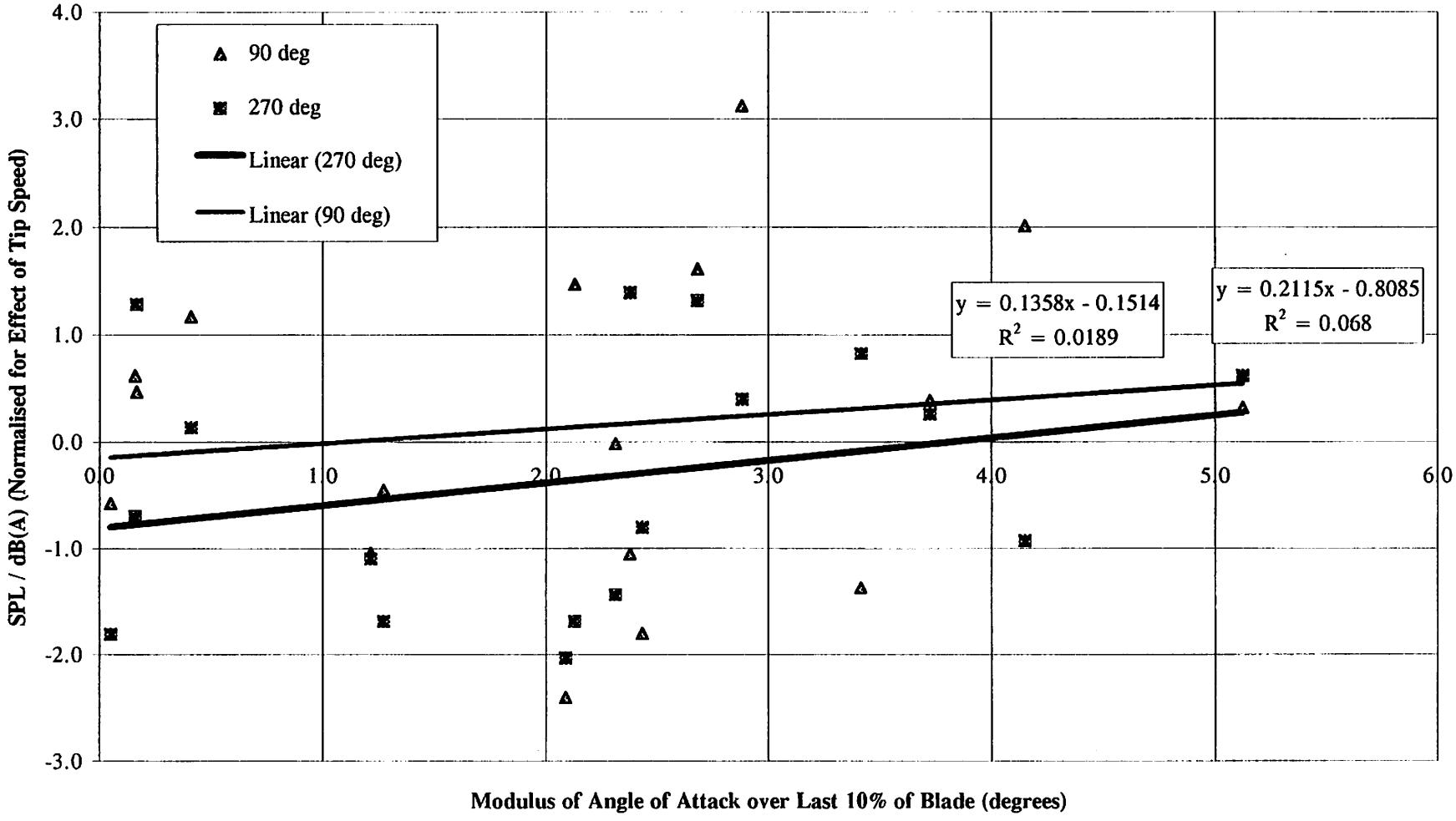

Figure 4.12
Graph of SPL (Normalised for Tip Speed) Against Square of Angle of Attack over the Outermost 10% of the Blade

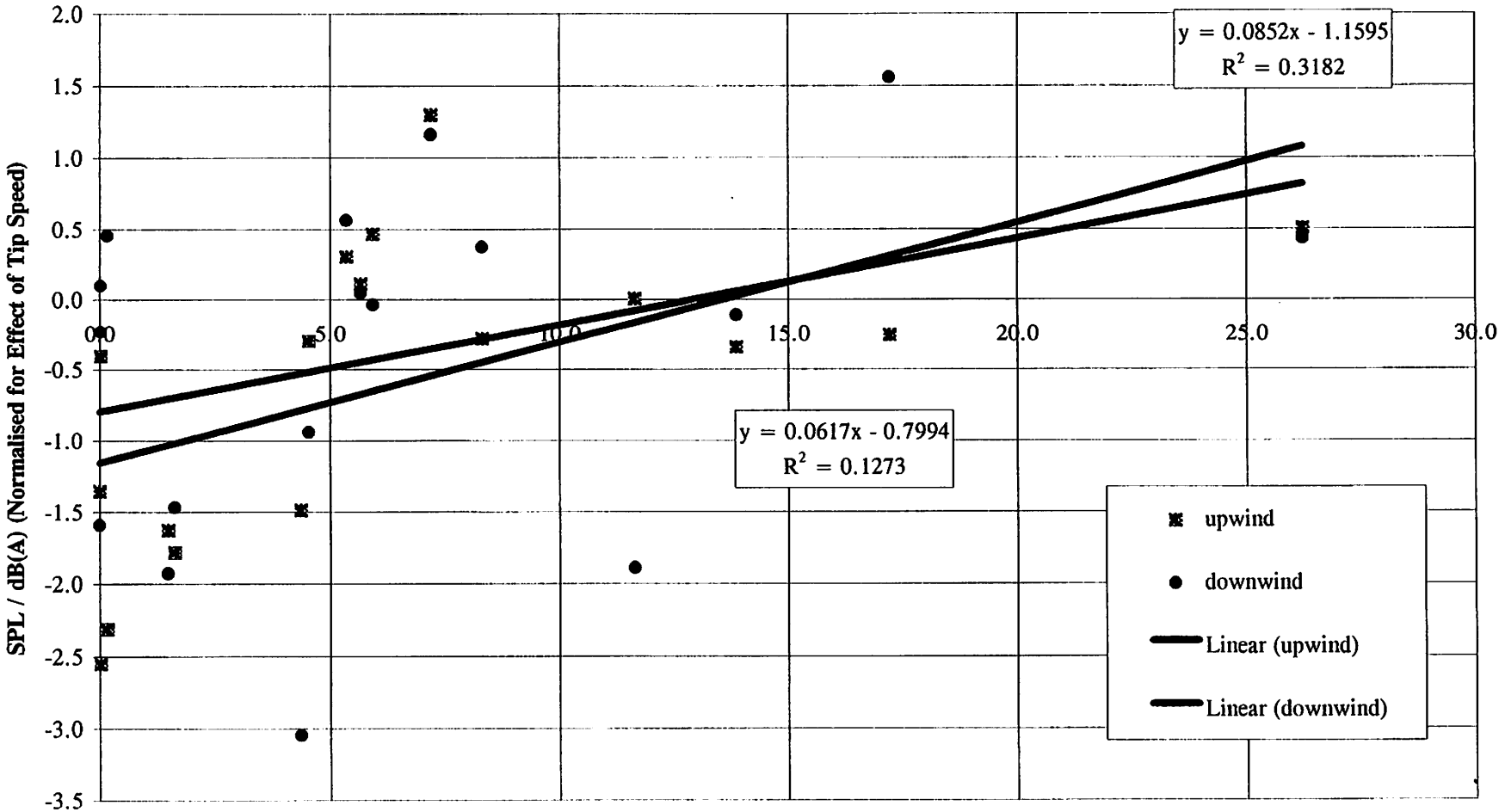

Figure 4.13
Graph of SPL (Normalised for Tip Speed) Against Square of Angle of Attack over the Outermost 10% of the Blade

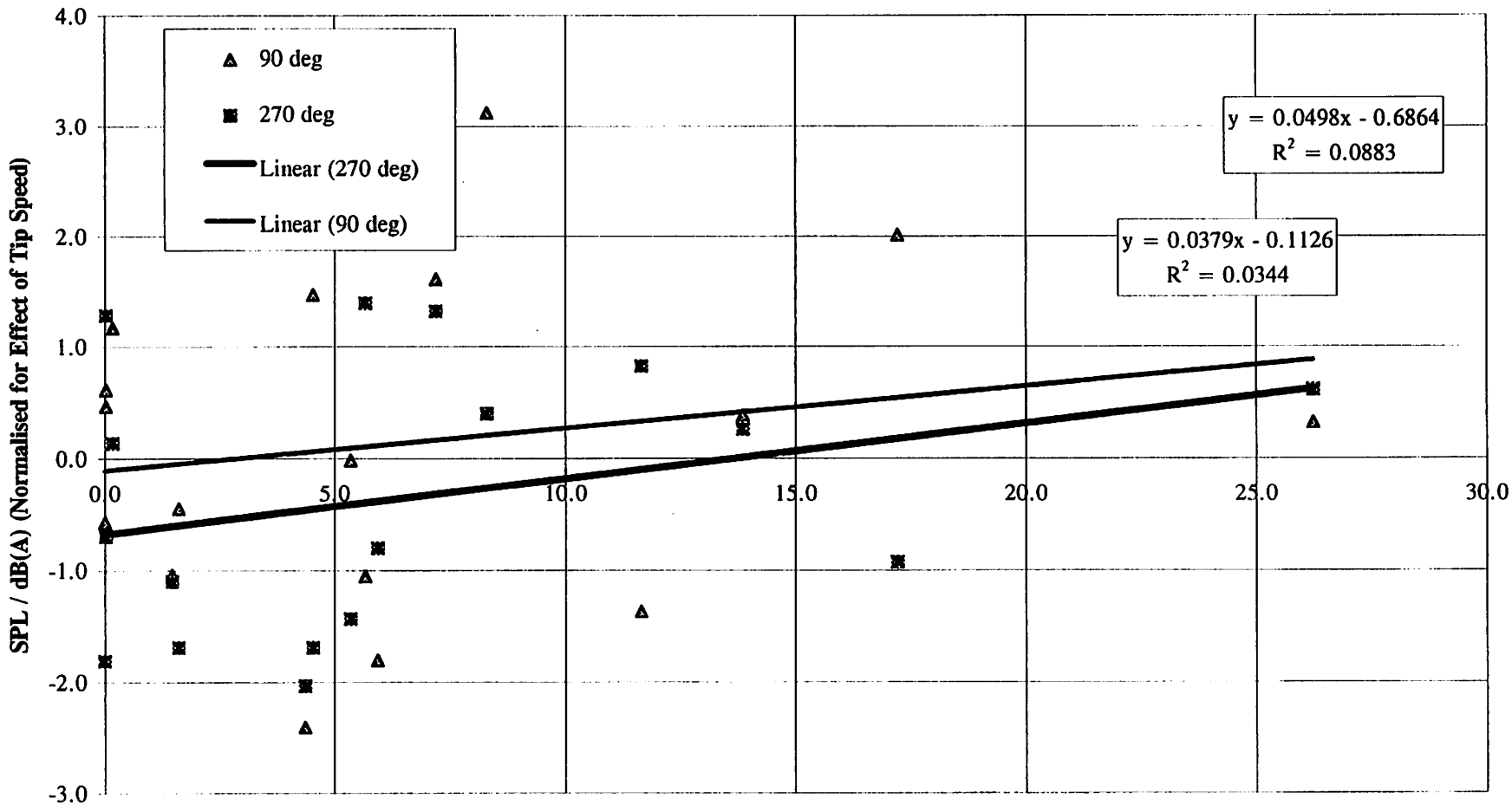

Figure 4.14
Example of Third Octave SPL Versus Angle of Attack
Microphone upwind, data normalised for tip speed)

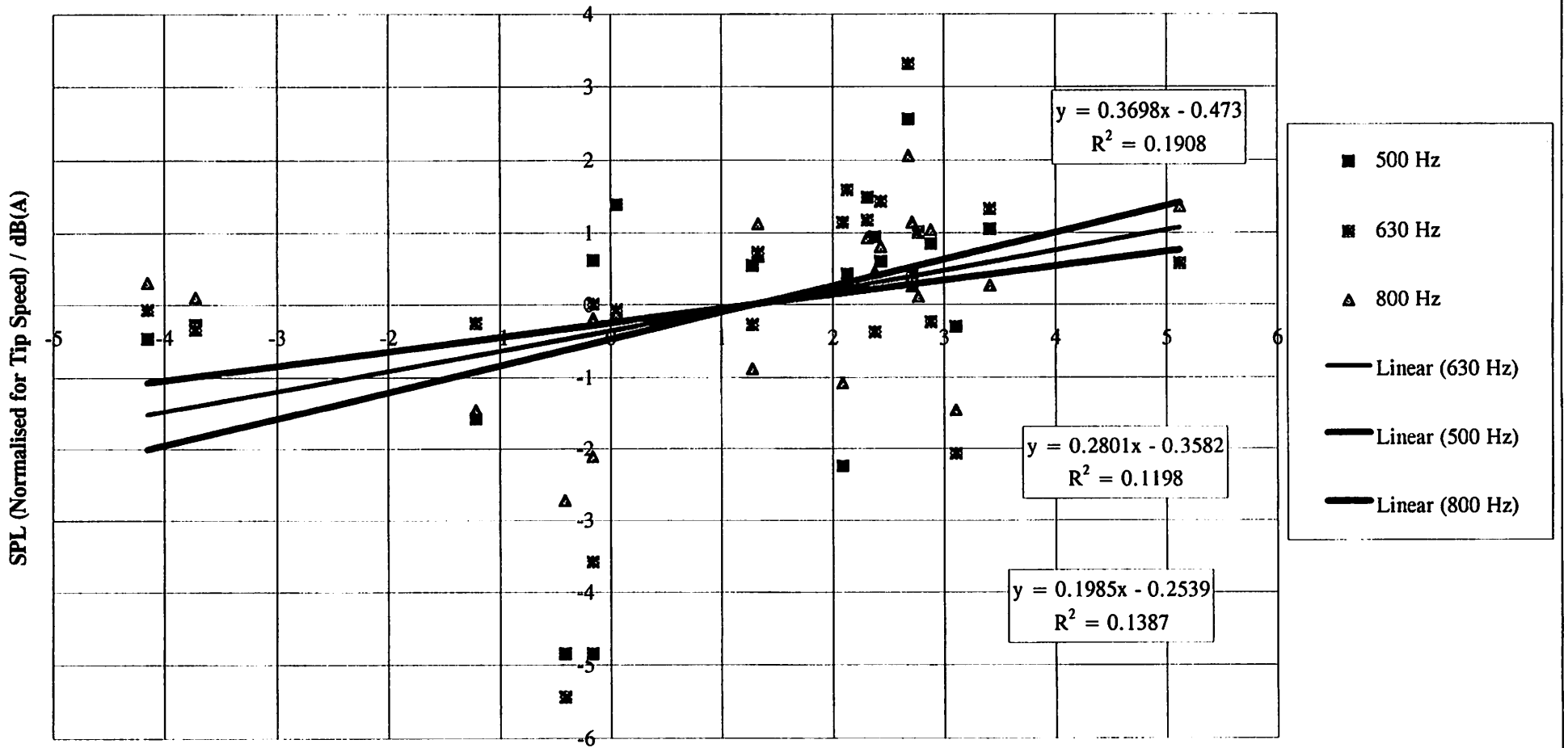

Figure 4.15
Example of Third Octave SPL Versus Angle of Attack,
Microphone Crosswind (270 degrees), Data Normalised for Tip Speed

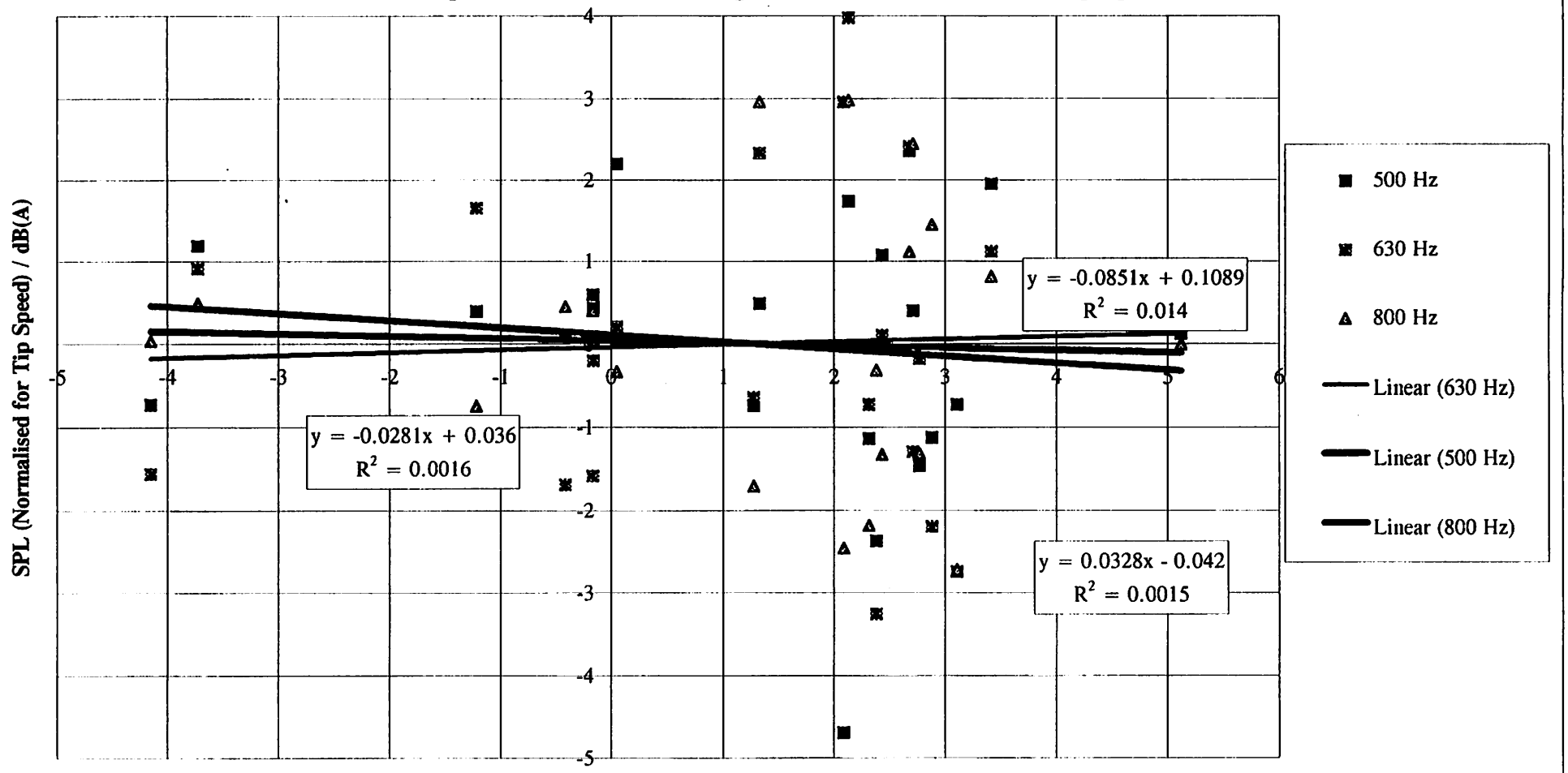

Aeroacoustic Computation of Low Mach Number Flow*

Kristian Skriver Dahl
Risø National Laboratory
DK-4000 Roskilde, Denmark
☎ (+45) 4677 5036
kristian.s.dahl@risoe.dk

March 13, 1997

Abstract

The possibilities of applying a recently developed numerical technique to predict aerodynamically generated sound from wind turbines is explored. The technique is a perturbation technique that has the advantage that the underlying flow field and the sound field are computed separately. Solution of the incompressible, time dependent flow field yields a hydrodynamic density correction to the incompressible constant density. The sound field is calculated from a set of equations governing the inviscid perturbations about the corrected flow field. Here, the emphasis is placed on the computation of the sound field. The nonlinear partial differential equations governing the sound field are solved numerically using an explicit MacCormack scheme. Two types of nonreflecting boundary conditions are applied; one based on the asymptotic solution of the governing equations and the other based on a characteristic analysis of the governing equations. The former condition is easy to use and it performs slightly better than the characteristic based condition. The technique is applied to the problems of the sound generation of a co-rotating vortex pair, which is a quadrupole, and the viscous flow over a circular cylinder, which is a dipole. Numerical results agree very well with the analytical solution for the problem of the co-rotating vortex pair. Numerical results for the viscous flow over a cylinder are presented and evaluated qualitatively.

*Presentation at IEA Expert Meeting on Aeroacoustics, March 17–18, 1997, Milano

Aeroacoustic Computation of Low Mach Number Flow

Kristian Skriver Dahl
Risø National Laboratory
DK-4000 Roskilde, Denmark
kristian.s.dahl@risoe.dk

o

IEA Meeting on Aeroacoustics, March 17–18, 1997, Milano

Reference

Dahl, Kristian Skriver," Aeroacoustic Computation of Low Mach Number Flow," Risø–R–947(EN), 1996, (Ph.D. thesis)

95

Outline

1. Objective
2. Governing equations
3. Numerical scheme
4. Boundary conditions
5. Numerical test cases
   - *Co-rotating vortex pair*
   - *Viscous flow over cylinder (video)*
6. Future work

Objective

RISØ

Application of a purely numerical method for prediction of aerodynamic noise

Two-dimensional aeroacoustic computation is perhaps possible for

- *separation-stall*
- *vortex shedding from the blunt trailing edge*

97

CAA vs CFD

RISØ

CFD: Flowfield
CAA: Flowfield and acoustic field

CFD: Time independent and time dependent
CAA: Only time dependent

CFD: Interest is on near-field, e.g., lift and drag on airfoil
CAA: Interest is on far-field, sound at the receiver

CFD: Smaller computational domains
CAA: Larger computational domains

CFD: Stretched meshes for good resolution of viscous layers
CAA: Uniform meshes for good wave tracking

Direct Numerical Simulation

RISØ

Time dependent, compressible N.S. equations describe both flow and acoustics.

Problems are:

- one scheme and one mesh
- numerical errors in flow variables may corrupt the weak acoustic field

99

Acoustic/Viscous splitting, Hardin&Pope 1992

Split problem into a viscous, incompressible flow part and an inviscid, compressible, acoustic part.

Advantages over direct numerical simulation:

- inaccuracies in flow field do not dominate acoustic field
- different schemes and meshes can be used for each field

Other characteristics:

- flow is incompressible
- constant density is corrected
- no feedback from acoustics to flow

100

Incompressible flow equations

Continuity equation,

$$\nabla \cdot V = 0,$$

and momentum equations,

$$\rho_0 \left(\frac{\partial V}{\partial t} + V \cdot \nabla V \right) = -\nabla P + \mu_0 \nabla^2 V,$$

gives

$$\rho_0,\ V(x,t), \text{and } P(x,t).$$

Hydrodynamic density correction

$$\rho_1(\boldsymbol{x},t) = \frac{P(\boldsymbol{x},t) - \overline{P}(\boldsymbol{x})}{c_0^2},$$

$$\overline{P}(\boldsymbol{x}) = \lim_{T\to\infty} \frac{1}{T} \int_0^T P(\boldsymbol{x},t)dt,$$

gives corrected flow field:

$$\rho_0 + \rho_1(\boldsymbol{x},t),\ \boldsymbol{V}(\boldsymbol{x},t), \text{and } P(\boldsymbol{x},t).$$

Perturbation equations

$$\rho = \rho_0 + \rho_1 + \rho', \; \boldsymbol{v} = \boldsymbol{V} + \boldsymbol{v}', \; p = P + p'.$$

$$\frac{\partial \rho'}{\partial t} + \boldsymbol{v}\cdot\nabla\rho' + \rho\nabla\cdot\boldsymbol{v}' = -\frac{\partial \rho_1}{\partial t} - \boldsymbol{v}\cdot\nabla\rho_1,$$

$$\frac{\partial \boldsymbol{v}'}{\partial t} + \boldsymbol{v}\cdot\nabla\boldsymbol{v}' + \frac{\nabla p'}{\rho} = -\frac{\rho_1 + \rho'}{\rho}\frac{\partial \boldsymbol{V}}{\partial t} - \left(\frac{\rho_1 + \rho'}{\rho}\boldsymbol{V} + \boldsymbol{v}'\right)\cdot\nabla\boldsymbol{V},$$

$$\frac{\partial p'}{\partial t} + \boldsymbol{v}\cdot\nabla p' + \rho c^2\nabla\cdot\boldsymbol{v}' = 0.$$

MacCormack scheme

Model equation: $\frac{\partial u}{\partial t} = -\frac{\partial u}{\partial x}$

Predictor step: $\left(\frac{\partial u}{\partial t}\right)_i^n = -\frac{u_{i+1}^n - u_i^n}{\Delta x}$

$$\overline{u_i^{n+1}} = u_i^n + \left(\frac{\partial u}{\partial t}\right)_i^n \Delta t$$

Corrector step: $\left(\frac{\partial u}{\partial t}\right)_i^{\overline{n+1}} = -\frac{\overline{u_i^{n+1}} - \overline{u_{i-1}^{n+1}}}{\Delta x}$

$$u_i^{n+1} = u_i^n + \frac{1}{2}\left[\left(\frac{\partial u}{\partial t}\right)_i^n + \left(\frac{\partial u}{\partial t}\right)_i^{\overline{n+1}}\right] \Delta t$$

Boundary conditions, Tam&Webb 1993

Asymptotic solution of the linearized, Fourier-Laplace transformed Euler equations yields:

$$\phi(r,\, t) = \frac{f(r - (V_r + c)t)}{r^{1/2}},$$

Taking time and r derivatives yields upon elimination of f:

$$\frac{1}{V_r + c}\frac{\partial \phi}{\partial t} + \frac{\partial \phi}{\partial r} + \frac{\phi}{2r} = 0.$$

A center of radiation should be chosen to define the radial distance r.

Boundary conditions, Thompson 1987

Characteristic form of governing equations:

$$l_i \frac{\partial U}{\partial t} + \mathcal{L}_i + l_i C = 0, \; \mathcal{L}_i = \begin{cases} \lambda_i l_i \dfrac{\partial U}{\partial x} & \text{for outgoing waves,} \\ 0 & \text{for incoming waves.} \end{cases}$$

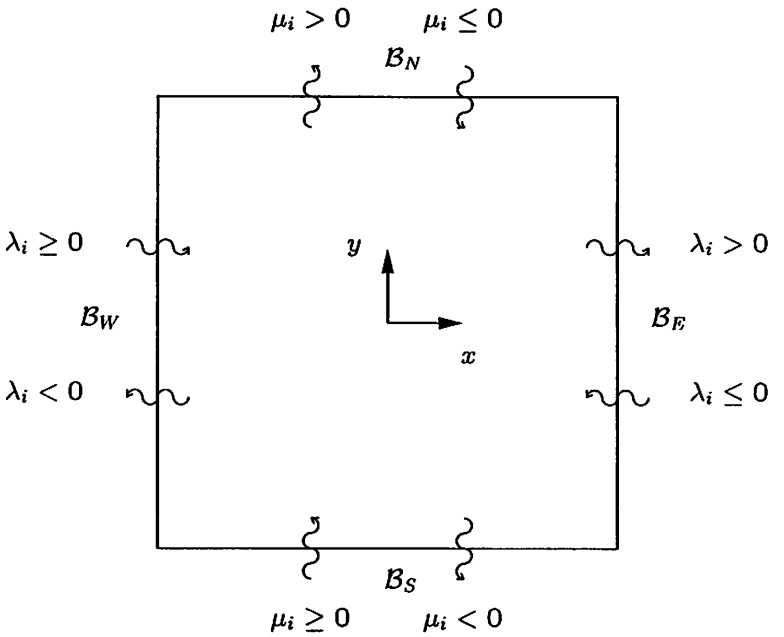

Numerical test cases

1. Co-rotating vortex pair
2. Viscous flow over cylinder

Co-rotating vortex pair

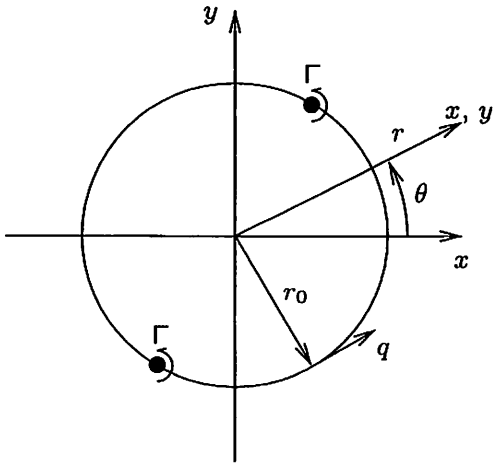

- Quadrupole
- Two-dimensional
- Cartesian coordinates
- Exact solution for flow field
- Computational domain: $-100 \leq x/r_0 \leq 100$, $-100 \leq y/r_0 \leq 100$, 81×81 mesh points

Results for co-rotating vortex pair

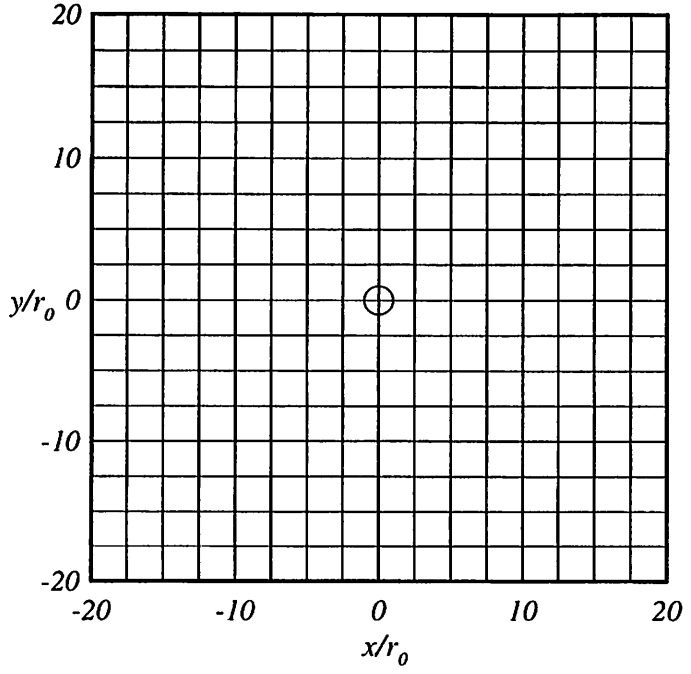

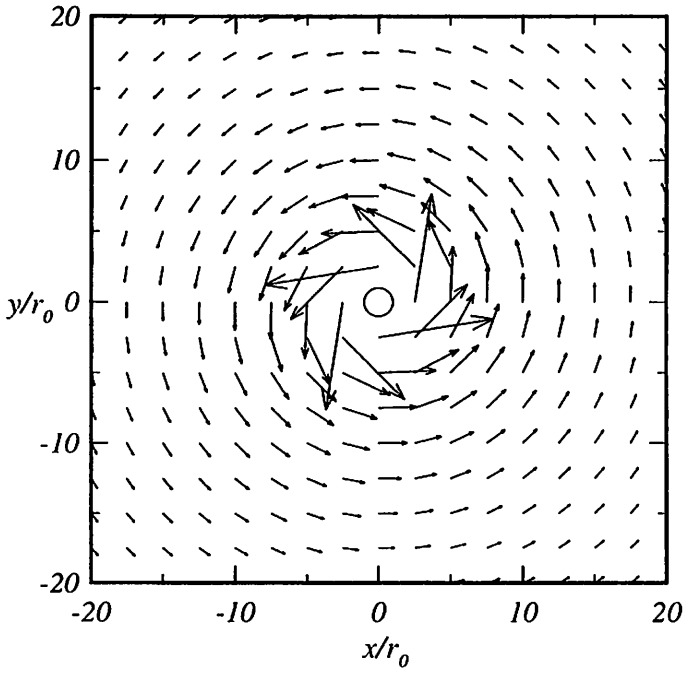

Acoustic pressure for co-rotating vortex pair

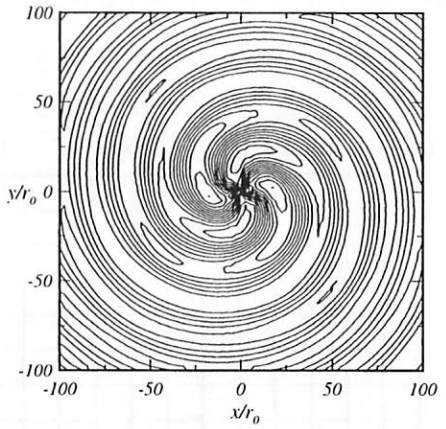

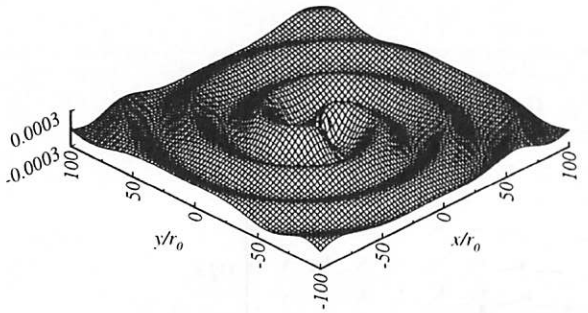

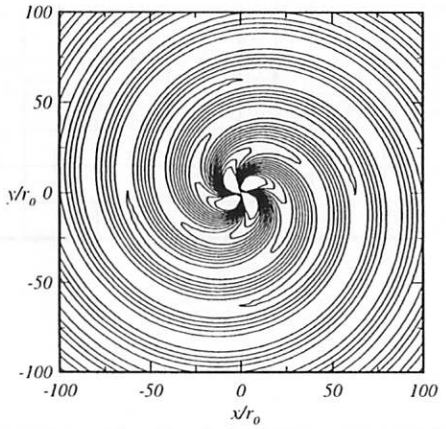

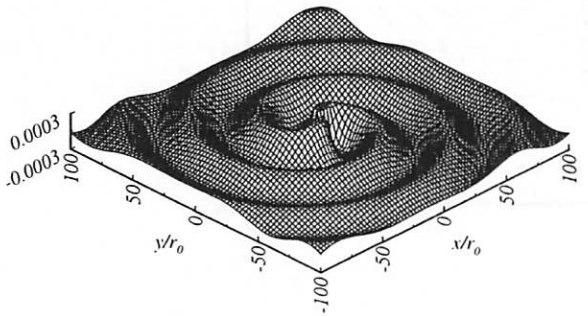

Acoustic pressure on diagonal

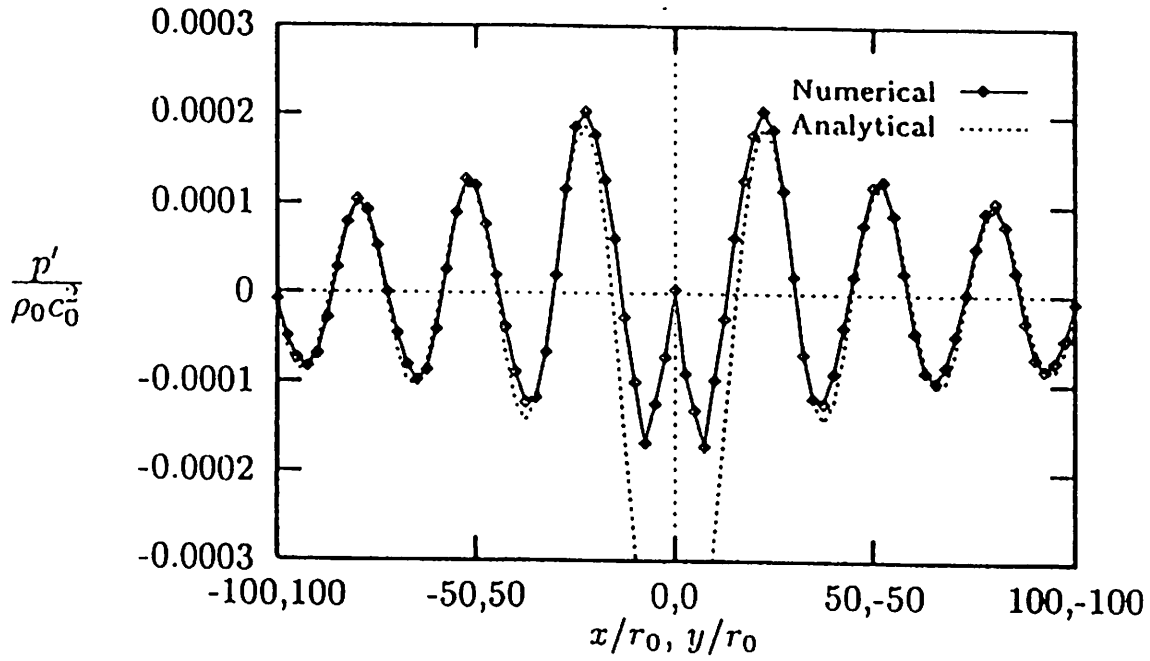

(b) Tam and Webb boundary condition (TWBC)

Effect of boundary location

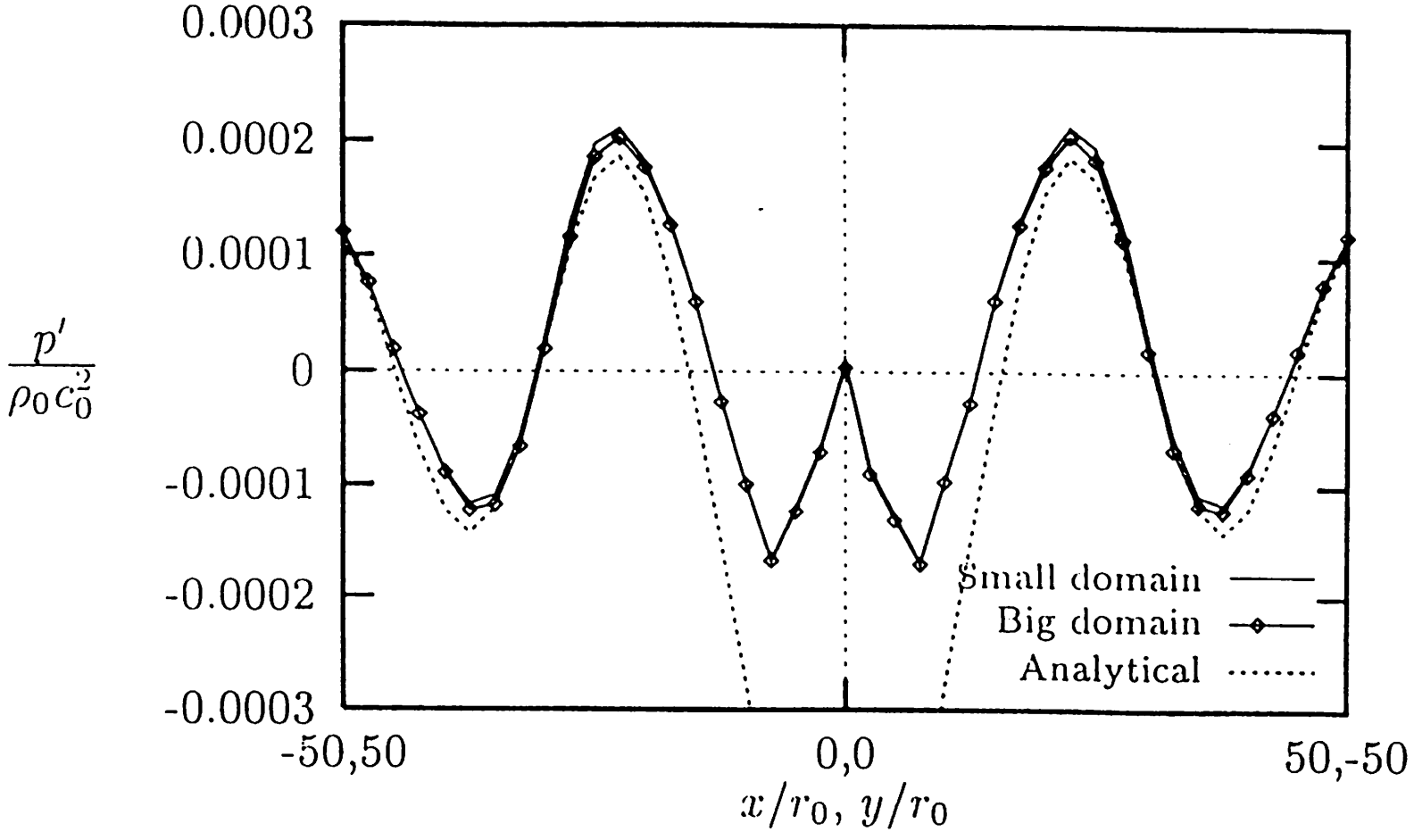

Viscous flow over cylinder

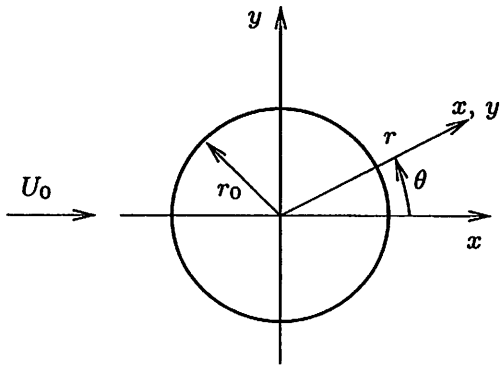

- Dipole
- Two-dimensional
- Cylindrical coordinates
- Numerical solution of flow field
- $Re = 200$, $M = 0.5$
- Computational domain: $r_{max} = 40r_0$, 189×161(viscous mesh), 151×161(acoustic mesh)

Results for cylinder

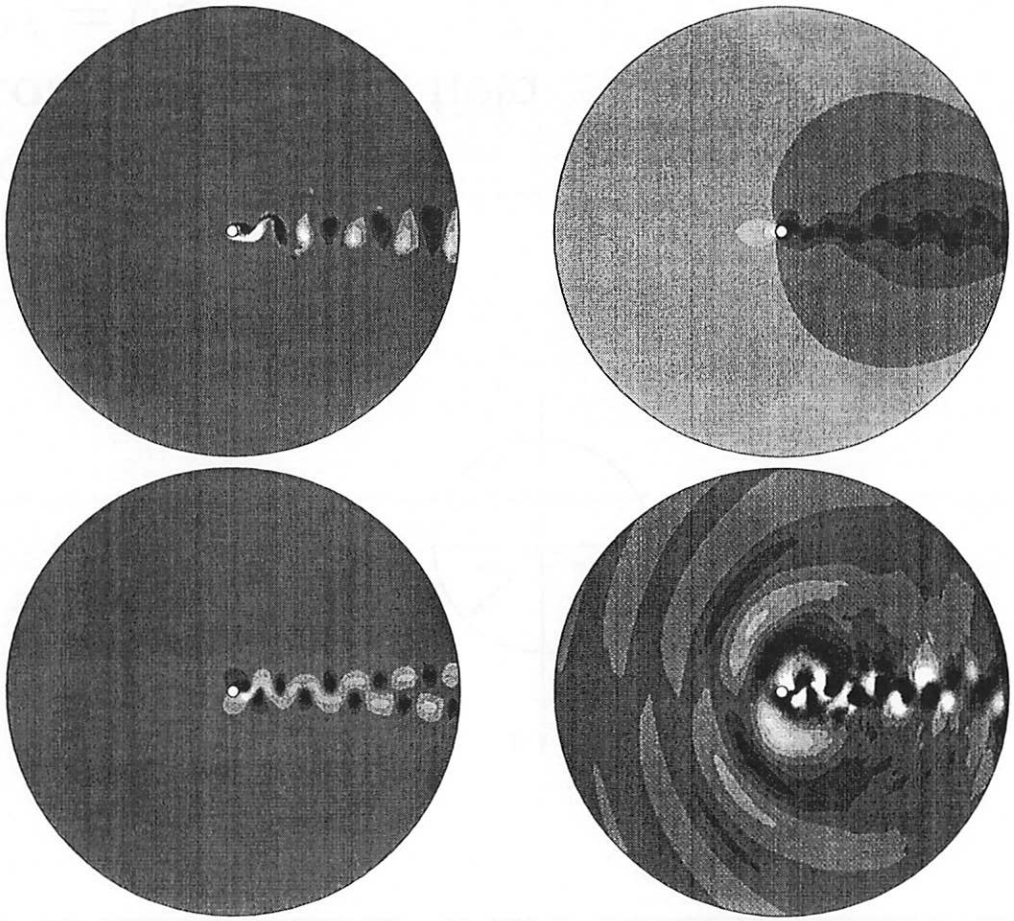

The Future

Future (and ongoing) work:

Interfacing of perturbation solver (in generalized coordinates) with general purpose flow solver.

The Dutch research on aerodynamic noise of wind turbines; past and present

T. Dassen[1], R. Parchen[2]
[1]National Aerospace Laboratory NLR, P.O. Box 153, NL-8300 AD, Emmeloord, The Netherlands
[2]TNO Institute of Applied Physics, P.O. Box 155, NL-2600 AD, Delft, The Netherlands

In the Netherlands, it was recognized in the early eighties that noise nuisance experienced by residents neighbouring stand-alone wind turbines or wind farms would be one of the major threats to governmental wind energy targets. Therefore, several substantial research efforts aimed at the understanding, modelling and reduction of aerodynamic noise of wind turbines were carried out during the last fifteen years. These efforts were initiated by a cluster of Dutch research institutes and manufacturers and co-ordinated by the Netherlands Agency for Energy and Environment (NOVEM).

In the eighties, research was mainly aimed at the prediction of the aerodynamic noise of wind turbines. For this, the semi-empirical prediction code RHOAK, which includes several noise sources, was developed and validated using large numbers of data obtained from outdoor measurements. The code reliably predicts the noise of a number of existing wind turbines for a certain range of conditions but can not be developed towards a full rotor blade design tool. The RHOAK code is adapted whenever new insights and/or useful data become available and has recently been coupled to a blade loading prediction code.

In the early nineties when the national TWIN-I programme started, research became more and more focused on the reduction of wind turbine noise. For this, several existing ideas about the 'quietening' of airfoils by applying irregularities (f.i. sawteeth) at the airfoil trailing edge were verified by performing flow and acoustic measurements in an anechoic wind tunnel. In the TWIN-II programme, the improvement of semi-empirical models describing the main sources of airfoil self-noise followed rather successfully, mainly as a consequence of the fact that the wind tunnel set-up allowed for detailed studies of the flow and the separate measurement of different noise sources. As a result, new airfoils expected to be silent with respect to inflow-turbulence noise could be defined and were tested successfully.

In the JOULE-III programme two acoustic projects, STENO and DRAW, with a substantial Dutch contribution were accepted. In STENO it is the aim to assess the noise-reducing capabilities and the optimal geometry of serrations when applied at the outer part of the rotor blade. The insights needed to define this geometry are obtained from a comprehensive series of flow and acoustic measurements performed in the Low Speed Wind Tunnel and the Small Anechoic Wind Tunnel of the National Aerospace Laboratory NLR. In DRAW all wind turbine broadband noise sources are studied with the aim to enable the development of prediction codes which consider the exact blade shape. Again, the experimental part of this research is carried out in the aforementioned wind tunnels of NLR and makes use of a large series of generic models. The experimental data are used by the TNO Institute of Applied Physics for the development and validation of a prediction code which is based on the correlation of boundary-layer turbulence and the field of unsteady pressures at the noise-radiating surface on the one hand and these pressures and the far-field noise on the other.

The substantial Dutch involvement in the research on aerodynamic noise of wind turbines has yielded a clear overview of the state-of-the-art (f.i. the possibilities and limitations of prediction codes) and of ways to fill up existing gaps in the understanding of this noise. The presentation will be concluded by surveying these gaps and will make a proposal for future work.

NOTES FROM DISCUSSION ON AEROACOUSTIC NOISE FROM WIND TURBINES IEA MEETING, MILANO, MONDAY 17th MARCH 1997

Prepared by Penny Dunbabin

The following people were present:

Gerard Schepers	ECN	Netherlands
Gianfranco Guidati	IAG	Germany
Peter Fuglsang	Risø	Denmark
Kristian Dahl	Risø	Denmark
Penny Dunbabin	RES	UK
Jim Tangler	NREL	USA
Emil Moroz	El Paso University	USA
B.Maribo Pedersen	DTU	Denmark

Ton Dassen of TNO, Netherlands, was unable to attend.

The discussion was centered on four questions:

1. What noise sources are the most important?
2. How are the sources best modelled?
3. What needs to be done to improve predictions?
4. Does it boil down to correct prediction of the unsteady aerodynamics around the rotor, or is the difficult part to convert the aerodynamics into acoustics?

There was a certain amount of digression on all these subjects. The notes given below are approximately in chronological order, and may not quite refer to the questions at the start of each section. For clarity, a few references have been added, although they may be familiar to the participants.

What noise sources are the most important?

It was generally agreed that once tonal noise from the gearbox and generator have been eliminated, aerodynamic noise becomes dominant. It is well known that sharpening the trailing edge can result in dramatic noise reductions, as shown by the paper submitted by J. Tangler.

For sharp trailing edges, the dominant aerodynamic noise mechanisms are:

turbulent boundary layer trailing edge noise
inflow turbulence noise.

Under normal circumstances, it is believed that trailing edge noise contributes more to the overall A-weighted noise level, although the precise amount is probably a function of turbine design.

Guidati referred to some experiments currently being investigated as part of the STENO project in which it was shown that serrated trailing edges can reduce trailing edge noise by 5 dB. These measurements were made both in the wind tunnel and on a full-scale wind turbine (the NedWind 1 MW). As part of the STENO project, the orientation and dimensions of serrations is beeing investigated. It appears that skewed flow may be a problem.

Guidati went on to say that once trailing edge noise has been successfully reduced, e.g. by serrations, inflow noise could become dominant again. The DRAW project has found significant reductions in inflow noise using thicker aerofoils. Fuglsang pointed out that Danish wind turbines already use very thick aerofoils near the tip (15-18%), for structural reasons. This should have the effect of minimising inflow turbulence noise.

Guidati discussed the implications of rigid and porous surfaces for the emission of noise from the trailing edge. A porous surface should have the effect of reducing the efficiency of noise radiation from the trailing edge. Tangler referred to some wind tunnel experiments conducted by Ainslie in the US to investigate this. For a full-scale wind turbine, there are questions as to whether a porous trailing edge could remain so for any length af time when exposed to the elements.

There was some discussion concerning tip noise. Most of the delegates agreed that tip noise is simply an enhanced form of trailing edge noise, i.e. that the tip vortex causes a region of separated flow over the blade near the tip, and that turbulent eddies in this region produce noise as they are convected over the trailing edge. The experimental work of Tangler (presented in the proceedings of this meeting), appears to confirm this. Pedersen and Schepers noted that Bonus currently manufactures blades with torpedo tips, while Enercon modifies the tip so that it turns towards the pressure side.

A second theory, by Sen, concerning secondary vortices was also discussed, but no firm conclusions were reached.

Infra-sound was discussed briefly. The advantages of upwind turbines from this point of view have been well documented. Moroz discussed some of the measurements made by Hubbard et al. on a downwind turbine (the MOD-2), which was found to be annoying at large distances, partly because of the interaction of the low frequency noise with the resonance frequencies of buildings or windows. Reference [1].

Dunbabin referred to some measurements reported by Legerton et al. (reference [2]), in which it was found that noise levels at frequencies below 31.5 Hz were well below the required limits, as were vibration levels, but that, occasionally tones in the range 1-20 Hz may be detectable at distances up to 800 m.

Tangler discussed laminar separation bubbles and the noise that can result from them. Some aerofoils, such as the NACA 23000 series have been found to be unsuitable for wind turbines, as they are prone to laminar separation bubbles that can cause Tollmein-Schlichting noise radiation. The presence or absence of these bubbles can be predicted by using codes such as XFOIL and EPLA, but a considerable level of experience is required to operate the programs. Tangler pointed out that keeping the maximum aerofoil thickness too far aft could result in strong bubbles.

There was some discussion of bevelled trailing edges. Guidati said that these can give a reduction in noise, as shown by experiments on the UNIWEX turbine. Moroz and Tangler mentioned that US Windpower uses bevelled trailing edges.

How are sources best modelled?

Guidati's vorticity wave model appears to be accurate for predicting the inflow turbulence noise. This model is presented in the proceedings of this conference. Both Guidati and Schepers mentioned that models may be of more use for predicting trends in data than for predicting absolute values.

Guidati referred to the work of Rene Parchen of TNO on the modelling of trailing edge noise. The fundamental theory of this modelling is described by Howe (reference [3]). The trailing edge noise is modelled as a function of the Fourier transform of the pressure field on the aerofoil. The pressure field on the aerofoil can be estimated from mean boundary layer quantities predicted by the k - ε method, or the Reynolds stress models.

Dunbabin referred to the work of Lowson on the subject of relating boundary layer turbulence intensity and absolute noise levels to boundary layer shape factor. H, (reference [4]).

What other measurements should be made?

Fuglsang & Dahl described some ongoing experiments to measure the angle of attack using a pitot tube, and to relate this to noise. It was planned to measure the angle of attack at one blade, and to record noise from the other two. The experiments are beeing conducted at Risø, and should be finished later this year.

What needs to be done to improve predictions?

Dahl and Guidati stated that once the source distribution has been established, the acoustic radiation can be calculated with relative ease. Guidati went on to say that a model is required to convert the turbulent kinetic energy to a source distribution.

---

1 Hubbard, H.H. & Shepherd, K.P. "Physical Characteristics and Perception of Low Frequency Noise from Wind Turbines", Noise Control Engineering, Vol.36, 1991, p5-15

2 "Low Frequency Noise & Vibration Levels at a Modern Wind Farm", Ledgerton, M.L., Manley, D.M., Sargent, J.W., Styles, P., Proceedings of the 25th Internoise Conference, Liverpool, UK, August 1996. Published by the Institute of Acoustics, 5 Holywell Hill, St. Albans AL1 1EU, UK. ISBN 873082 91 6

3 "A Review of the Theory of Trailing edge Noise" Howe, M.S., Journal of Sound & Vibration, Vol 61, no 3, pp437-465, 1978

4 "Design Prediction Model for Wind Turbine Noise, Part 1, Basic Aerodynamic and Acoustic Models", Lowson, M.V. & Fiddes, S.P., Flow Solutions report 93/06, 15/11/96, published by ETSU, Harwell Laboratories, Near Chilton, Didcot, Oxfordshire OX11 0RA, UK.

29th IEA Meeting of Experts
Aero-acoustic Noise of Wind Turbines

Milano, march 17-18, 1997

List of Participants

NAME	ADDRESS	PHONE/FAX NUMBERS
Gerard Schepers	ECN PO Box 1 1755 ZG Petten the Netherlands	Tel: (+31) 224 56 4233 Fax: (+31) 224 56 3214
Peter Fuglsang Kristian Dahl	RISØ National Laboratory P.O.box 49 4000 Roskilde Denmark	Tel: (+45) 4677 5071 5036 Fax: (+45) 4237 2965
Penny Dunbabin	Renewable Energy Systems Ltd. 11 Elmbank street Glasgow G2 4PB United Kingdom	Tel: (+44) 1412 212467 Fax: (+44) 1412 212470
Gianfranco Guidati	IAG, University of Stuttgart Pfaffenwaldring 21 70550 Stuttgart Germany	Tel: (+49) 711 685 3421 Fax: (+49) 711 685 3438
Emil Moroz	University of Texas at El Paso Dept. of Mech. & Ind. Eng. El Paso, TX 79968 U.S.A.	Tel:(+1) 915 747 5031 Fax: (+1) 915 747 5019 e-mail: emil@wind.me.utep.edu
James Tangler	NREL 1617 Cole Boulevard Golden, CO 80401 U.S.A.	Tel: (+1) 303 384 6934 Fax: (+1) 303 384 6901 e-mail: tanglerj@ tcplink.nrel.gov
B.Maribo Pedersen	Dept. of Energy Engineering Building 404 Techn. Univ. of Denmark 2800 Lyngby Denmark	Tel: (+45) 4525 4312 Fax: (+45) 4588 2421 e-mail: bmp@et.dtu.dk

IEA R&D WIND - ANNEX XI
TOPICAL EXPERT MEETINGS

1. Seminar on Structural Dynamics, Munich, October 12, 1978

2. Control of LS-WECS and Adaptation of Wind Electricity to the Network, Copenhagen, April 4, 1979

3. Data acquisition and Analysis for LS-WECS, Blowing Rock, North Carolina, September 26 - 27, 1979

4. Rotor Blade Technology with Special Respect to Fatigue Design Problems, Stockholm, April 21 -22, 1980

5. Environmental and Safety Aspects of the Present LS WECS, Munich, September 25 - 26, 1980

6. Reliability and Maintenance Problems of LS WECS, Aalborg, April 29 - 30, 1981

7. Costings for Wind Turbines, Copenhagen, November 18 - 19, 1981

8. Safety Assurance and Quality Control of LS WECS during Assembly, Erection and Acceptance Testing , Stockholm, May 26 - 27, 1982

9. Structural Design Criteria for LS WECS, Greenford, March 7 - 8, 1983

10. Utility and Operational Experiences and Issues from Major Wind Installations, Palo Alto, October 12 - 14, 1983

11. General Environmental Aspects, Munich, May 7 - 9, 1984

12. Aerodynamic Calculational Methods for WECS, Copenhagen, October 29 - 30, 1984

13. Economic Aspects of Wind Turbines, Petten, May 30 - 31, 1985

14. Modelling of Atmospheric Turbulence for Use in WECS Rotor Loading Calculations, Stockholm, December 4 - 5, 1985

15. General Planning and Environmental Issues of LS WECS Installations, Hamburg, December 2, 1987

16. Requirements for Safety Systems for LS WECS, Rome, October 17 - 18, 1988

17. Integrating Wind Turbines into Utility Power Systems, Virginia, April 11 - 12, 1989

18. Noise Generating Mechanisms for Wind Turbines, Petten, November 27 - 28, 1989

19. Wind Turbine Control Systems, Strategy and Problems, London, May 3 - 4, 1990

20. Wind Characteristics of Relevance for Wind Turbine Design, Stockholm, March 7 - 8, 1991

21. Electrical Systems for Wind Turbines with Constant or Variable Speed, Göteborg, October 7 - 8, 1991

22. Effects of Environment on Wind Turbine Safety and Performance, Wilhelmshaven, June 16, 1992

23. Fatigue of Wind Turbines, Golden Co., October 15 - 16, 1992

24. Wind Conditions for Wind Turbine Design, Risø, April 29 - 30, 1993

25. Increased Loads in Wind Power Stations, "Wind Farms", Göteborg, May 3 - 4, 1993

26. Lightning Protection of Wind Turbine Generator Systems and EMC Problems in the Associated Control Systems, Milan, March 8 - 9, 1994

27. Current R&D Needs in Wind Energy Technology, Utrecht, Sept. 11 - 12, 1995

28. State of the Art of Aeroelastic Codes for Wind Turbine Calculations, Lyngby, Denmark, April 11 - 12, 1996

29. Aero-acoustic Noise of Wind Turbines,Noise Prediction Models, Milano, Italy, March 17 - 18, 1997